



January 2017

Semi-Empirical Methods For Electronic Properties Of Surface Adsorbed Molecules.

Rajesh Dhakal

Follow this and additional works at: <https://commons.und.edu/theses>

Recommended Citation

Dhakal, Rajesh, "Semi-Empirical Methods For Electronic Properties Of Surface Adsorbed Molecules." (2017). *Theses and Dissertations*. 2107.
<https://commons.und.edu/theses/2107>

This Dissertation is brought to you for free and open access by the Theses, Dissertations, and Senior Projects at UND Scholarly Commons. It has been accepted for inclusion in Theses and Dissertations by an authorized administrator of UND Scholarly Commons. For more information, please contact zeinebyousif@library.und.edu.

SEMI-EMPIRICAL METHODS FOR ELECTRONIC
PROPERTIES OF SURFACE ADSORBED MOLECULES

by

Rajesh Dhakal

Bachelor of Science, Minnesota State University-Moorhead, 2010

A Dissertation

Submitted to the Graduate Faculty

of the

University of North Dakota

in partial fulfillment of the requirements

for the degree of

Doctor in Philosophy

Grand Forks, North Dakota

May

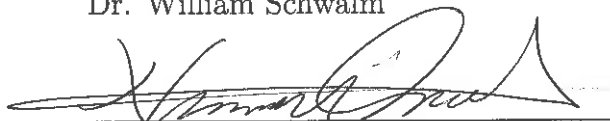
2017

Copyright 2015 Rajesh Dhakal

This dissertation, submitted by Rajesh Dhakal in partial fulfillment of the requirements for the Degree of Doctor of Philosophy from the University of North Dakota, has been read by the faculty Advisory Committee whom the work has been done and is hereby approved.



Dr. William Schwalm



Dr. Nuri Oncel



Dr. Yen Lee Loh

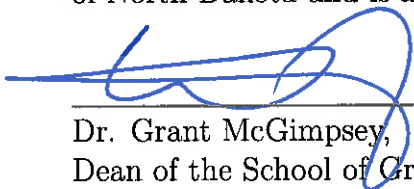


Dr. Graeme Dewar



Dr. Bruce Dearden

This dissertation is being submitted by the appointed advisory committee as having met all of the requirements of the School of Graduate Studies at the University of North Dakota and is hereby approved.



Dr. Grant McGimpsey,
Dean of the School of Graduate Studies



Date

Permission

Title Semi-empirical methods for electronic properties of surface adsorbed molecules.

Department Physics

Degree Doctor of Philosophy

In presenting this dissertation in partial fulfillment of the requirements for a graduate degree from the University of North Dakota, I agree that the library of this University shall make it freely available for inspection. I further agree that permission for extensive copying for scholarly purposes may be granted by the professor who supervised my dissertation work or, in his absence, by the chairperson of the department or the dean of the Graduate School. It is understood that any copying or publication or other use of this dissertation or part thereof for financial gain shall not be allowed without my written permission. It is also understood that due recognition shall be given to me and to the University of North Dakota in any scholarly use which may be made of any material in my dissertation.

Rajesh Dhakal
May 08, 2017

TABLE OF CONTENTS

LIST OF FIGURES	viii
LIST OF TABLES	xii
ACKNOWLEDGEMENTS	xiv
ABSTRACT	xvi
CHAPTER	
I FAKE METHOD	1
1.1 Schrödinger's equation and one-electron theory	1
1.2 Rayleigh Ritz's Variational Principle Method	5
1.3 FAKE METHOD	9
1.3.1 Extended Hückel empirical methods	10
1.3.2 Outline of FAKE method	11
1.3.3 Method	13
1.3.4 Results and Discussion	20
II STO AND GTO	21
2.1 Slater-type orbitals	21
2.2 STO to GTO expansion method	22
2.3 Results	24
2.4 Generating Functions	27
2.4.1 Overlap integrals	27

2.4.2	Kinetic Energy integrals	29
III	TIGHT BINDING METHOD	32
3.1	Introduction	32
3.1.1	Hamiltonian matrix element	35
IV	GRAPHENE	38
4.1	Introduction	38
4.2	The π -orbital model	42
4.3	LCAO model	48
V	GREENIAN AND LOCAL DENSITY OF STATES	52
5.1	Green functions	52
5.2	Local density of states	56
5.3	Monkhorst-Pack method	57
5.3.1	Results	62
VI	EDGE SHEET OF GRAPHENE	65
6.1	An effective dimer method	66
6.1.1	Results and Discussion	69
VII	HOLES AND DEFECTS ON GRAPHENE	74
VIIIA	SIMPLE MODEL OF GRAPHITE	82
8.1	Introduction	82
8.2	Method	82
8.2.1	Two layers	86
8.2.2	Three layers	87
8.2.3	Results and Discussion	88

IX	EXTENSION THEORY FOR GRAPHENE	90
9.1	Extended Hamiltonian	90
9.1.1	Extended Green functions	92
9.1.2	Boundary region	94
9.1.3	Extended lattice results	95
X	ADSORBATE SYSTEMS	99
10.1	Löwdin partitioning technique	99
10.2	Chemisorption of Hydrogen	102
10.2.1	Hydrogen right on top of carbon	102
10.2.2	Hydrogen above the center of a ring	107
10.2.3	Hydrogen above and in between the bonds	109
XI	SUMMARY AND DISCUSSIONS	114
	REFERENCES	118

LIST OF FIGURE

1.1	Occupied-orbital energies, ψ_n indexing the energy levels in ascending order for ethylene.	18
1.2	Occupied-orbital energies, ψ_n indexing the energy levels in ascending order for cyclopropene.	18
1.3	Occupied-orbital energies, ψ_n indexing the energy levels in ascending order for formic acid.	19
1.4	Occupied-orbital energies, ψ_n indexing the energy levels in ascending order for formaldehyde.	19
2.1	STO $1s$, $\sqrt{\frac{1}{\pi}} \zeta^{\frac{3}{2}} \exp(-\zeta r)$ into GTO-3G, $\zeta = 1$, STO(Red), GTO(Blue). 24	
2.2	STO $2s$, $\sqrt{\frac{1}{3\pi}} \zeta^{\frac{5}{2}} r \exp(-\zeta r)$ into GTO-3G, $\zeta = 1$, STO(Red), GTO(Blue). 25	
2.3	STO $2p$, $\sqrt{\frac{1}{\pi}} \zeta^{\frac{5}{2}} r \exp(-\zeta r)$ into GTO-3G, $\zeta = 1$, STO(Red), GTO(Blue). 25	
2.4	STO $3d_{xy}$, $\sqrt{\frac{2}{3\pi}} \zeta^{\frac{7}{2}} r^2 \exp(-\zeta r)$ into GTO-3G, $\zeta = 1$, STO(Red), GTO(Blue).	26
2.5	Comparison of the least-squares fit of a $1s$ Slater atomic orbital to a contracted gaussian 1-G, 2-G and 3-G for $\zeta = 1$ by Szabo ¹	26
4.1	Lattice of Graphene. There are two carbons atoms per unit cell, denoted by $\alpha = 1, 2$ or A and B . These lie on interlocking triangular sublattices with Bravais lattice vectors \vec{h}_1 and \vec{h}_2 . The interatomic distance is a	38
4.2	Symmetrized first Brillouin zone.	41
4.3	Schematic diagram of atoms in the neighborhood of (m, n) unit cell.	42
4.4	Plot of bands E_1 and E_2 of graphene near the Fermi level as a function of \vec{k} . The vertical axis is energy in Hückel units and the horizontal axes are momentum in the x and y directions. The conduction band (upper cone) and the valence band (lower cone) meet at six points known as Dirac points that lie at the corners of the Brillouin zone.	44
4.5	Positions of the Dirac cones in the zone. Two of the cone-shaped structures (K and K') are independent and the others are constructed translating by reciprocal basis vectors.	45

4.6	ΓMK Irreducible Brillouin zone (IBZ). Band energies of the lower band are shown as superimposed local contours. The energy zero corresponds to the Dirac cones at the K, K' points and the sharp peaks in the DOS come from saddle points at M_1, M_2 and M_3 . The points Γ, K, M , are called zone center, the corner and the center of the edge respectively. The green lines show the borders of the irreducible BZ along which the extrema occur. One moves along these lines to get the energy that an electron can have within the solid. The \vec{k} grid is replaced with a list of high symmetry points along the $\Gamma - M - K - \Gamma$ path in \vec{k} space.	47
4.7	Band diagram for graphene in π orbital theory. The vertical axis is energy and the horizontal axis is the momentum in x and y directions. M, K and Γ are the symmetry points inside a first Brillouin zone given as $\vec{\Gamma} = (0, 0, 0)$, $\vec{M} = \frac{1}{2} \frac{2\pi}{a} (0, \frac{2}{3}, 0)$, $\vec{K} = \frac{2\pi}{a} (\frac{1}{3\sqrt{3}}, \frac{1}{3}, 0)$ The Dirac point is at the Fermi-level, energy, which occurs at point K . The saddle points are at M	48
4.8	Band diagram for graphene using LCAO with a Bloch symmetrized basis of $2s, 2p_x, 2p_y$ and $2p_z$ orbitals for a unit cell. The vertical axis is energy in eV and the horizontal axis is momentum in the x and y directions.	50
4.9	Graphene band structure from first principles-LAPW method ²	50
5.1	Zone transformed into a trapezoid.	60
5.2	(Left) Making of the Brillouin zone (a) The symmetrized zone comprises sector 1 through 6. Other segments shown dashed are equivalent by translation (b) Translation is used to assemble an equivalent trapezoidal zone.	60
5.3	PDOS of an infinite graphene sheet for different valence orbitals using solid state matrix elements from FAKE method.	62
5.4	DOS of a graphene by DFT study using two basis sets for graphene by Stewart and Derek ³ to study how the choice of basis functions impacts characterization techniques and calculated electronic transport properties.	62
5.5	DOS of an infinite graphene sheet with all four valence orbitals combined using FAKE method.	63
5.6	DOS of a graphene using QUANTUM ESPRESSO ⁴	63
6.1	The two simple edge geometries of graphene. The armchair termination consists of both the sub-lattice sites but the zigzag termination is made of only one sub-lattice and the edge atoms are all equivalent to one another chemically. In the picture above, one can see the red sites in zigzag termination.	65
6.2	Effective dimer used to calculate the matrix elements.	66
6.3	Schematic diagram showing the zigzag states for different values of n	69

6.4	π orbital DOS at site 1 of Fig(6.2) a zigzag state representing α sublattice before removing site 1.	69
6.5	π orbital DOS at site 2 of Fig(6.2) a zigzag state representing β sublattice before removal of site 1.	70
6.6	π LDOS of sites in the vicinity of a zigzag line defect ⁵	70
6.7	Contour plot of spectral density of Fig(6.2) at site 1 before its removal. The white area is where the probability of finding the electron is maximum and darker the area lesser the probability is.	71
6.8	Contour plot of spectral density at site 2 before removal of site 1.	72
6.9	π LDOS at site 2 after removing site 1 from Fig(6.2).	72
6.10	Spectral density at the edge state after the removal of site 1.	73
7.1	Schematic diagram of a graphene where a carbon (β) sublattice is removed, the numbers are the neighboring atoms with respect to the vacancy.	74
7.2	LDOS for an adjacent site to the vacancy, site 1 (α) sublattice in Fig(7.1). The red, blue, green and orange curves are PDOS for $2s$, $2p_x$, $2p_y$ and $2p_z$ respectively. The black curve is the total DOS at site 1. There is a peak at Fermi level that is caused due to the vacancy.	76
7.3	LDOS for an adjacent site to the vacancy, site 2 (β) in Fig(7.1). The red, blue, green and orange curves are PDOS for $2s$, $2p_x$, $2p_y$ and $2p_z$ respectively. The black curve is the total DOS at site 2. There is a zero DOS at fermi level. The site is the same sublattice as the vacancy.	77
7.4	LDOS for an adjacent site to the vacancy, site 3 (α) sub lattice in Fig(7.1).The red, blue, green and orange curves are PDOS for $2s$, $2p_x$, $2p_y$ and $2p_z$ respectively. The black curve is the total DOS at site 3 which is the third nearest neighbor with respect to the vacancy. Because it is an α sublattice, one can see a peak in a Fermi level as we saw from site 1.	77
7.5	LDOS for an adjacent site to the vacancy, site 4 (α) sub lattice in Fig(7.1). The red, blue, green and orange curves are PDOS for $2s$, $2p_x$, $2p_y$ and $2p_z$ respectively. The black curve is the total DOS at site 4. Because site 4 is α sublattice in the graphene system, it can be seen there is a very small peak in the Fermi level. However it is not as big we saw on 1st and 3rd neighbor DOS.	78
7.6	LDOS for an adjacent site to the vacancy, site 5 (β) sub lattice in Fig(7.1). The red, blue, green and orange curves are PDOS for $2s$, $2p_x$, $2p_y$ and $2p_z$ respectively. The black curve is the total DOS at site 5. It is the fifth nearest neighbor from the vacancy and is a β sublattice. The effect of vacancy is significantly less here compared to other sites. However, the DOS at Fermi level looks flat compared to the original one.	79
7.7	Only π LDOS at a site next to vacancy (Red) and at a site far-far away from it (Blue).	79

7.8	π LDOS at a lattice site next to the vacancy ($r = a$) and at a site far away from vacancy (black solid line) ⁵	80
7.9	Only π LDOS of first five neighboring sites due to vacancy. Red, blue, green, orange and black are 1st, 2nd, 3rd, 4th and 5th neighbors respectively. Red, green and orange represent α sublattice whereas blue and black represent the β sublattice, the same kind where the vacancy was made.	80
8.1	AA stacked graphene where two layers aren't shifted horizontally.	83
8.2	AB stacked graphene where two layers are shifted horizontally.	83
8.3	ABC stacked graphene where two layers are shifted horizontally.	83
8.4	Tight binding matrix element V 's reproduced from (B. A. McKinnon) ⁶	85
8.5	Schematic diagram of the connection.	86
8.6	Density of states for one layer(Red) and two layers(Blue): $v_1 = 1$ and $v_2 = 0.35$ in Hückel units.	88
8.7	Density of states for one layer(Red) and three layers(Blue): $v_1 = 1$, $v_2 = 0.35$, $v_3 = 0.035$ and $v_4 = 0.035$ in Hückel units.	88
9.1	Schematic diagram of graphene showing its first five neighbors.	90
9.2	Contour plot of the ellipse formed by the resultant of g . The x -axis is α and y -axis is β	96
9.3	π -theory bands for an extended Hamiltonian. Red is when $(\alpha, \beta) = (0, 0)$ and blue is when $(\alpha, \beta) = (0.18, 0.003)$	96
9.4	π -theory bands for an extended Hamiltonian. Left is when $(\alpha, \beta) = (0.055, -0.0215)$ and right is when $(\alpha, \beta) = (-0.3178, -0.2152)$	97
9.5	π -theory bands for an extended Hamiltonian in the BB region. On the left is some extra dips in the band so the number of van Hove singularities on the right changes at those points.	97
9.6	π theory bands for an extended Hamiltonian. Left is when $(\alpha, \beta) = (0, 0)$ and right is when $(\alpha, \beta) = (0.1798, 0.0002958)$ outside the ellipse.	98
9.7	π theory bands for an extended Hamiltonian. Left is when $(\alpha, \beta) = (0.055, -0.0215)$ and right is when $(\alpha, \beta) = (-0.3178, -0.2152)$ inside the ellipse.	98
10.1	Schematic diagram of a Hydrogen atom placed right on top of a carbon atom, namely atom 0. The labels 1,2,3,4,5 are the first, second, third, fourth and fifth neighbors with respect to carbon 0.	102
10.2	FAKE DOS for a single isolated hydrogen atom without coupling to the substrate.	103
10.3	FAKE PDOS of hydrogen atom that is located at a distance of $2.5A^\circ$. A splitting in it's energy level can be seen when it is coupled to a carbon atom as shown in Fig(10.1). The H atom is directly on top of carbon 0 is allowed to interact with 22 carbon atoms as shown.	103

10.4	π theory: p_z PDOS of an adjacent carbon atom, site 1 at Fig(10.1). Here the zero of the DOS is still located at the Fermi energy, which is taken as zero on the graphene. There is also a change in van Hove singularity on the valence band.	104
10.5	FAKE DOS of an adjacent carbon atom, site 1 at Fig(10.1). The DOS is not significantly changed anywhere in the energy spectrum.	104
10.6	The DOS of the first neighbor is changed from blue to red. The change is coming from p_z contribution that was seen in Fig(10.4).	106
10.7	An isolated atomic hydrogen is placed at a distance of $2.5 A^\circ$ above from the center of 2D graphene ring.	107
10.8	FAKE PDOS on hydrogen. There are two more peaks that have arised in the valence part after the coupling of hydrogen with graphene. . .	108
10.9	π theory. The induced π DOS on adjacent carbon atoms due to the coupling of hydrogen at a distance of $2.5A^\circ$ above the center of the ring in the sites 1, 2, 5, 14, and 16 as shown in Fig(10.7).	108
10.10	FAKE DOS: The DOS of one of the carbon site inside the ring has changed from blue to red. It is seen that there is a small change is DOS which is coming from the contribution of p_z orbital. The other PDOS stays the same.	109
10.11	An isolated hydrogen placed $2.5A^\circ$ above the mid distance between site 1 and 4.	110
10.12	The PDOS of the hydrogen from the kind of configuration described in Fig(10.11) is only shifted and broadened from atomic hydrogen . .	110
10.13	The π DOS at sites 1, 2, 7, 16, and 18. Only the first neighbor seems to change its shape. However, the change is not as significant as from other registries shown above.	111
10.14	The total DOS at site 1. Blue is the uncoupled DOS whereas the red is new coupled DOS. There is no change is total DOS for this kind of registry at all.	111
10.15	The distortion of the lattice due to displacement of the adsorbent carbon atom and rehybridization from its initial sp^2 hybridization to sp^3 . The H atom (above) distorts the carbon lattice and causes rehybridization. The rehybridization describes approximately the local change in the Hamiltonian	112

LIST OF TABLES

1.1	FAKE orbital parameters. Harris and his group optimized ζ and α^0 using 37 sets of molecules containing H, C, N, O and F . ζ_{at} are single-STO values to find $\langle \vec{r} \rangle$ from ab-initio calculations. α' and α'' are from Moore's atomic data. Units for α are eV and for ζ is Bohr ⁻¹	20
2.1	Coefficients and exponent parameters for Gaussian expansion of Slater orbitals using Least Square Fit for $\zeta = 1$	24

Acknowledgements

I wish to express my sincere appreciation for my research advisor Dr. William Schwalm; I attribute the level of my Doctorate degree to his encouragement and efforts. I take this opportunity to express my sincere gratitude for his time, as it would have been impossible for the degree to be incomplete without him. His one-on-one communication, generous advice, feedbacks and reminders have not only increased my knowledge but also shaped me into a better researcher.

I would also like to thank Dr. Yen Lee Loh, Dr. Nuri Oncel, Dr. Graeme Dewar, and Dr. Bruce Dearden for serving on my dissertation committee and their guidance and suggestions. I would also like to thank the rest of the Physics and AstroPhysics Department for their support throughout the graduate studies.

Finally, thanks to all those individuals whose name does not appear, yet have contributions to the successful completion of my studies and research.

Dedications

I would to dedicate this dissertation to my parents Bhagawati Pd. and Indira Devi Dhakal and my wife Dawa Lama Tamang, who have always been supportive and great source of inspiration and motivation.

ABSTRACT

In the work described here, semi-empirical, theoretical tools have been developed to address one-electron properties of substrate/adsorbate systems. The tools are adaptations of the simple, Hückel π -electron theory and of the fast accurate-kinetic energy theory of F. Harris et al. (FAKE) to systems involving an infinite, mostly periodic substrate via a Green-function formalism. These tools are applied here to study graphene with vacancies and adsorbates, but can be generalized. In π theory, only a small subset of substrate basis states having odd reflection symmetry through the graphene layer are used to treat electrons near the Fermi level, to a very crude level of approximation. The substrate model Hamiltonian has been extended to contain second third and fourth nearest neighbor interactions. In the FAKE method, a semi-empirical tight-binding, charge self-consistent Hamiltonian is developed in which kinetic energy integrals are evaluated exactly and potential energy terms are extrapolated via a Müllikan formula using the overlaps. The methods are applied to an isolated atomic hydrogen adsorbate, and to vacancy and edge states on the graphene substrates. By comparing to experiments including scanning tunneling microscopy and to theoretical work including augmented plane wave (APW) and first principles density functional and other theoretic work, the theoretical tools developed here are seen to give good results and can in principle provide an efficient, potentially faster way of handling very large adsorbed molecules.

CHAPTER I

FAKE METHOD

1.1 Schrödinger's equation and one-electron theory

The independent one-electron Schrödinger equation is given by,

$$-\frac{\hbar^2}{2m}\nabla^2\phi(\vec{r}) + U(\vec{r})\phi(\vec{r}) = \epsilon \phi(\vec{r}) \quad (1.1)$$

which represents a single electron but is not useful because of the effects of electron-electron interactions. A more accurate calculation of the electronic properties of a system should have N -particle wavefunction for all N electrons. The Schrödinger equation from classical Hamiltonian for N electrons with ψ as a wavefunction of the N -electron system is,

$$H\psi = \sum_{i=1}^N \left(-\frac{\hbar^2}{2m}\nabla_i^2 \psi - Z e^2 \sum_{R_k} \frac{1}{|\vec{r}_i - \vec{R}_k|} \psi \right) + \frac{1}{2} \sum_{i \neq j} \frac{e^2}{|\vec{r}_i - \vec{r}_j|} \psi = E \psi \quad (1.2)$$

where the first term is the kinetic energy, the second term is the attractive electrostatic potential with the bare nuclei fixed at points \vec{R}_k and the last term is the electron-electron interactions between the electrons positioned at \vec{r}_i and \vec{r}_j . It's not possible to solve the equation above exactly thus one needs to find an approximate method. Consider ψ as the product wavefunction of the N -electron system,

$$\psi(\vec{r}_1\sigma_1, \vec{r}_2\sigma_2, \dots, \vec{r}_N\sigma_N) = \phi_1(\vec{r}_1, \sigma_1)\phi_2(\vec{r}_2, \sigma_2)\dots\phi_N(\vec{r}_N, \sigma_N), \quad (1.3)$$

where \vec{r}_k is a position variable and σ_j is a spin variable. The wavefunction $\phi_k(\vec{r}_k, s_k)$ is the independent one-electron eigenfunction for k^{th} electron. The second term in the N -electron Hamiltonian can be expressed as

$$U^{el-pro}(\vec{r}_i) = -Z e^2 \sum_{R_k} \frac{1}{|\vec{r}_i - \vec{R}_k|}. \quad (1.4)$$

The i^{th} electron experiences the electric repulsive force from all other electrons. One can attempt to treat these other electrons as a smooth negative charge distribution with charge density ρ . Then the potential energy for the i^{th} electron due to the presence of the charge density ρ is given by:

$$U_i^{el-el} = -e \int \frac{\rho(\vec{r}')}{|\vec{r}_i - \vec{r}'|}. \quad (1.5)$$

But the charge density due to i^{th} one-electron eigenfunction is given by,

$$\rho_i(\vec{r}) = -e|\phi_i(\vec{r})|^2 \quad (1.6)$$

only if it is occupied. The total electronic charge density is the sum of all one-electron individual charge densities

$$\rho(\vec{r}) = -e \sum_i^N |\phi_i(\vec{r})|^2 \quad (1.7)$$

In this way one can reduce the N -electron system Schrödinger equation into a one-electron relation approximately as

$$\begin{aligned} -\frac{\hbar^2}{2m} \nabla^2 \phi_i(\vec{r}) - Z e^2 \sum_{R_k} \frac{1}{|\vec{r} - \vec{R}_k|} \phi_i(\vec{r}) + \\ e^2 \left(\sum_{j, j \neq i} \int |\phi_j(\vec{r}')|^2 \frac{1}{|\vec{r} - \vec{r}'|} d^3x' \right) \phi_i(\vec{r}) = \epsilon_i \phi_i(\vec{r}), \end{aligned} \quad (1.8)$$

which is the set of *Hartree equations*⁷. These can be solved iteratively to minimize the expectation value of the Hamiltonian $\langle H \rangle$. Although, Hartree's equation is physically reasonable and intuitive, it is not enough to explain how the configuration of other $(N - 1)$ electrons effect the i^{th} electron. Hartree's product wavefunction is incompatible with Pauli's exclusion principle because the electron wavefunctions should be antisymmetric and they have to change sign when any pair of electron coordinates is exchanged. It is clearly not possible to treat the exchange features of electron-electron interactions just by Hartree's product form of ψ and so one has to extend the self-consistent field to a higher level of approximation. So Fock and Slater generalized Hartree's results by including the proper exchange symmetry and this results in the Hartree-Fock Self-Consistent theory⁸.

A linear combination of product wavefunctions is used in which the other products are obtained by permutations of $\vec{r}_i\sigma_i$ added together with weights of $+1$ or -1 so that the overall sum of products is antisymmetrized. It can also be written as a determinant of a $N \times N$ matrix because the determinant changes sign when any two columns or rows are interchanged.

$$\psi(\vec{r}_1\sigma_1, \dots, \vec{r}_N\sigma_N) = \frac{1}{\sqrt{N!}} \sum_P \epsilon_P \prod_{i=1}^N \phi_{Pi}(\vec{r}_i\sigma_i) \quad (1.9)$$

where, i runs over all the permutations, and ϵ_P is $+$ for even and $-$ for odd permutations. In each case σ_k is the spin coordinate. The one-electron wavefunction $\phi_i(\vec{r}_j)\chi_i(\sigma_j)$ is a product of the space and a spin part and its normalization condition requires,

$$\int \phi_i^*(\vec{r}_k)\phi_j(\vec{r}_k) d^3x_k = \delta_{ij} \quad \text{and} \quad \sum_{\sigma_k = -\frac{1}{2}}^{\frac{1}{2}} \chi_i^*(\sigma_k)\chi_j(\sigma_k) = \delta_{ij}.$$

where $s = \uparrow, \downarrow$ and

$$\chi_i(\sigma_k) = \begin{cases} \chi_\uparrow(\sigma_k) & \text{spin up } \uparrow \\ \chi_\downarrow(\sigma_k) & \text{spin down } \downarrow. \end{cases}$$

The expectation value of \hat{H} is given by,

$$\begin{aligned} \langle \hat{H} \rangle &= \int \psi^* \hat{H} \psi d^3x \\ &= \frac{1}{N!} \int \sum_Q \epsilon_Q \prod_{m=1}^N \phi_m^*(Q\vec{r}_m) \hat{H} \sum_P \epsilon_P \prod_{n=1}^N \phi_{Pn}(\vec{r}_n) d^3x_n. \end{aligned} \quad (1.10)$$

For a one-electron operator $\sum_{m=1}^N \hat{A}_m$, with A_m acting only on functions of $\vec{r}_m \sigma_m$, the only case where a term in $\langle \hat{H} \rangle$ survives is when $\epsilon_P \phi_{Pm}(\vec{r}_m) = \phi_m(\vec{r}_m)$. Thus the only contributing permutation is an operator identity \hat{I} . For the two electron operator $\sum'_{m,n} \hat{A}_{mn}$, the contributing permutations are $\hat{P} = \hat{I}$ and the odd permutation $\hat{P} = P_{mn}$ which exchanges two coordinates and for which $\epsilon_P = -1$. The odd minus sign for the permutation comes from the fact that there is an interchange of electrons between m and n since electrons are fermions. Finally the expectation value of \hat{H} for an N -electron system is given by,

$$\begin{aligned} \langle \hat{H} \rangle &= \sum_{i,k} \int \phi_i^*(\vec{r}_1) \left(\frac{\hbar^2}{2m} \nabla^2 - \frac{Ze^2}{|\vec{r}_1 - \vec{R}_k|} \right) \phi_i(\vec{r}_1) d^3x_1 \\ &\quad + \frac{1}{2} e^2 \sum_{j,i \neq j} \left(\int \frac{|\phi_i^*(\vec{r}_1)|^2 |\phi_j^*(\vec{r}_2)|^2}{|\vec{r}_1 - \vec{r}_2|} d^3x_1 d^3x_2 \right. \\ &\quad \left. - \delta_{s_i s_j} \int \frac{\phi_i^*(\vec{r}_1) \phi_j^*(\vec{r}_2) \phi_j(\vec{r}_1) \phi_i(\vec{r}_2)}{|\vec{r}_1 - \vec{r}_2|} d^3x_1 d^3x_2 \right). \end{aligned} \quad (1.11)$$

There are two terms inside the second sum in Eq(1.11), the first one is the direct and the latter is the exchange term that has a $\delta_{s_i s_j}$ for the exchange of spin and the coordinates are swapped.

1.2 Rayleigh Ritz's Variational Principle Method

It is impossible to solve the N -electron Schrödinger exactly so one must use approximate methods. One useful way of getting approximate solutions is to set up the trial wavefunction containing a number of parameters and varying them to find the extreme value of the expectation value of the Hamiltonian. The parameterization should be chosen cleverly so that the trial wavefunction will be qualitatively like the expected solutions to the given Schrödinger equation. Let's take a wavefunction ϕ that is varied subjected to the condition that it's normalized. So the expectation value of the Hamiltonian for this function is:

$$\langle \hat{H} \rangle = \int \phi^* H \phi d^3x. \quad (1.12)$$

The wavefunction ϕ is varied in such a way that it varies the expectation value $\langle \hat{H} \rangle$ too. One can prove that only for certain unknown choices of the function ϕ , the expectation value of H will be stationary and so a small change in ϕ shouldn't make any first-order change in $\langle \hat{H} \rangle$. Of all the eigenfunctions ϕ_n of the Hamiltonian \hat{H} , one will have the lowest eigenvalue which must be the absolute minimum which is the ground-state eigenfunction that is lower than for any other functions varied. The functions thus obtained are the eigenfunctions of Schrödinger's equation. In this way, Schrödinger's equation can be solved by using this variational principle⁹.

If the ϕ 's are a set of trial one-electron basis wavefunctions, then ϕ is varied to make $F = \langle \phi | \hat{H} | \phi \rangle$ stationary, subjected to the constraint ϕ is normalized, i.e., $\langle \phi | \phi \rangle = 1$. Suppose, $\tilde{\phi} \rightarrow \phi + \alpha \delta\phi$, where $\delta\phi$ is an arbitrary but a continuous function so that as $\alpha \rightarrow 0$, $\tilde{\phi} \rightarrow \phi$. Suppose further that

$$G = F - \left(\sum_i \lambda_{ii} \langle \phi_i | \phi_i \rangle + \sum_{i \neq j} \delta_{ij} \left(\lambda_{ij} \langle \phi_i | \phi_j \rangle + \lambda_{ji} \langle \phi_j | \phi_i \rangle \right) \right) \quad (1.13)$$

where the λ 's are Lagrange's undetermined multipliers⁹. When one maximizes or minimizes the function $F = \langle \phi | \hat{H} | \phi \rangle$, the solution will depend on λ and it is adjusted in such a way that F takes the extremal value subjected to the condition that $\langle \phi | \phi \rangle = 1$. If, $F = \langle \hat{H} \rangle$, and

$$\begin{aligned}
& \left(\sum_i \lambda_{ii} \langle \phi_i | \phi_i \rangle + \sum_{i \neq j} \delta_{ij} \left(\lambda_{ij} \langle \phi_i | \phi_j \rangle + \lambda_{ji} \langle \phi_j | \phi_i \rangle \right) \right) \\
&= \sum_i \lambda_{ii} \int \phi_i^*(\vec{r}_1) \phi_i^*(\vec{r}_1) d^3 x_1 \\
&+ \sum_{i,j,i \neq j} \delta_{ij} \left(\lambda_{ij} \int \phi_i^*(\vec{r}_1) \phi_j^*(\vec{r}_1) d^3 x_1 + \lambda_{ji} \int \phi_j^*(\vec{r}_1) \phi_i^*(\vec{r}_1) d^3 x_1 \right)
\end{aligned} \tag{1.14}$$

Choosing $\lambda_{ji} = \lambda_{ij}^*$ makes the last two terms the complex conjugate of each other providing the correct number of independent multipliers. The undetermined multipliers are λ_{ii} and λ_{ij} for $j \neq i$ running over all the spin-orbitals of the atom. Thus, varying ϕ_i yields:

$$\begin{aligned}
\tilde{G} &= \langle \tilde{\phi} | \hat{H} | \tilde{\phi} \rangle - \left(\sum_i \lambda_{ii} \langle \tilde{\phi}_i | \tilde{\phi}_i \rangle + \sum_{i \neq j} \delta_{ij} \left(\lambda_{ij} \langle \tilde{\phi}_i | \tilde{\phi}_j \rangle + \lambda_{ji} \langle \tilde{\phi}_j | \tilde{\phi}_i \rangle \right) \right) \\
&= \sum_{i,k} \int \left(\phi_i^*(\vec{r}_1) + \alpha \delta \phi_i^*(\vec{r}_1) \right) \left(\frac{\hbar^2}{2m} \nabla_1^2 - \frac{Ze^2}{|\vec{r}_1 - \vec{R}_k|} \right) \left(\phi_i(\vec{r}_1) + \alpha \delta \phi_i(\vec{r}_1) \right) d^3 x_1 \\
&\quad \sum_{i \neq j} \int \frac{e^2 \left(\phi_i^*(\vec{r}_1) + \alpha \delta \phi_i^*(\vec{r}_1) \right) \phi_j^*(\vec{r}_2)}{|\vec{r}_1 - \vec{r}_2|} \left(\left(\phi_i(\vec{r}_1) + \alpha \delta \phi_i(\vec{r}_1) \right) \phi_j(\vec{r}_2) - \delta_{s_i s_j} \right. \\
&\quad \left. \left(\phi_j(\vec{r}_1) \left(\phi_i(\vec{r}_2) + \alpha \delta \phi_i(\vec{r}_2) \right) \right) \right) d^3 x_1 d^3 x_2 \\
&- \sum_i \lambda_{ii} \int \left(\phi_i^*(\vec{r}_1) + \alpha \delta \phi_i^*(\vec{r}_1) \right) \left(\phi_i(\vec{r}_1) + \alpha \delta \phi_i(\vec{r}_1) \right) d^3 x_1 \\
&+ \sum_{i \neq j} \delta_{ij} \lambda_{ij} \left(\phi_i^*(\vec{r}_1) + \alpha \delta \phi_i^*(\vec{r}_1) \right) \phi_j(\vec{r}_1) d^3 x_1.
\end{aligned}$$

Let,

$$\hat{g}_1 = \sum_k \left(\frac{\hbar^2}{2m} \nabla_1^2 - \frac{Ze^2}{|\vec{r}_1 - \vec{R}_k|} \right) \quad \& \quad \hat{g}_{12} = \frac{e^2}{|\vec{r}_1 - \vec{r}_2|}.$$

Since for the maximum, minimum, or any stationary points of G , one has the condition,

$$\left. \frac{\partial \tilde{G}}{\partial \alpha} \right|_{\alpha=0} = 0, \quad (1.15)$$

this implies

$$\begin{aligned} & \sum_i \int \delta\phi_i^*(\vec{r}_1) g_1 \phi_i(\vec{r}_1) d^3x_1 \\ & + \sum_{i \neq j} \int \delta\phi_i^*(\vec{r}_1) \int \left(\phi_j^*(\vec{r}_2) g_{12} \phi_j(\vec{r}_2) d^3x_2 \right) \phi_i(\vec{r}_1) d^3x_1 \\ & - \sum_{i \neq j} \delta_{s_i s_j} \int \delta\phi_i^*(\vec{r}_1) \int \left(\phi_j^*(\vec{r}_2) g_{12} \phi_i(\vec{r}_2) d^3x_2 \right) \phi_j(\vec{r}_1) d^3x_1 \\ & - \sum_i \lambda_{ii} \int \delta\phi_i^*(\vec{r}_1) \phi_i(\vec{r}_1) d^3x_1 \\ & - \sum_{i \neq j} \delta_{ij} \int \delta\phi_i^*(\vec{r}_1) \phi_j(\vec{r}_1) d^3x_1 + \text{complex conjugate of the given term} = 0 \end{aligned} \quad (1.16)$$

When the conditions $i = j$ and $i \neq j$ are combined, the above equation can be written as,

$$\begin{aligned} & \int \delta\phi_i^*(\vec{r}_1) \left\{ g_1 \phi_i(\vec{r}_1) + \sum_j \int \left(\phi_j^*(\vec{r}_2) g_{12} \phi_j(\vec{r}_2) d^3x_2 \right) \phi_i(\vec{r}_1) \right. \\ & \left. - \delta_{s_i s_j} \int \left(\phi_j^*(\vec{r}_2) g_{12} \phi_i(\vec{r}_2) d^3x_2 \right) \phi_j(\vec{r}_1) - \sum_j \delta_{ij} \lambda_{ij} \phi_j(\vec{r}_1) \right\} d^3x_1 = 0. \end{aligned} \quad (1.17)$$

Let's suppose the expression inside the curly bracket be Ψ so Eq(1.17) becomes,

$$\int \delta\phi_i^*(\vec{r}_1) \Psi d^3x_1 = 0 \quad (1.18)$$

Because $\delta\phi_i^*$ is arbitrary if Ψ is continuous then the integrand must be zero. I will show this by way of contradiction. Lets assume Ψ is not identically zero. Hence, there must be some point at which the function is not zero. I assume ϕ is positive and continuous near the point. So there exists a sphere small enough centered at

that point, such that the function is positive inside this sphere. $\delta\phi^*$ is a continuous and arbitrary function so it can be chosen to be zero outside but positive inside the sphere where Ψ is positive and continuous. Then the product of these two functions is zero outside but positive inside the sphere. Thus the integrand is positive inside and zero outside causing the whole integral to take on a positive value. This contradicts the fact that $\int \delta\phi_i^*(\vec{r}_1) \Psi d^3x_1 = 0$, so Ψ has to be zero inside a sphere of volume centered at any point.

$$\therefore \Psi = 0$$

that implies,

$$\begin{aligned} g_{12} \phi_i(\vec{r}_1) + \sum_j \int \phi_j^*(\vec{r}_2) g_{12} \phi_j(\vec{r}_2) d^3x_2 \phi_i(\vec{r}_1) \\ - \delta_{ij} \int \phi_j^*(\vec{r}_2) g_{12} \phi_i(\vec{r}_2) d^3x_2 \phi_j(\vec{r}_1) = \sum_j \delta_{s_i s_j} \lambda_{ij} \phi_j(\vec{r}_1) \end{aligned} \quad (1.19)$$

Thus obtained equation above is the Hartree-Fock equation¹⁰. A unitary transformation can be made on ϕ_i without leaving the determinantal wavefunction now the minimization results changed yields

$$\phi_l = \sum_m C_{lm} \phi'_m \quad \text{and} \quad \phi'_m = \sum_n C_{nm}^* \phi_n.$$

The Lagrange multiplier λ_{ij} is transformed with respect to the unitary transformation made above. One finds after some algebra that the Hartree-Fock equation is not altered undergoing any unitary transformations. The fact that λ_{ij} is Hermitian allows one to choose a unitary transformation that diagonalizes λ_{ij} so that the elements of λ_{ij} form a diagonal matrix. Thus chosen ϕ'_i s are the solution to the Hartree-Fock

equation that diagonalizes the matrix λ resulting in

$$\begin{aligned} & \sum_k \left(\frac{\hbar^2}{2m} \nabla_1^2 - \frac{Ze^2}{|\vec{r}_1 - \vec{R}_k|} \int d^3x_2 \right) \phi_i(\vec{r}_1) + \frac{1}{2} \left(\sum_j \int |\phi_j(\vec{r}_2)|^2 \frac{e^2}{|\vec{r}_1 - \vec{r}_2|} \right) \phi_i(\vec{r}_1) \\ & - \sum_j \delta_{s_i s_j} \left(\int \phi_j^*(\vec{r}_2) \frac{e^2}{|\vec{r}_1 - \vec{r}_2|} \phi_i(\vec{r}_2) d^3x_2 \right) \phi_j(\vec{r}_1) = \epsilon_i \phi_i(\vec{r}_1) \end{aligned} \quad (1.20)$$

where ϵ_i represent the energy that is required to remove the i^{th} electron from orbital i provided the other electrons are held fixed on the system. The wavefunction ϕ_i a one-electron eigenfunction, implies that the variational principle not only applies for the ground state but also to other stationary states. In other words, stationary values of G correspond to eigenstates of H^8 .

1.3 FAKE METHOD

Some time ago Frank E. Harris et al. developed a minimal approximation to one-electron quantum theory of molecules based on a linear combination of atomic orbitals (LCAO)¹¹. They called it the fast, accurate-kinetic energy (FAKE) method for semi-empirical electronic structure. This is an extended-Huckel method that should be able to handle large systems with less computational effort than ab-initio methods¹². The kinetic-energy integrals are calculated accurately while the potential-energy integrals are determined empirically by fitting to atomic and molecular data. The neighboring atom coulombic interactions are also included. This treatment of kinetic-energy improves the convergence of the iterative process and omits the *ad hoc* adjustment factors like those of Wolfsberg, Helmholz and Cusachs^{13,14}.

In the LCAO method, the diagonal and non-diagonal matrix elements of the

Hamiltonian are given by,

$$\langle \phi_i | H | \phi_j \rangle = \langle \phi_i | \hat{T}(\vec{r}) - \sum_A \frac{Z_A}{|\vec{R}_A - \vec{r}|} + e^2 \int \frac{\rho(\vec{r}')}{|\vec{r} - \vec{r}'|} d^3x' - E(\text{exch}, \vec{r}) | \phi_j \rangle \quad (1.21)$$

where \hat{T} is the kinetic energy operator and $E(\text{exch}, \vec{r})$ is the contribution due to the exchange and correlation energy. The correlation accounts for relaxation of the multielectron wavefunction in higher order and the antisymmetric part goes with the exchange energy that arises due to the antisymmetry of electron coordinates.

1.3.1 Extended Hückel empirical methods

In the extended Hückel type of empirical one-electron methods¹², the off-diagonal Hamiltonian matrix elements are interpolated simply by a Wolfsberg -Helmholz¹³ interpolation formula for $i \neq j$, where

$$H_{ij} = \frac{K}{2} S_{ij} (H_{ii} + H_{jj}). \quad (1.22)$$

Here H_{ii} is the valence state ionization energy for orbital i and S_{ij} is the overlap integral for basis orbitals i and j . However the method does not represent the two-body electrostatic interactions well¹⁵. It does not account sufficiently for electron-electron repulsion, and even a large electron density does not inhibit the attraction of more electrons into a more electronegative atom¹⁶. Charge builds up resulting in unrealistic atomic charges. One must include self-consistent iteration of charges in calculations of this kind.

In order to make the effective electronegativity closer to measured values, an iterative extended Hückel theory can be introduced¹⁶. The diagonal Hamiltonian is expressed as a function of net atomic charge. This makes the Hamiltonian depend upon the net atomic charges that is to be determined iteratively¹⁷. A quadratic

dependence of the diagonal matrix element on the net atomic charge q_A is included, which is an extension of the ω technique described by A. Streweiser¹⁸.

$$\alpha_{i_A} = \alpha_{i_A}^0 + q_A \alpha'_{i_A} + q_A^2 \alpha''_{i_A} \quad (1.23)$$

where $-\alpha_i$ is the diagonal Hamiltonian entry with respect to orbital i in iterative extended Hückel theory. The other coefficients are obtained by fitting ionization potentials in an isoelectronic series of atoms and ions.

This way the Hamiltonian matrix will depend upon the solution to the molecular orbital problem, and one requires to solve it iteratively for a self-consistent set of charges and matrix elements using the output charges from one iteration to form the input Hamiltonian matrix elements for the next iteration.

1.3.2 Outline of FAKE method

The FAKE method is an improved iterative extended Hückel method developed also by Harris et al^{11,12}. The current section follows the description given in references^{11,12}. The kinetic and potential energy matrix elements are treated separately. The FAKE calculations are based on an effective one-electron Hamiltonian with diagonal elements H_{ii} which consists of the following terms^{12,19}:

1. A Kinetic energy, T_{ii} calculated for a single Slater-type orbital i .
2. A one-center potential energy, given as an empirical expression $-\alpha_{i_A}^0 - q_A \alpha'_{i_A} - q_A^2 \alpha''_{i_A} - T_{ii}$ with constants $\alpha_{i_A}^0$, α'_{i_A} and α''_{i_A} depending on the type of atom and orbital involved and which depends on the net charge q_A of the atom as in Eq.(1.23). The Hamiltonian is determined self-consistently by iteration.
3. Two-electron repulsion between an electron in an orbital i on atom A and the core and electron charges of each of the other atoms B . The sum of 2 and 3 is

the potential energy associated with orbital ϕ_i .

$$H_{ii,A} = -\alpha_i^0 q_A - q_A \alpha_i' - q_A^2 \alpha_i'' - \sum_{B \neq A} (q_B - n_{BA}) [ii|B] - \sum_{B \neq A} n_{BA} [ii|e_B]. \quad (1.24)$$

where, the overlap -charges is given as.

$$n_{BA} = \sum_{i \text{ on } A, j \text{ on } B} P_{ij} S_{ij} \quad (1.25)$$

The term $[ii|B]$ is the interaction of the i th orbital of atom A with the core of atom B given by the relation,

$$[ii|B] = [R_{A_i B_j} + 1/\gamma_B]^{-1}. \quad (1.26)$$

The empirical parameter γ_B is parameterized to take very large values ($\gamma_B \rightarrow \infty$). The repulsion term $[ii|e_B]$ is the interaction of the i th orbital on atom A with the j th orbital on atom B , that is interpolated using the Nishigo-Mataga^{20,21} formula,

$$[ii|e_B] = 1/(R_{A_i B_j} + 2/[(ii|ii) + jj|jj]) \quad (1.27)$$

where

$$(ii|ii) = I_i - EA_i, \quad (1.28)$$

and I_i is the ionization potential and EA_i is the electron affinity of orbital ϕ_i . Note that the term defined by $(ii|ii)$ is not to be confused with two electron multicenter integrals as

$$(ij|kl) = \int \phi_i^*(\vec{r}_1) \phi_j(\vec{r}_1) \frac{1}{|\vec{r}_1 - \vec{r}_2|} \phi_k^*(\vec{r}_2) \phi_l(\vec{r}_2) d^3x_1 d^3x_2. \quad (1.29)$$

The expressions $[ii|B]$ and $[ii|e_B]$ in Eq.(1.24) are interpolated between short and long distance limits . The α_i' and α_i'' are fitted to an isoelectronic series of atoms

and ions. The empirical parameter e_B was adjusted using the formula of Mataga-Nishimoto²⁰ to optimize the orbital energies and equilibrium distances. Off diagonal matrix elements between orbital i and j on different atoms consist of actually computed kinetic-energy matrix elements plus two-centered potential matrix elements V_{ij} determined by interpolation from the overlap integral S_{ij} by Mulliken’s formula without an adjustable parameter K ,

$$V_{ij} = \frac{1}{2}S_{ij}(H_{ii} - T_{ii} + H_{jj} - T_{jj}). \quad (1.30)$$

The traditional extended Hückel method interpolates both kinetic and potential parts of H_{ij} , resulting in an approximation Eq(1.22). The FAKE method extrapolates only the potential part, V_{ij} , as in Eq.(1.30). Because the kinetic and potential terms do not scale the same way with length, the latter method is expected to work better and be more nearly comparable between different physical situations. The atomic charge q_A is computed at each iteration starting from the formal core charge Z_A and subtracting orbital charges computed using overlap and bond-order matrices. The net atomic charge on atom A in a molecule, q_A , is given by

$$q_A = Z_A - \sum_{m@A} \sum_n P_{mn} S_{mn}, \quad (1.31)$$

where P is the bond order matrix as defined in Eq(1.41).

1.3.3 Method

The molecular or solid state wavefunction ψ_i , is expressed as a linear combination of Slater atomic-like orbitals ϕ_j :

$$\psi_i = \sum_m a_{im} \phi_m$$

where the molecular eigenstates ψ_i is normalized, i.e.,

$$\langle \psi_i | \psi_j \rangle = \sum_{mn} a_{im}^* a_{jn} \langle \phi_m | \phi_n \rangle = \sum_{mn} a_{im}^* a_{jn} S_{mn} = \delta_{ij}. \quad (1.32)$$

The overlap integral $S_{mn} = \langle \phi_m | \phi_n \rangle$ for Slater-type atomic orbitals m and n are further expanded in terms of three Gaussian orbitals (STO-3G). In work reported below three Gaussians are used per Slater basis function. If E_i is the energy associated with ψ_i ,

$$E_i = \langle \psi_i | H | \psi_i \rangle = \sum_{mn} a_{im}^* a_{in} H_{mn} \quad (1.33)$$

where H_{mn} satisfies the condition

$$H_{mn} = T_{mn} + \frac{1}{2} S_{mn} (V_{mm} + V_{nn}). \quad (1.34)$$

For $m = n$,

$$H_{mm} = T_{mm} + \frac{1}{2} S_{mm} (2V_{mm}) = T_{mm} + V_{mm}. \quad (1.35)$$

the Slater type ϕ 's must be normalized so that the diagonal term reduces correctly.

The potential energy term V_{mm} is simply

$$V_{mm} = H_{mm} - T_{mm}. \quad (1.36)$$

$$H_{mn} = T_{mn} + \frac{1}{2} S_{mn} (H_{mm} - T_{mm} + H_{nn} - T_{nn}) \quad (1.37)$$

The diagonal energy H_{mm} where ϕ_m is on atom A is given by,

$$H_{mm} = -\alpha_m^0 - q_A \alpha_m' - q_A^2 \alpha_m'' - \sum_{B \neq A} (q_B - n_{BA}) [mm|B] - \sum_{B \neq A} n_{BA} [mm|e_B]. \quad (1.38)$$

Therefore,

$$\begin{aligned}
H_{jk} = & T_{jk} + \frac{1}{2} S_{jk} \left(-\alpha_j^0 - q_A \alpha'_j - q_A^2 \alpha''_j - \sum_{B \neq A} (q_B - n_{BA}) [jj|B] - \sum_{B \neq A} n_{BA} [jj|e_B] \right. \\
& - T_{jj} - \alpha_k^0 - q_{A'} \alpha'_k - q_{A'}^2 \alpha''_m - \sum_{B' \neq A'} (q_{B'} - n_{B'A'}) [kk|B'] \\
& \left. - \sum_{B' \neq A'} n_{B'A'} [kk|e'_B] - T_{kk} \right)
\end{aligned} \tag{1.39}$$

where there is no sum on repeated indices and it is clear that H_{mn} depends upon the net atomic charges. According to the variational principle, E_i takes on a stationary value by varying the expansion coefficients subjected to the constraint $\langle \psi_i | \psi_i \rangle = 1$. This leads to the secular equation

$$\det | \hat{H} - E \hat{S} | = 0, \tag{1.40}$$

where \hat{H} and \hat{S} are the Hamiltonian and Overlap matrices with respect to the basis orbitals. The secular equation yields energy eigenvalues, each with it's corresponding eigenvector, the i^{th} one of which having entries a_{ij} . A charge distribution is defined by assigning electrons in a pair to each one-electron molecular wavefunction ψ_i in the ascending order of E_i until all the available electrons are accounted for in the process. At finite temperature, of course, the levels are occupied partially as prescribed by a Fermi function. For self-consistency, the bond-order matrix P_{mn} is introduced. This is defined in terms of the generalized eigenvectors of H ¹⁹

$$P_{mn} = \sum_i^{occ} N_i a_{im}^* a_{in} \tag{1.41}$$

where $N_i = 2$ is the maximum number of electrons that occupies each molecular orbital ψ_i such that,

$$\sum_{mn} P_{mn} S_{mn} = N \quad (\text{total number of valence electrons}). \quad (1.42)$$

The net atomic charge q_A on atom A is then given by

$$q_A = Z_A - \sum_m \sum_n P_{mn} S_{mn} , \quad (1.43)$$

where m is summed over the basis orbitals on atom A but n is summed everywhere and Z_A is the number of active valence electrons on atom A .

The matrices \hat{S} and \hat{T} are computed only once for each choice of a basis set of orbitals and an initial set of net atomic charges q_A is estimated. The iteration converges rapidly if the initial estimation of q_A is closer to the final value of net atomic charge. For simplicity, one can start the iteration putting all q'_A s equal or putting them all to zero .

The iteration process proceeds as follows. With the q'_A s on hand, S_{mn} and T_{mn} , the Hamiltonian matrix element H_{mn} , is re-calculated. This leads to a new secular equation for the molecular orbital and energies as described above. Then P_{mn} is recalculated again from the newly iterated eigenvectors. On the basis of this new bond order matrix P_{mn} , q'_A s are calculated again and the process is repeated over until the values of the q'_A s and P_{mn} become consistent, which means until they no longer change between iterations. The speed of the convergence depends upon the efficiency of the solutions for the secular equation, and mostly, in solid state case, on the efficiency of calculating net-charges on atoms. The transformation of the atomic orbitals into an orthonormal basis helps speed up the convergence of its calculation.

During the iterations, the attainment of self-consistency depends directly only upon the atomic charges q_A not directly upon the individual eigenvector components

a_{mn} . The attempt to obtain convergence on eigenvectors leads to extra work because they can fluctuate chaotically if there are degenerate eigenvalues. One has to examine q_A carefully for consistency. The divergence of the charges under iteration is typical when one substitutes the output charge of one iteration directly as input for next iteration. A simple method of damping can be used by applying an intermediate atomic charge with a value somewhere between that calculated for two successive iterations. If $q_{A,n}$ and $q'_{A,n}$ are the input and output charges for atom A at n^{th} iteration, the input for $(n + 1)^{th}$ iteration can be calculated as:

$$q_{A,n+1} = q_{A,n} + \lambda(q'_{A,n} - q_{A,n}). \quad (1.44)$$

The smaller the values of λ , stronger is the damping of the iteration. The FAKE method is not variational hence so the quality of results is determined by the parameters like the orbital exponents ζ_i and the orbital energy parameters α_i that depend in turn upon the atoms and associated quantum numbers of STO i and net atomic charge q_i as explained in Ref.^{18,22} for the ω technique. The quantities α'_i and α''_i were kept fixed at values consistent with Moore's atomic data^{12,23} while α_i^0 and ζ_i were optimized with respect to ab-initio SCF orbital energies and charge distributions.

The theory was applied to a calibration set limited of 37 molecules to find optimum atomic parameters¹². That calibration set contained H, C, N, O and F and for them near optimum molecular values of ζ and α_0 were found. The ab initio calculation for the same set has been found also by Snyder and Basch²⁴. It turns out that the optimized ζ values are contracted (more compact orbitals means large ζ values) relative to the free-atom orbitals¹².

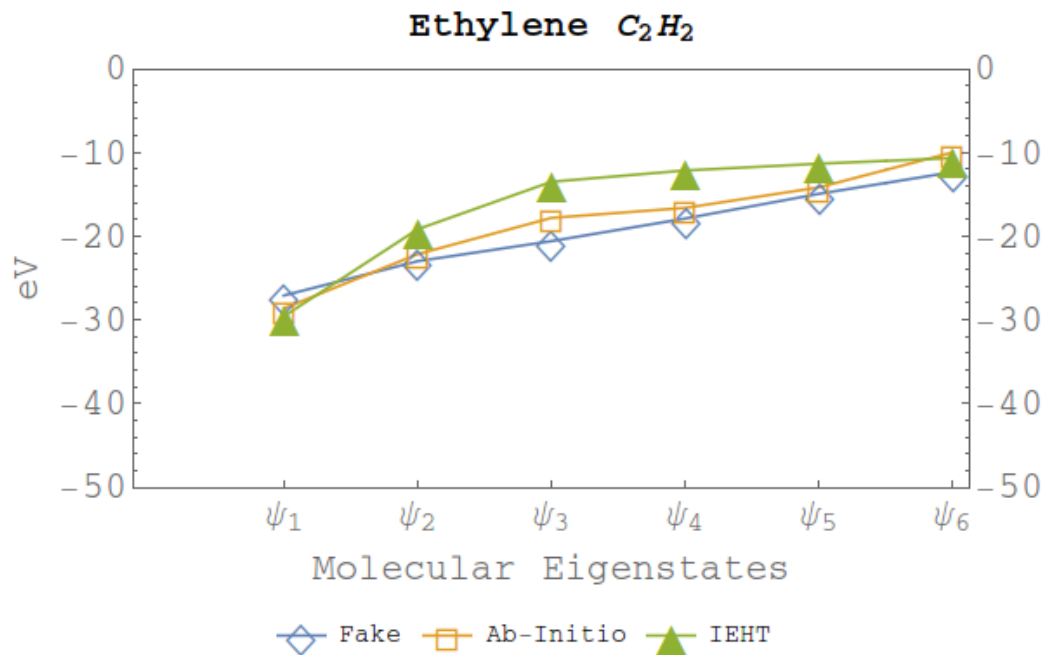


Figure 1.1: Occupied-orbital energies, ψ_n indexing the energy levels in ascending order for ethylene.

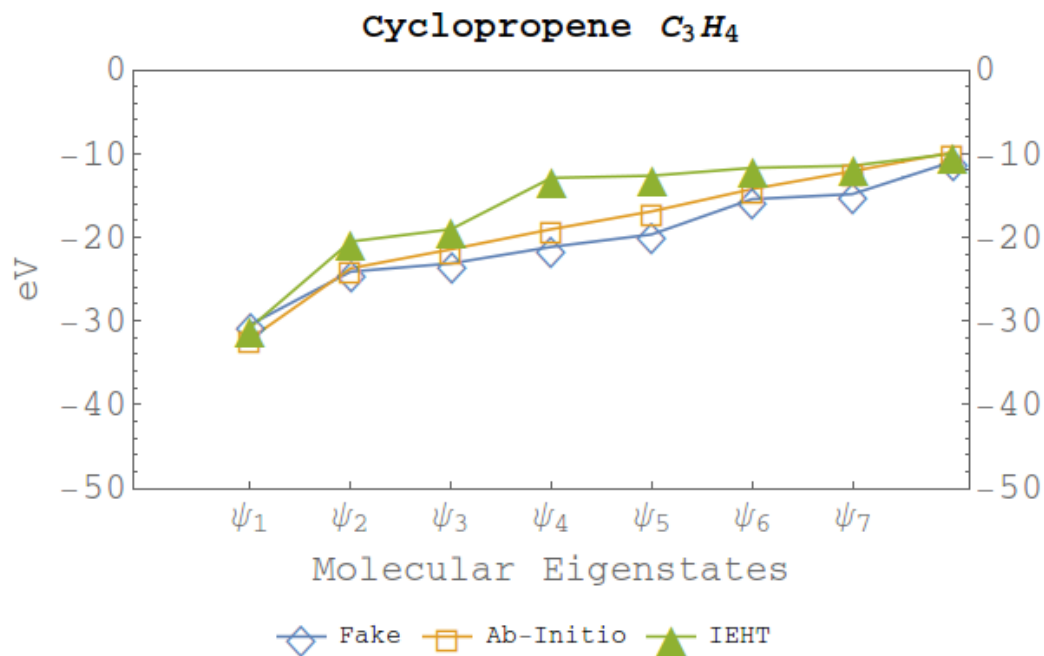


Figure 1.2: Occupied-orbital energies, ψ_n indexing the energy levels in ascending order for cyclopropene.

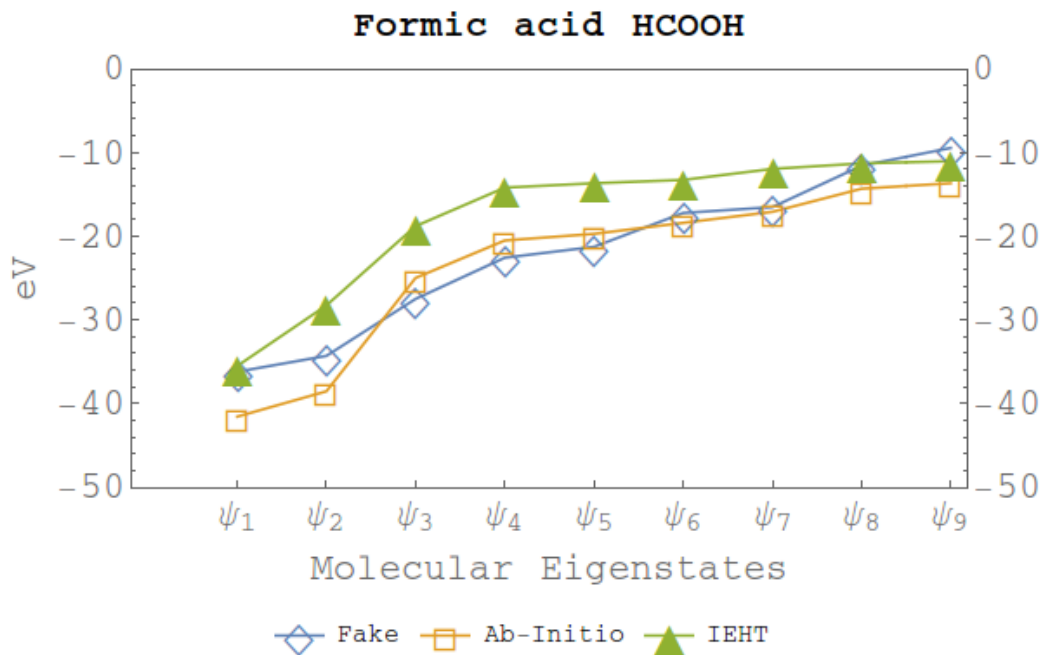


Figure 1.3: Occupied-orbital energies, ψ_n indexing the energy levels in ascending order for formic acid.

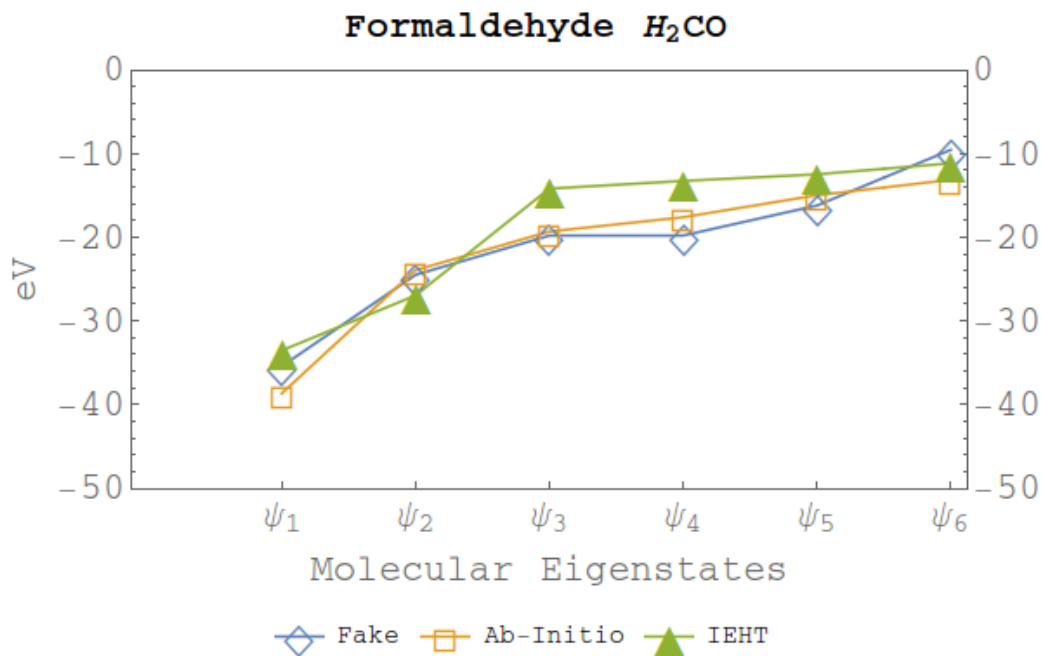


Figure 1.4: Occupied-orbital energies, ψ_n indexing the energy levels in ascending order for formaldehyde.

	α^0	α'	α''	ζ	ζ_{at}
H 1s	10.0	14.0	0.0	1.4	1.0
C 2s	19.0	10.6	1.6	2.2	1.57
2p	5.0	11.3	1.6	2.2	1.46
N 2s	25	12	2.1	2.7	1.88
2p	11.0	13.8	0.9	2.7	1.77
O 2s	33.0	13.4	1.7	3.2	2.19
2p	15.0	16.3	2.6	3.2	2.03
F 2s	41.0	15.2	1.7	3.7	2.5
2p	20.0	17.2	2.2	3.7	2.32

Table 1.1: FAKE orbital parameters. Harris and his group optimized ζ and α^0 using 37 sets of molecules containing H, C, N, O and F . ζ_{at} are single-STO values to find $\langle \vec{r} \rangle$ from ab-initio calculations. α' and α'' are from Moore's atomic data. Units for α are eV and for ζ is Bohr⁻¹.

1.3.4 Results and Discussion

I studied some molecules that contained H , C and O like ethylene, cyclopropene, formic acid and formaldehyde using the parameters from Table(1.1) and the results are shown in Fig(1.1), Fig(1.2), Fig(1.3) and Fig(1.4). The results were compared with iterative extended Hückel theory calculations by Harris et. al^{12,19} and the ab-initio calculations by Snyder and Basch²⁴. The results for energy eigenvalues among the three sets of calculations agreed satisfactorily to some level. The detailed studies are too expensive computationally compared to the calculation described here. The FAKE method would be a suitable approach to use in the qualitative study of large molecules and crystals.

CHAPTER II

STO AND GTO

2.1 Slater-type orbitals

As mentioned previously, most integrals are done semi-analytically. Here I give some details.

I express the usual Slater-type atomic orbitals (STO) in terms of three Gaussian-type orbitals (GTO). At large distances, the atomic electron density normally decreases exponentially with distance r from the nucleus. The s orbital electron density has a cusp at the nucleus with a non-zero derivative. The STO's satisfy both of these requirements as basis functions and have the form

$$\psi(r, \theta, \Phi) = N_n r^{n-1} e^{-\zeta r} Y_l^m(\theta, \Phi) \quad (2.1)$$

appropriate for solutions to the atomic eigenvalue equation where N is the normalization constant, n is the principal quantum number of the orbital, ζ is the orbital exponent and $Y_l^m(\theta, \phi)$ is the angular part of the orbital. The STO's don't have radial nodes unlike the $2s$ orbital of the hydrogen-like orbitals. They are not actual atomic eigenfunctions but are basis functions, and they are not orthogonal radially. One can define the Slater exponent ζ and radial wavefunction $R(r)$ by

$$\zeta = \frac{Z - \sigma}{n}, \quad R_n(r) = N r^{n-1} e^{-\zeta r}, \quad (2.2)$$

with Z being the atomic number and σ a screening constant. Such radial wavefunctions are normalized as

$$\int_0^{\infty} R_n^2(r) r^2 dr = 1. \quad (2.3)$$

The atomic orbitals for many-electron atoms are usually approximated by linear combinations of several STO's and the ζ 's are evaluated by means of self-consistent field methods.

2.2 STO to GTO expansion method

Let us take the Gaussian type orbitals, GTO's to be defined as

$$\phi_{nlm}(\zeta, r) = N_n(\xi) r^{n-1} e^{-\zeta r^2} Y_l^m(\theta, \Phi), \quad (2.4)$$

N being the normalizing factor. If $\psi_{nlm}(\zeta, r)$ is the STO expanded in terms of k of these GTOs, namely

$$\psi_{nlm}(\xi, r) = \sum_{i=1}^k C_i \phi_{nlm}(\xi_i, r). \quad (2.5)$$

The orbitals on both sides of the above equation should have the same angular dependence i.e. one can only include n with the same l and m . The STO-3G fits to a Slater function shown in Fig(2.1), Fig(2.2), Fig(2.3), Fig(2.4) are for a Slater exponent of $\zeta = 1$. For calculation purposes, the Slater functions have different orbital exponents. The orbital exponents are scaled with a function of r . Doing so they expand or contract the function but still do not change the functional form¹. The scale factor multiply r as

$$e^{-r} = \sum_i C_i e^{-\alpha_i r^2}, \quad (2.6)$$

and if

$$\alpha_i \rightarrow \zeta^2 \alpha_i \quad (2.7)$$

then

$$e^{-\zeta r} = \sum_i C_i e^{-\alpha_i \zeta r^2}. \quad (2.8)$$

Thus, the appropriate exponent parameter α_i for a particular expansion becomes independent of the value of ζ but the expansion coefficient C_i 's are adjusted as they depend on the normalization N . Therefore,

$$\psi_{nlm}(\zeta, r, \theta, \Phi) = \sum_{i=1}^k C_i N_n(\zeta, \alpha) r^{n-1} e^{-\zeta \alpha_i r^2} Y_l^m(\theta, \Phi). \quad (2.9)$$

We expand all s -type orbitals in terms of Gaussian $1s$ -orbitals ($n = 1$), the p -type orbitals are expanded in terms of $2p$ -GTO ($n = 2$) and d types STO also in terms of $3d$ -GTO ($n = 3$) which can be written explicitly as

$$\begin{aligned} \psi_{1s}(\zeta, r) &= \sum_{i=1}^k C_i^{1s} \phi_{1s}(\zeta, \alpha_i^{1s}, r), \\ \psi_{2s}(\zeta, r) &= \sum_{i=1}^k C_i^{2s} \phi_{1s}(\zeta, \alpha_i^{2s}, r), \\ \text{and } \psi_{2p}(\zeta, r) &= \sum_{i=1}^k C_i^{2p} \phi_{2p}(\zeta, \alpha_i^{2p}, r). \end{aligned} \quad (2.10)$$

where

$$\phi_{1s}(\zeta, \alpha_i, r) = N(\zeta, \alpha_i) e^{-(\zeta \alpha_i r^2)} \quad (2.11)$$

and

$$\phi_{2p_{z,x,y}}(\zeta, \alpha_i, r) = N(\zeta, \alpha_i) r e^{-(\zeta \alpha_i r^2)} \begin{cases} \cos \theta \\ \cos \theta \sin \Phi \\ \sin \theta \sin \Phi \end{cases} \quad (2.12)$$

where Φ is the azimuthal angle. The optimum values of C_i and α_i were obtained by using the method of **Least Square Fit** by fitting the Gaussian expansion to the

STO's, based on minimization of the integral given

$$\epsilon = \int \left[\psi_{nlm}(\zeta, r) - \sum_i^k C_i \phi_{nlm}(\zeta \alpha_i, r) \right]^2 d^3x. \quad (2.13)$$

2.3 Results

	C_1	C_2	C_3	α_1	α_2	α_3
1s	1.55208	0.217994	0.112008	4.49978	0.681191	0.151363
2s	-0.0330378	-0.09068329	0.134448	39.9677	4.49938	0.107989
2p(x, y, z)	0.190622	0.162201	0.0456471	1.34829	0.31932	0.098736
3d(xy, yz, zx)	0.180002	0.0620761	0.00593466	0.517115	0.141978	0.0592772
3d(x ² - y ²)	0.180002	0.0620761	0.00593466	0.517115	0.141978	0.0592772
3d(3z ² - r ²)	0.145625	0.0502206	0.00480124	0.517115	0.141978	0.0592772
	-0.0651253	-0.0224593	-0.00214718			

Table 2.1: Coefficients and exponent parameters for Gaussian expansion of Slater orbitals using Least Square Fit for $\zeta = 1$.

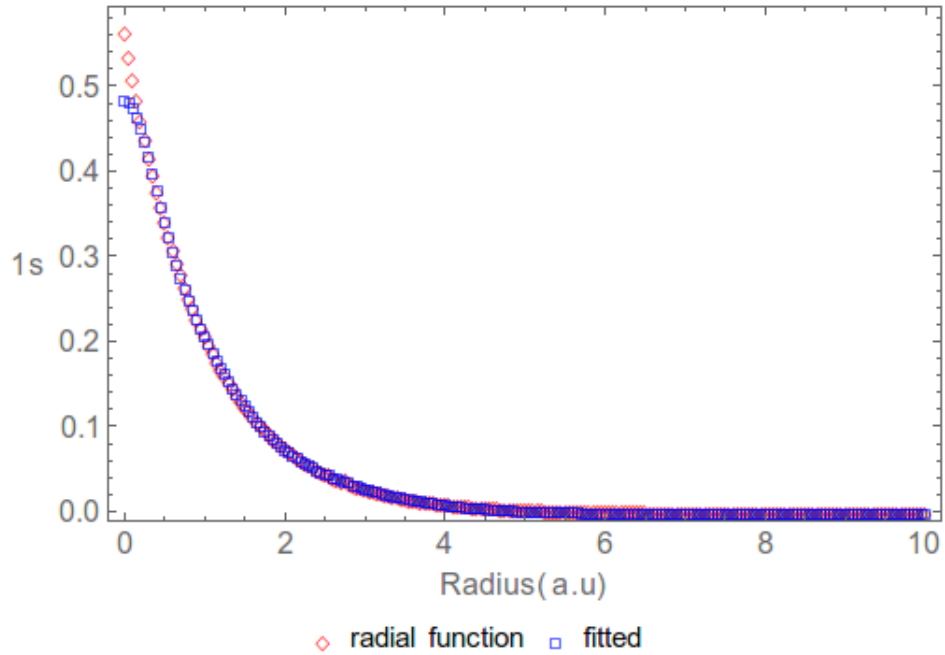


Figure 2.1: STO 1s, $\sqrt{\frac{1}{\pi}} \zeta^{\frac{3}{2}} \exp(-\zeta r)$ into GTO-3G, $\zeta = 1$, STO(Red), GTO(Blue).

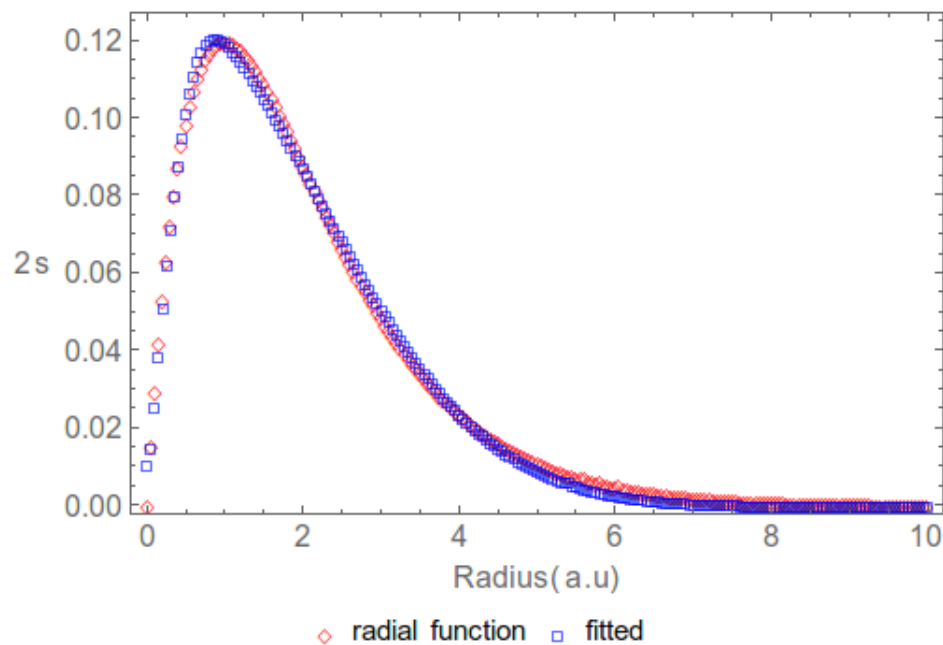


Figure 2.2: STO $2s$, $\sqrt{\frac{1}{3\pi}} \zeta^{\frac{5}{2}} r \exp(-\zeta r)$ into GTO-3G, $\zeta = 1$, STO(Red), GTO(Blue).

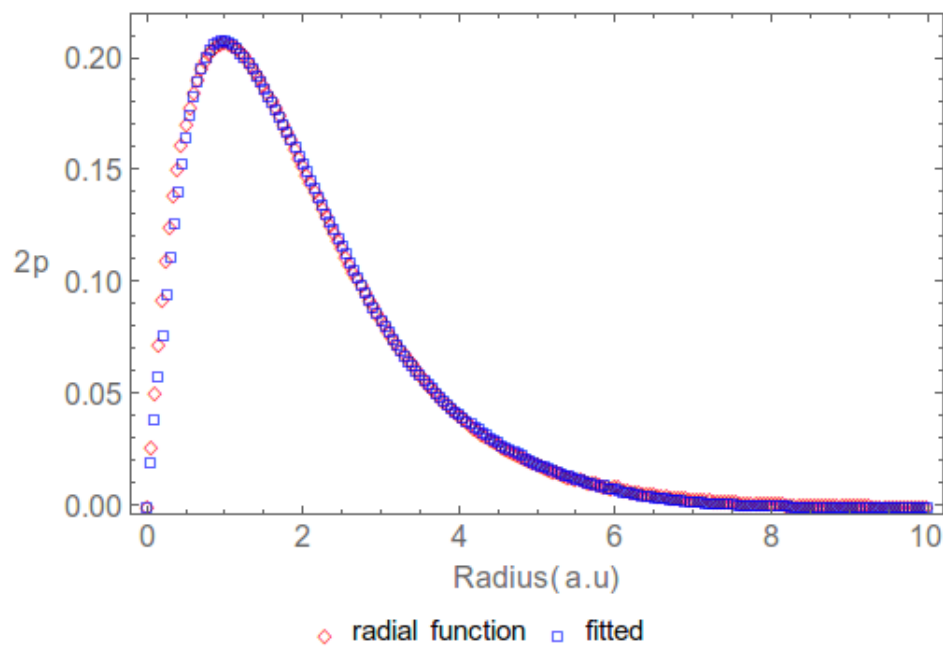


Figure 2.3: STO $2p$, $\sqrt{\frac{1}{\pi}} \zeta^{\frac{5}{2}} r \exp(-\zeta r)$ into GTO-3G, $\zeta = 1$, STO(Red), GTO(Blue).

Each STO basis function is expanded in terms of three contracted Gaussian basis functions. The scaling procedure is general and the parameters α and ζ are

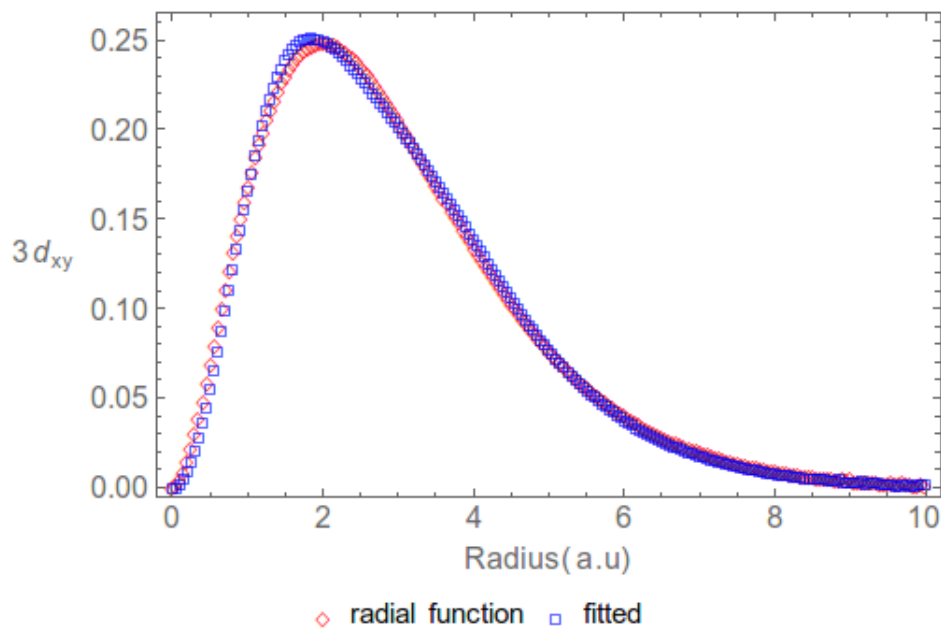


Figure 2.4: STO $3d_{xy}$, $\sqrt{\frac{2}{3\pi}} \zeta^{\frac{7}{2}} r^2 \exp(-\zeta r)$ into GTO-3G, $\zeta = 1$, STO(Red), GTO(Blue).

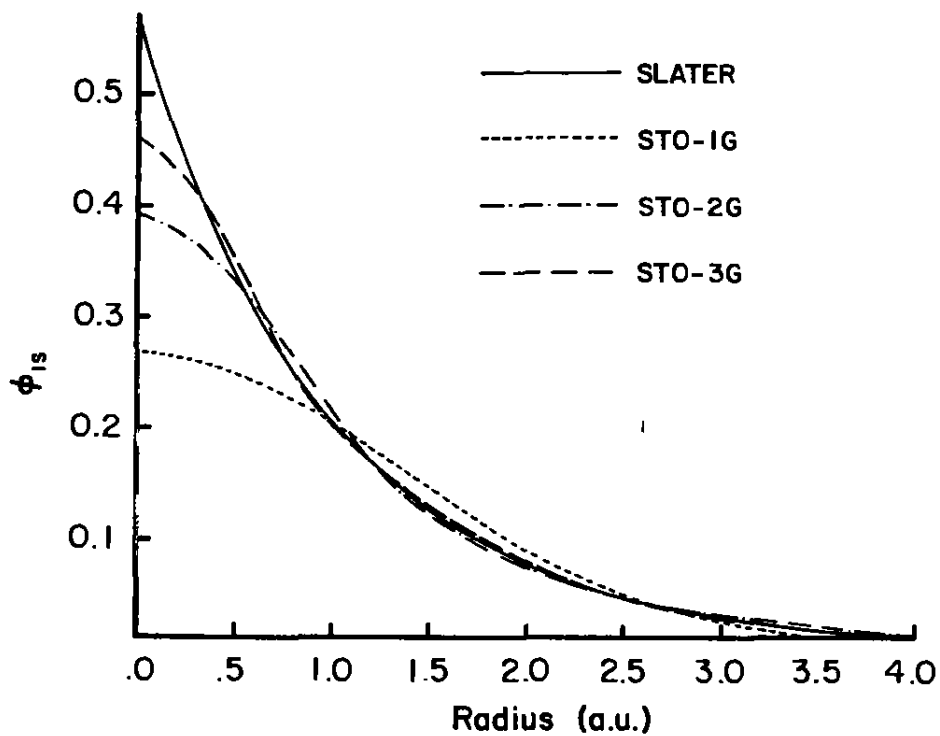


Figure 2.5: Comparison of the least-squares fit of a 1s Slater atomic orbital to a contracted gaussian 1-G, 2-G and 3-G for $\zeta = 1$ by Szabo¹.

only to be determined once for each basis function. In our case, they were acquired from Table(1.1) and Table(2.1). Those values are standard for functions centered on corresponding atoms. Thus, the new 3-GTOs were used as basis functions for our calculations.

2.4 Generating Functions

2.4.1 Overlap integrals

The most basic integrals involve the underlying Gaussian basis set. Let,

$$g_l(\vec{r} - \vec{a}) = (x - a_1)^{l_1}(y - a_2)^{l_2}(z - a_3)^{l_3} \exp(-\alpha|\vec{r} - \vec{a}|^2) \quad (2.14)$$

and

$$g_m(\vec{r} - \vec{b}) = (x - b_1)^{m_1}(y - b_2)^{m_2}(z - b_3)^{m_3} \exp(-\alpha|\vec{r} - \vec{b}|^2), \quad (2.15)$$

where, l_1, l_2, l_3 and m_1, m_2, m_3 denote the orbital quantum numbers and $a_1, a_2, a_3, b_1, b_2, b_3$ denote the position of the orbitals. In shifted variables, this become a linear combination of functions as in Eq(2.4). The overlap matrix element between these two gaussian orbitals is given by,

$$\begin{aligned} s_{lm} &= \langle g_l | g_m \rangle = \langle g_l(\vec{r} - \vec{a}) | g_m(\vec{r} - \vec{b}) \rangle \quad (2.16) \\ &= \int_{x=-\infty}^{\infty} \int_{y=-\infty}^{\infty} \int_{z=-\infty}^{\infty} (x - a_1)^{l_1}(y - a_2)^{l_2}(z - a_3)^{l_3} e^{-\alpha((x-a_1)^2+(y-a_2)^2+(z-a_3)^2)} \\ &\quad (x - b_1)^{m_1}(y - b_2)^{m_2}(z - b_3)^{m_3} e^{-\beta((x-b_1)^2+(y-b_2)^2+(z-b_3)^2)} dx dy dz \quad (2.17) \end{aligned}$$

$$\begin{aligned}
&= \int_{x=-\infty}^{\infty} (x - a_1)^{l_1} e^{-\alpha(x-a_1)^2} (x - b_1)^{m_1} e^{-\beta(x-b_1)^2} dx \\
&\quad \int_{y=-\infty}^{\infty} (y - a_2)^{l_2} e^{-\alpha(y-a_2)^2} (y - b_2)^{m_2} e^{-\beta(y-b_2)^2} dy \\
&\quad \int_{z=-\infty}^{\infty} (z - a_3)^{l_3} e^{-\alpha(z-a_3)^2} (z - b_3)^{m_3} e^{-\beta(z-b_3)^2} dz.
\end{aligned}$$

I introduce s_1 and t_1 as generating sum parameters to form a generating function for each factor of the above integral such that,

$$\begin{aligned}
&\int_{x=-\infty}^{\infty} e^{(s_1(x-a_1))} e^{-\alpha(x-a_1)^2} e^{(t_1(x-b_1))} e^{-\beta(x-b_1)^2} dx \\
&= \int_{x=-\infty}^{\infty} \sum_{l_1} \left(\frac{s_1^{l_1}}{l_1!} \right) (x - a_1)^{l_1} e^{-\alpha(x-a_1)^2} \sum_{m_1} \left(\frac{t_1^{m_1}}{m_1!} \right) (x - b_1)^{m_1} e^{-\beta(x-b_1)^2} dx.
\end{aligned} \tag{2.18}$$

In this way, the full generating integral in $3D$ becomes a product, of three factors:

$$\begin{aligned}
&\int_{x=-\infty}^{\infty} e^{(s_1(x-a_1))} e^{-\alpha(x-a_1)^2} e^{(t_1(x-b_1))} e^{-\beta(x-b_1)^2} dx \\
&\quad \int_{y=-\infty}^{\infty} e^{(s_2(y-a_2))} e^{-\alpha(y-a_2)^2} e^{(t_2(y-b_2))} e^{-\beta(y-b_2)^2} dy \\
&\quad \int_{z=-\infty}^{\infty} e^{(s_3(z-a_3))} e^{-\alpha(z-a_3)^2} e^{(t_3(z-b_3))} e^{-\beta(z-b_3)^2} dz
\end{aligned}$$

After doing the integral one has,

$$\begin{aligned}
I_s &= \frac{\pi^{3/2}}{(\alpha + \beta)^{3/2}} \exp \left(\frac{s_1^2 + t_1^2 + 4(a_1 - b_1)t_1\alpha - 4(a_1 - b_1)^2\alpha\beta + 2s_1(t_1 + 2\beta(b_1 - a_1))}{4(\alpha + \beta)} \right) \\
&\exp \left(\frac{s_2^2 + t_2^2 + 4(a_2 - b_2)t_2\alpha - 4(a_2 - b_2)^2\alpha\beta + 2s_2(t_2 + 2\beta(b_2 - a_2))}{4(\alpha + \beta)} \right) \\
&\exp \left(\frac{s_3^2 + t_3^2 + 4(a_3 - b_3)t_3\alpha - 4(a_3 - b_3)^2\alpha\beta + 2s_3(t_3 + 2\beta(b_3 - a_3))}{4(\alpha + \beta)} \right). \\
&= \frac{\pi^{3/2}}{(\alpha + \beta)^{3/2}} \exp \left(|\vec{t} + \vec{s}|^2 + 4(\alpha\vec{t} - \beta\vec{s}) \cdot (\vec{a} - \vec{b}) - 4\alpha\beta|\vec{a} - \vec{b}|^2 \right)
\end{aligned} \tag{2.19}$$

The coefficient of the n th order term in a power series expansion of the integral I_s gives the desirable powers of x , y and z . For example, the overlap between a $1s$ and a $2p_x$ orbital is given as:

$$\langle \psi_{1s} | \psi_{2p_x} \rangle = \sum_{l=1}^3 \sum_{m=1}^3 C_l^* C_m \langle g_l | g_m \rangle \tag{2.20}$$

where $\langle g_l | g_m \rangle$ is expressed in terms of the generating functions I_s .

2.4.2 Kinetic Energy integrals

Other important basic integrals involve the calculation of the kinetic energy integral underlying Gaussian basis set. The kinetic energy matrix element between two Gaussian type orbitals is given by,

$$\left\langle g_l(\vec{r} - \vec{a}) \mid \hat{K} \mid g_m(\vec{r} - \vec{b}) \right\rangle = \left(\frac{-\hbar^2}{2m^*} \right) \left\langle g_l(\vec{r} - \vec{a}) \mid \nabla^2 g_m(\vec{r} - \vec{b}) \right\rangle \tag{2.21}$$

$$\begin{aligned}
&= \left(\frac{-\hbar^2}{2m^*} \right) \int_{x=-\infty}^{\infty} \int_{y=-\infty}^{\infty} \int_{z=-\infty}^{\infty} (x-a_1)^{l_1} (y-a_2)^{l_2} (z-a_3)^{l_3} e^{-\alpha((x-a_1)^2+(y-a_2)^2+(-a_3)^2)} \\
&\quad \left(\frac{d^2}{dx^2} + \frac{d^2}{dy^2} + \frac{d^2}{dz^2} \right) (x-b_1)^{m_1} (y-b_2)^{m_2} (z-b_3)^{m_3} \\
&\quad e^{-\beta((x-b_1)^2+(y-b_2)^2+(z-b_3)^2)} dx dy dz.
\end{aligned}$$

Again I introduce the generating function parameter sets \vec{s} and \vec{t} as was done for the overlap integral, and form generating function, $I_k(\vec{s}, \vec{a}, \alpha; \vec{t}, \vec{b}, \beta)$.

$$\begin{aligned}
I_k &= \int_{x,y,z=-\infty}^{\infty} \sum_{l_1,l_2,l_3} \left(\frac{s_1^{l_1}}{l_1!} \right) \left(\frac{s_2^{l_2}}{l_2!} \right) \left(\frac{s_3^{l_3}}{l_3!} \right) (x-a_1)^{l_1} (y-a_2)^{l_2} (z-a_3)^{l_3} \\
&\quad e^{-\alpha((x-a_1)^2+(y-a_2)^2+(-a_3)^2)} \\
&\quad \left(\nabla^2 \sum_{m_1,m_2,m_3} \left(\frac{t_1^{m_1}}{m_1!} \right) \left(\frac{t_2^{m_2}}{m_2!} \right) \left(\frac{t_3^{m_3}}{m_3!} \right) (x-b_1)^{m_1} (y-b_2)^{m_2} (z-b_3)^{m_3} \right. \\
&\quad \left. e^{-\beta((x-b_1)^2+(y-b_2)^2+(z-b_3)^2)} \right) dx dy dz \\
&= \int_{x,y,z=-\infty}^{\infty} e^{s_1(x-a_1)} e^{s_2(y-a_2)} e^{s_3(z-a_3)} e^{-\alpha((x-a_1)^2+(y-a_2)^2+(-a_3)^2)} \\
&\quad \left(\frac{\partial^2}{\partial x^2} + \frac{\partial^2}{\partial y^2} + \frac{\partial^2}{\partial z^2} \right) e^{t_1(x-b_1)} e^{t_2(y-b_2)} e^{t_3(z-b_3)} e^{-\beta((x-b_1)^2+(y-b_2)^2+(z-b_3)^2)} dx dy dz
\end{aligned} \tag{2.22}$$

In this way the full kinetic energy generating integral in 3D becomes,

$$\begin{aligned}
I_k &= \int e^{s_1(x-a_1)} e^{-\alpha(x-a_1)^2} \frac{d^2}{dx^2} e^{t_1(x-b_1)} e^{-\beta(x-b_1)^2} dx \times \\
&\int e^{s_2(y-a_2)} e^{-\alpha(y-a_2)^2} e^{t_2(y-b_2)} e^{-\beta(y-b_2)^2} dy \times \\
&\int e^{s_3(z-a_3)} e^{-\alpha(z-a_3)^2} e^{t_3(z-b_3)} e^{-\beta(z-b_3)^2} dz + \int e^{s_1(x-a_1)} e^{-\alpha(x-a_1)^2} e^{t_1(x-b_1)} e^{-\beta(x-b_1)^2} dx \times \\
&\int e^{s_2(y-a_2)} e^{-\alpha(y-a_2)^2} \frac{d^2}{dy^2} e^{t_2(y-b_2)} e^{-\beta(y-b_2)^2} dy \times \int e^{s_3(z-a_3)} e^{-\alpha(z-a_3)^2} e^{t_3(z-b_3)} e^{-\beta(z-b_3)^2} dz \\
&+ \int e^{s_1(x-a_1)} e^{-\alpha(x-a_1)^2} e^{t_1(x-b_1)} e^{-\beta(x-b_1)^2} dx \times \int e^{s_2(y-a_2)} e^{-\alpha(y-a_2)^2} e^{t_2(y-b_2)} e^{-\beta(y-b_2)^2} dy \times \\
&\int e^{s_3(z-a_3)} e^{-\alpha(z-a_3)^2} \frac{d^2}{dz^2} e^{t_3(z-b_3)} e^{-\beta(z-b_3)^2} dz \\
&= \sqrt{\frac{\pi^3}{(\alpha + \beta)^7}} \exp \left(\frac{|\vec{s} + \vec{t}|^2 + 4(\vec{a} - \vec{b}) \cdot (\alpha \vec{t} - \beta \vec{s}) - 4\alpha\beta|\vec{a} - \vec{b}|^2}{(\alpha + \beta)} \right) \\
&\left(|\alpha \vec{t} - \beta \vec{s}|^2 + 4\alpha\beta(\vec{a} - \vec{b}) \cdot (\alpha \vec{t} + \beta \vec{s}) + 4\alpha^2\beta^2|\vec{a} - \vec{b}|^2 - 6\alpha\beta(\alpha + \beta) \right)
\end{aligned}$$

The integration simplifies due to the way the Gaussians factor out. The coefficients of the power series expansion of the integrals $I_k(\vec{s}, \vec{a}, \alpha; \vec{t}, \vec{b}, \beta)$ give the desirable Gaussian kinetic energy integrals. So for any Hermitian operator \hat{A} ,

$$\begin{aligned}
&\left\langle g_l(\vec{r} - \vec{a}) \mid \hat{A} \mid g_m(\vec{r} - \vec{b}) \right\rangle \\
&= \int (x - a_1)^{l_1} (y - a_2)^{l_2} (z - a_3)^{l_3} e^{\alpha|\vec{r} - \vec{a}|^2} \\
&\quad \hat{A} (x - b_1)^{m_1} (y - b_2)^{m_2} (z - b_3)^{m_3} e^{\alpha|\vec{r} - \vec{b}|^2} d^3x \\
&= \left(\frac{\partial}{\partial s_1} \right)^{l_1} \left(\frac{\partial}{\partial s_2} \right)^{l_2} \left(\frac{\partial}{\partial s_3} \right)^{l_3} \left(\frac{\partial}{\partial t_1} \right)^{m_1} \left(\frac{\partial}{\partial t_2} \right)^{m_2} \\
&\quad \left(\frac{\partial}{\partial t_3} \right)^{m_3} I_{\hat{A}}(\vec{s}, \vec{a}, \alpha; \vec{t}, \vec{b}, \beta) \Big|_{\{\vec{s}=\vec{0}, \vec{t}=\vec{0}\}}
\end{aligned} \tag{2.23}$$

where $I_{\hat{A}}(\vec{s}, \vec{a}, \alpha; \vec{t}, \vec{b}, \beta)$ is the generating function for any operator \hat{A} which can be found using the method described above.

CHAPTER III

TIGHT BINDING METHOD

3.1 Introduction

In a pseudo-potential method, the electrons are assumed to be nearly free so plane waves are used to approximate their wavefunctions. Such a Fourier basis is often used in density functional theory as well. However, to reduce the basis and to concentrate on lower valence bands, the electrons are assumed to be tightly bound to their nuclei as in the atoms. As atoms are brought together until their separations become comparable to the lattice constant of the solid, overlap and spreading of their wavefunctions is expected. The electronic wavefunctions in this case can be approximated reasonably well by a linear combination of atomic wavefunctions. This approximation is the Tight-Binding Method (TBM) or Linear Combination of Atomic Orbitals(LCAO) method. The atomic wavefunctions die out at infinity but have overlap, with a few neighboring atoms.

In non-metallic solids or semi-metals the electrons are expected to be influenced more strongly by the ionic ones. Especially for the valence and low-lying conduction bands and states related to them, a localized description is expected to be relatively more appropriate. The tight-binding model can be the best model if the atomic shell radius is much smaller than a lattice constant. The model is not as applicable to simple metals where electrons are free or nearly-free. For larger atoms, then d -like and f -like orbitals become important. However, one can often use the TB method to study covalent semiconductors and other solids. This section follows closely the

description by Warren Pickett (2006).

The electron's potential $V(\vec{r})$ in a crystal can be approximated as a sum of atomic potentials:

$$V_{crystal}(\vec{r}) = \sum_m V_{atomic}(\vec{r} - \vec{R}_m) \quad (3.1)$$

where m runs over all the lattice vectors and this potential is periodic. To see this, consider

$$\begin{aligned} V_{crystal}(\vec{r} + \vec{R}_n) &= \sum_m V_{atomic}(\vec{r} - \vec{R}_m + \vec{R}_n) \\ &= \sum_m V_{atomic}(\vec{r} - (\vec{R}_m - \vec{R}_n)), \quad \vec{R}'_m = \vec{R}_m - \vec{R}_n \\ &= \sum_{m'} V_{atomic}(\vec{r} - \vec{R}'_m) = V_{crystal}(\vec{r}). \end{aligned} \quad (3.2)$$

Hence the potential is periodic as expected. The electron's atomic-like wavefunction is influenced by the other atoms in the crystal so a slight modification to an atomic wavefunction should be expected. Due to the presence of other atoms, a proper Bloch symmetrized basis function with a translation quantum number $\vec{k} = k_x\hat{x} + k_y\hat{y} + k_z\hat{z}$ can be constructed such that,

$$\langle \vec{r} | \chi_{\mu,i}(\vec{k}) \rangle = \frac{1}{\sqrt{N}} \sum_{m=1}^N e^{i\vec{k}\cdot\vec{R}_m} \phi_{\mu}(\vec{r} - \vec{\rho}_i - \vec{R}_m), \quad (3.3)$$

with the summation running over all the N unit cells in the crystal with positions given by the vectors \vec{R}_m and the $\vec{\rho}_i$ give the position of electron relative to the atomic wavefunction ϕ_{μ} , which is one of the atomic states associated with each atom. The index μ takes the values of the minimal set of basis states ϕ_{μ} ($\mu = 2s, 2p_x, 2p_y, 2p_z, \dots$) of atomic orbitals. The atomic basis function has significant amplitude in the neighborhood of the atomic site but decays rapidly away from it. It becomes almost negligible by the time it reaches the corresponding site in neighboring cell. The overlap between the neighboring atomic orbitals is significantly less. This is a basic assumption of the

Tight-Binding model (TB). The factor \sqrt{N} is used to normalize the Bloch's function $|\chi_{\mu,i}(\vec{k})\rangle$ and the atomic wavefunctions $\phi_{\mu}(\vec{r})$ are normalized too, although due to the overlap of atomic wavefunctions they are not orthogonal. The Bloch basis states can be used as a suitable basis for expansion of the crystal wavefunctions since they satisfy Bloch's theorem²⁵. Thus,

$$\begin{aligned}
\langle \vec{r} | \chi_{\mu,i}(\vec{k}) \rangle &= \chi_{\mu,i,\vec{k}}(\vec{r}) = \frac{1}{\sqrt{N}} \sum_{m=1}^N e^{i\vec{k}\cdot\vec{R}_m} \phi_{\mu}(\vec{r} - \vec{\rho}_i - \vec{R}_m) \\
\therefore \chi_{\mu,i,\vec{k}}(\vec{r} + \vec{R}_n) &= \frac{1}{\sqrt{N}} \sum_{m=1}^N e^{i\vec{k}\cdot(\vec{R}_m - \vec{R}_n)} e^{i\vec{k}\cdot\vec{R}_n} \phi_{\mu}(\vec{r} - \vec{\rho}_i - \vec{R}_m + \vec{R}_n) \\
&= \frac{1}{\sqrt{N}} \sum_{m=1}^N e^{i\vec{k}\cdot(\vec{R}_m - \vec{R}_n)} e^{i\vec{k}\cdot\vec{R}_n} \phi_{\mu}(\vec{r} - \vec{\rho}_i - (\vec{R}_m - \vec{R}_n)) \\
&= e^{i\vec{k}\cdot\vec{R}_n} \frac{1}{\sqrt{N}} \sum_{m'=1}^N e^{i\vec{k}\cdot\vec{R}_{m'}} \phi_{\mu}(\vec{r} - \vec{\rho}_i - \vec{R}'_m) \\
&= e^{i\vec{k}\cdot\vec{R}_n} \chi_{\mu,i,\vec{k}}(\vec{r}).
\end{aligned} \tag{3.4}$$

The Bloch basis state can also be written as,

$$\langle \vec{r} | \chi_{\mu,i}(\vec{k}) \rangle = \frac{1}{\sqrt{N}} e^{i\vec{k}\cdot\vec{R}_n} \sum_{m=1}^N e^{i\vec{k}\cdot(\vec{R}_m - \vec{R}_n)} \phi_{\mu}(\vec{r} - \vec{\rho}_i - \vec{R}_m). \tag{3.5}$$

The phase factor inside the summation $e^{i\vec{k}\cdot(\vec{R}_m - \vec{R}_n)}$ is periodic with the periodicity of the lattice. The basis function $|\chi_{\mu,i}(\vec{k})\rangle$ is a Bloch form that represents a propagating electron wave. Near the center of the $(m, i)^{th}$ atom,

$$\langle \vec{r} | \chi_{\mu,i}(\vec{k}) \rangle \simeq e^{i\vec{k}\cdot\vec{R}_n} \phi_{\mu}(\vec{r} - \vec{\rho}_i - \vec{R}_m) \sim \phi_{\mu}(\vec{r} - \vec{\rho}_i - \vec{R}_m), \tag{3.6}$$

which means the Bloch symmetrized functions are proportional near the atoms to the atomic orbitals. The crystal orbitals behave like atomic orbitals in the neighborhood of each atom. Since $|\chi_{\mu,i}(\vec{k})\rangle$ satisfies both the mathematical requirement of the Bloch's theorem and basic assumption of the TB model, it is a suitable basis to

calculate energies of the bands in a solid crystal. Thus, one assumes that a crystal single-particle eigenstate can be expanded in this basis as

$$|\psi_{(n)}(\vec{k})\rangle = \sum_{\mu,i} C_{(n,\vec{k})\mu,i} |\chi_{\mu,i}(\vec{k})\rangle. \quad (3.7)$$

3.1.1 Hamiltonian matrix element

If $\psi_{(n)}(\vec{k}, \vec{r})$ is a solution to an effective single-particle Schrodinger's equation with Hamiltonian \hat{H} , then

$$\begin{aligned} \hat{H} \psi_{(n)}(\vec{k}, \vec{r}) &= \epsilon(\vec{k}) \psi_{(n)}(\vec{k}, \vec{r}) \\ \hat{H} \sum_{\mu,i} C_{(n,\vec{k})\mu,i} |\chi_{\mu,i}(\vec{k})\rangle &= \epsilon(\vec{k}) \sum_{\mu,i} C_{(n,\vec{k})\mu,i} |\chi_{\mu,i}(\vec{k})\rangle \\ \sum_{\mu,i} \langle \chi_{\nu,j}(\vec{k}) | \hat{H} | \chi_{\mu,i}(\vec{k}) \rangle C_{(n,\vec{k})\mu,i} &= \epsilon(\vec{k}) \sum_{\mu,i} \langle \chi_{\nu,j}(\vec{k}) | \chi_{\mu,i}(\vec{k}) \rangle C_{(n,\vec{k})\mu,i} \\ \sum_{\mu,i} \left[\langle \chi_{\nu,j}(\vec{k}) | \hat{H} | \chi_{\mu,i}(\vec{k}) \rangle - \epsilon(\vec{k}) \langle \chi_{\nu,j}(\vec{k}) | \chi_{\mu,i}(\vec{k}) \rangle \right] C_{(n,\vec{k})\mu,i} &= 0. \end{aligned} \quad (3.8)$$

The eigenstates have to be orthonormalized, which gives

$$\langle \psi_{(n)}(\vec{k}, \vec{r}) | \psi_{(n')}(\vec{k}', \vec{r}) \rangle \simeq \delta_{nn'} \Delta(\vec{k} - \vec{k}'). \quad (3.9)$$

$$\Delta(\vec{k} - \vec{k}') = \begin{cases} 1 & \text{if } \vec{k} - \vec{k}' \text{ belongs to the reciprocal lattice} \\ 0 & \text{otherwise.} \end{cases}$$

One only needs to consider the matrix elements of the states with the same \vec{k} index and the values of \vec{k} and \vec{k}' are restricted to the first Brioullin zone. The size of the secular equation is equal to the total number of atomic orbitals and the sum runs over the number of different types of atoms and the number of orbitals associated with each type of atom. This is exactly the number of solutions or (bands) to be expected at each \vec{k} point²⁶.

In order to find the solutions to Eq.(3.8) one needs to evaluate the integrals.

$$\langle \chi_{\nu,j}(\vec{k}) | \chi_{\mu,i}(\vec{k}) \rangle = \frac{1}{N} \sum_m \sum_n e^{i\vec{k} \cdot (\vec{R}_m - \vec{R}_n)} \langle \phi_\nu(\vec{r} - \vec{\rho}_j - \vec{R}_n) | \phi_\mu(\vec{r} - \vec{\rho}_i - \vec{R}_m) \rangle \quad (3.10)$$

Let $\vec{R}_m - \vec{R}_n = \vec{R}_l$. The translational symmetry with periodic boundary conditions permits one to write this as

$$\langle \chi_{\nu,j}(\vec{k}) | \chi_{\mu,i}(\vec{k}) \rangle = \frac{1}{N} \sum_m \sum_l e^{i\vec{k} \cdot \vec{R}_l} \langle \phi_\nu(\vec{r} - \vec{\rho}_j) | \phi_\mu(\vec{r} - \vec{\rho}_i - \vec{R}_l) \rangle \quad (3.11)$$

and doing that one has eliminated any reference to m from the summand. The sum is now independent of index m and the summation over m gives a factor of N . Finally,

$$\langle \chi_{\nu,j}(\vec{k}) | \chi_{\mu,i}(\vec{k}) \rangle = \sum_l e^{i\vec{k} \cdot \vec{R}_l} \langle \phi_\nu(\vec{r} - \vec{\rho}_j) | \phi_\mu(\vec{r} - \vec{\rho}_i - \vec{R}_l) \rangle \quad (3.12)$$

is the overlap matrix element written as,

$$S_{\nu,\mu}^{j,i}(\vec{k}) = \sum_l e^{i\vec{k} \cdot \vec{R}_l} \langle \phi_\nu(\vec{r}) | \phi_\mu(\vec{r} + \vec{\rho}_j - \vec{\rho}_i - \vec{R}_l) \rangle = \sum_l e^{i\vec{k} \cdot \vec{R}_l} S_{\nu,\mu}(\vec{\rho}_j - \vec{\rho}_i - \vec{R}_l)$$

The Hamiltonian matrix element between two Bloch-states is evaluated in a similar way.

$$\langle \chi_{\nu,j}(\vec{k}) | \hat{H} | \chi_{\mu,i}(\vec{k}) \rangle = \sum_l e^{i\vec{k} \cdot \vec{R}_l} \langle \phi_\nu(\vec{r} - \vec{\rho}_j) | \hat{H} | \phi_\mu(\vec{r} - \vec{\rho}_i - \vec{R}_l) \rangle. \quad (3.13)$$

This can be written as

$$H_{\nu,\mu}^{j,i}(\vec{k}) = \sum_l e^{i\vec{k} \cdot \vec{R}_l} \langle \phi_\nu(\vec{r}) | \phi_\mu(\vec{r} + \vec{\rho}_j - \vec{\rho}_i - \vec{R}_l) \rangle = \sum_l e^{i\vec{k} \cdot \vec{R}_l} H_{\nu,\mu}(\vec{\rho}_j - \vec{\rho}_i - \vec{R}_l). \quad (3.14)$$

The TB approximation is simplified if overlap matrix elements between the orbitals at the same atom are

$$\langle \phi_\nu(\vec{r} - \vec{\rho}_i) | \phi_\mu(\vec{r} - \vec{\rho}_i) \rangle = \delta_{\nu,\mu}. \quad (3.15)$$

Effectively any overlap between different orbitals on the same site is taken to be zero. Similarly, the hamiltonian matrix elements are non-zero if the orbitals are on the same atom which are regarded to be “on-site energies” ϵ_μ .

$$\langle \phi_\nu(\vec{r} - \vec{\rho}_i) | \hat{H} | \phi_\mu(\vec{r} - \vec{\rho}_i) \rangle = \delta_{\nu,\mu} \epsilon_\mu \quad (3.16)$$

The Hamiltonian matrix elements between orbitals on different atoms but situated on nearly sites are given by,

$$\langle \phi_\nu(\vec{r} - (\vec{R}_m + \vec{\rho}_i)) | \hat{H} | \phi_\mu(\vec{r} - (\vec{R}_n + \vec{\rho}_j)) \rangle = V_{\nu,\mu}^{i,j}. \quad (3.17)$$

The $V_{\nu,\mu}^{i,j}$ are the “hopping” matrix elements with respect to the atomic orbitals ϕ_ν and ϕ_μ centered at $\vec{\rho}_j$ and $\vec{\rho}_i$ respectively.

CHAPTER IV

GRAPHENE

4.1 Introduction

Graphene is among one of the four crystalline forms of carbon. It is a one-atom-thick allotrope of carbon with a honeycomb lattice structure that can be imagined to be benzene rings with the hydrogen atoms stripped out. It is known to have some remarkable properties depending on its 2D nature and on the peculiar features of its semi-metallic band structure. It is a single layer of graphite in which the scattering length can be as long as thousands of interatomic distances²⁷. Interest in graphene is extended by recent interest in adsorbates on the graphene, including, for instance, atomic hydrogen²⁸.

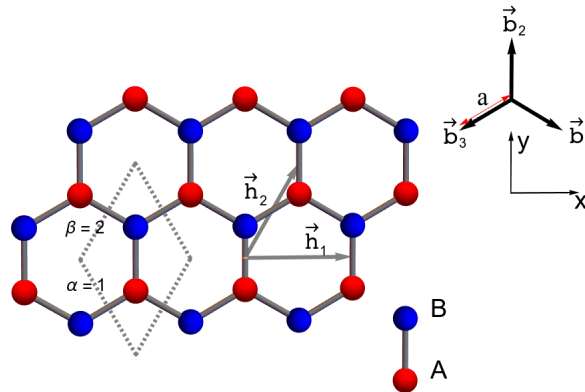


Figure 4.1: Lattice of Graphene. There are two carbon atoms per unit cell, denoted by $\alpha = 1, 2$ or **A** and **B**. These lie on interlocking triangular sublattices with Bravais lattice vectors \vec{h}_1 and \vec{h}_2 . The interatomic distance is a .

Carbon has four valence electrons. In graphene the first three electrons fill sigma

bonding orbitals that join the carbon atoms to their neighbors in the $2D$ plane. The atomic orbitals in a carbon atom are sp^2 hybridized into σ bonds with an angle of 120° in the xy plane. The electrons that take part in σ bonds don't take part in conductivity; to some level of approximation. Rather, transport involves the conduction π electron that is contributed from the atomic $2p_z$ state²⁷. The graphene lattice is made up of two equivalent carbon sublattices A and B associated with cosine-like energy bands. Those bands intersect at the Fermi energy (E_F) near the edges of a Brillouin zone forming conical band contacts and characteristic van Hove singularities in the energy spectrum.

The graphene structure can be seen as a triangular lattice with a basis of two atoms per unit cell α and β and the distance between interlocking triangular sublattices is shown in Fig(4.1). If \vec{h}_1 and \vec{h}_2 are the lattice vectors in the (\hat{x}, \hat{y}) basis, then

$$\vec{R}_{m,\alpha} = \vec{R}_m + \vec{\rho}_\alpha$$

where,

$$\vec{R}_m = m_1 \vec{h}_1 + m_2 \vec{h}_2 \quad \text{and} \quad \vec{\rho}_{1,2} = \pm \frac{1}{2} \vec{b}_2$$

and vectors \vec{b} 's are primitive translational vectors given by

$$\vec{b}_1 = \frac{\sqrt{3} a}{2} \hat{x} - \frac{a}{2} \hat{y}, \quad \vec{b}_2 = a \hat{y}, \quad \vec{b}_3 = -\frac{\sqrt{3} a}{2} \hat{x} - \frac{a}{2} \hat{y}.$$

The Bravais lattice vectors can be written as,

$$\vec{h}_1 = \vec{b}_1 - \vec{b}_3 = \sqrt{3} a \hat{x}, \quad \vec{h}_2 = \vec{b}_2 - \vec{b}_3 = \frac{\sqrt{3} a}{2} \hat{x} + \frac{3a}{2} \hat{y}.$$

The magnitude of the lattice vectors is $\sqrt{3} a = \sqrt{3} \times 1.42\text{\AA} = 2.46\text{\AA}$. For convenience,

one can set the lattice vector \vec{h}_3 arbitrarily to

$$\vec{h}_3 = a \hat{z}.$$

The reciprocal lattice vectors \vec{K} satisfy the condition

$$\vec{h}_i \cdot \vec{K}_j = 2\pi \delta_{ij}. \quad (4.1)$$

If V is a matrix with the Bravais basis vectors as columns, then

$$V = \begin{pmatrix} \vec{h}_1 & \vec{h}_2 & \vec{h}_3 \\ \downarrow & \downarrow & \downarrow \end{pmatrix} \quad \text{so that } 2\pi V^{-1} = \begin{pmatrix} \vec{K}_1 & \rightarrow \\ K_2 & \rightarrow \\ K_3 & \rightarrow \end{pmatrix},$$

therefore,

$$\vec{K}_1 = \frac{2\pi}{a} \left(\frac{1}{\sqrt{3}} \hat{x} - \frac{1}{3} \hat{y} \right) \quad \text{and} \quad \vec{K}_2 = \frac{2\pi}{a} \left(\frac{2}{3} \hat{y} \right),$$

where \vec{K}_1 and \vec{K}_2 are reciprocal lattice vectors used to set up Bloch symmetrized basis functions to construct the Brillouin zone and compute the band structure. A complete set of phase factors $e^{i\vec{k} \cdot \vec{r}}$ is represented by a set of points in \vec{k} -space that are subjected to periodic boundary conditions at the edges of the crystal lattice. It is useful to express \vec{k} in terms of the reciprocal basis vectors instead of the usual \hat{x} and \hat{y} components by

$$\vec{K}_{pq} = p\vec{K}_1 + q\vec{K}_2 \quad (4.2)$$

for any integers p and q that are both not zero as shown in Fig(4.2).

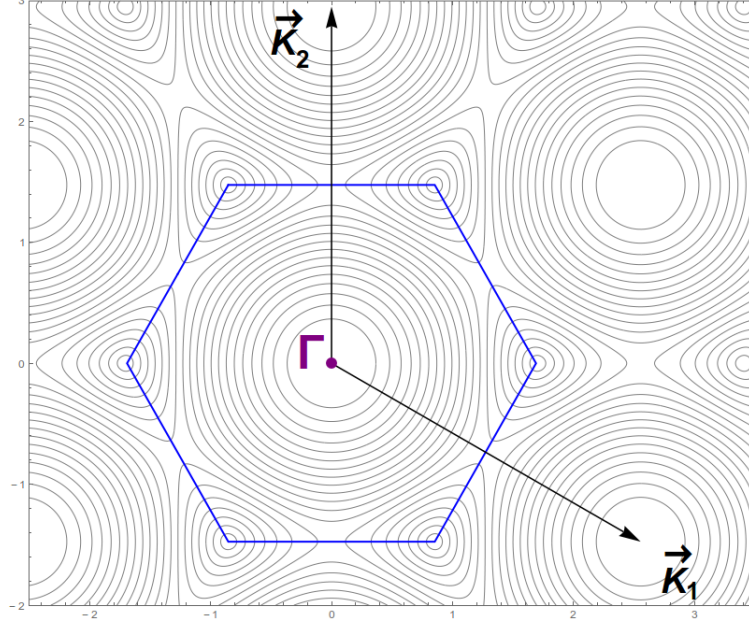


Figure 4.2: Symmetrized first Brillouin zone.

The tight-binding formalism described previously can be applied to graphene. The Bloch symmetrized basis function $|\chi_\mu^\alpha(\vec{k})\rangle$ with translation quantum number $\vec{k} = k_x \hat{x} + k_y \hat{y}$ is constructed from a valence basis set ϕ_μ ($\mu = 2s, 2p_x, 2p_y$ and $2p_z$) of Slater orbitals situated at the site α ($\alpha = 1$ or 2) in the unit cell is given by

$$\langle \vec{r} | \chi_\mu^\alpha(\vec{k}) \rangle = \frac{1}{\sqrt{N}} \sum_m e^{i\vec{k} \cdot \vec{R}_{m,\alpha}} \phi_\mu(\vec{r} - \vec{R}_{m,\alpha}), \quad (4.3)$$

where $m = 1, \dots, N$ labels the unit cells and $\vec{\rho}$ is the atom's position vector inside the unit cell. The Hamiltonian eigenstates are written as a linear combination of Bloch symmetrized basis functions for each choice of wave vector \vec{k} , with a different phase factor for each atom $\alpha = 1$ or 2 . In his study of the structure of the electronic energy bands and Brillouin zones for graphite using the tight-binding approximation, Wallace²⁹ used the same kind of representation, which is fairly standard, and can be found also for instance, in a well-known paper by Dresselhaus et al³⁰.

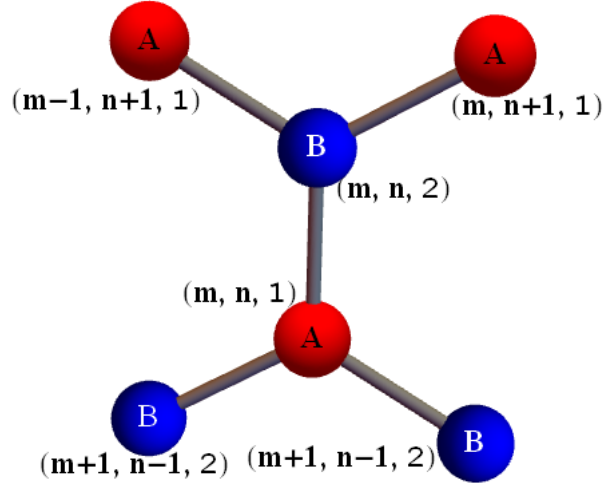


Figure 4.3: Schematic diagram of atoms in the neighborhood of (m, n) unit cell.

4.2 The π -orbital model

Before continuing with the full Hamiltonian, it is instructive to look first at only the π orbitals. In their 1970 study of a discrete variational method for the energy-band problem, Painter and Ellis³¹ found that the π bands are situated on either side of the Fermi level and they were responsible for the conduction properties. I will limit my calculation to the π bands here, too. One forms a Bloch symmetrized basis $|\chi(\vec{k}, \alpha)\rangle$ for the $\alpha = 1$ or 2 sublattices. This yields the Hamiltonian

$$\begin{aligned}
 H &= \begin{pmatrix} \langle \vec{k}, 1 | H | \vec{k}, 1 \rangle & \langle \vec{k}, 1 | H | \vec{k}, 2 \rangle \\ \langle \vec{k}, 2 | H | \vec{k}, 1 \rangle & \langle \vec{k}, 2 | H | \vec{k}, 2 \rangle \end{pmatrix} \\
 &= \begin{pmatrix} \epsilon_1 & \langle \vec{k}, 1 | H | \vec{k}, 2 \rangle \\ \langle \vec{k}, 2 | H | \vec{k}, 1 \rangle & \epsilon_2 \end{pmatrix}
 \end{aligned} \tag{4.4}$$

where ϵ_1 and ϵ_2 are the Hückel energies with scaling such that one is allowed to have two atoms that are chemically different as in boron nitride. However, graphene has equal diagonal energies. The parameter ϵ_α is equivalent to energy on the α site in a

Hückel model. The off diagonal matrix elements are calculated to be

$$\langle \vec{k}, 1 | H | \vec{k}, 2 \rangle = \beta \left(1 + \frac{1}{t} + \frac{s}{t} \right) \quad \text{and} \quad \langle \vec{k}, 2 | H | \vec{k}, 1 \rangle = \beta \left(1 + t + \frac{t}{s} \right), \quad (4.5)$$

where β takes a value of -1 if the two atoms are next to each other. The phase factors are given by,

$$s = e^{i\vec{k} \cdot \vec{h}_1} = e^{i\sqrt{3} k_x a} \quad \text{and} \quad t = e^{i\vec{k} \cdot \vec{h}_2} = e^{i \left(\frac{\sqrt{3}}{2} k_x a + \frac{3}{2} k_y a \right)}. \quad (4.6)$$

The translation symmetry reduced Hamiltonian becomes (2×2) ,

$$H(\vec{k}) = \begin{pmatrix} \epsilon_1 & -(1 + \frac{1}{t} + \frac{s}{t}) \\ -(1 + t + \frac{t}{s}) & \epsilon_2 \end{pmatrix} \quad (4.7)$$

Using Bloch symmetrized basis functions, one can reduce the problem of diagonalizing an “infinite” Hamiltonian matrix to a finite matrix (2×2) by treating the atoms of the unit cell and restricting the \vec{k} points to the first Brillouin zone. The Hamiltonian matrix obtained can be used to find the band structure for graphene, and since there are two basis states per \vec{k} value, there are two eigenfunctions (stationary states) for each wave vectors \vec{k} ,

$$H(\vec{k}) \left| \psi_{\vec{k},n} \right\rangle = E_n(\vec{k}) \left| \psi_{\vec{k},n} \right\rangle. \quad (4.8)$$

The index n is the band index and in each band the energy is a smooth function of \vec{k} , giving eigen-energies from the secular equation via

$$\begin{aligned} \det \left| H(\vec{k}) - \hat{I}E \right| &= 0 \\ \text{or } (\epsilon_1 - E)(\epsilon_2 - E) - \left(1 + t + \frac{t}{s} \right) \left(1 + \frac{1}{t} + \frac{s}{t} \right) &= 0 \end{aligned} \quad (4.9)$$

If $s = e^{i\theta_1}$ and $t = e^{i\theta_2}$, then the determinant in Eq(4.9) gives two solutions ,

$$E_{1,2} = \frac{\epsilon_1}{2} + \frac{\epsilon_2}{2} \pm \sqrt{3 + (\epsilon_1 - \epsilon_2)^2 + 2 \cos(\theta_1) + 2 \cos(\theta_1 - \theta_2) + 2 \cos(\theta_2)}. \quad (4.10)$$

The band energy is graphed as a function of \vec{k} i.e., energy versus crystal momentum, as shown in Fig(4.4). One can see that the energies are symmetrical at the Hückel level of approximation for the points $E \rightarrow -E$. This is because of the bipartite nature of the graphene lattice, i.e., partitions of $A(\alpha = 1)$ and $B(\alpha = 2)$ lattice sites. The Fermi level is the energy at which these two bands touch each other.

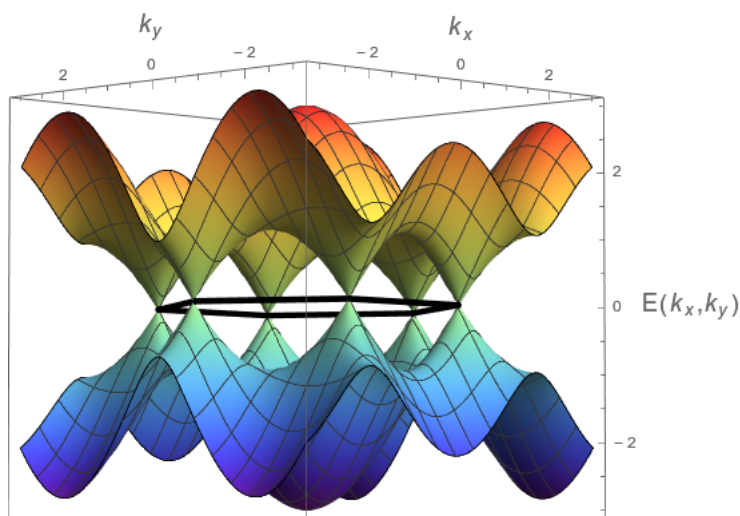


Figure 4.4: Plot of bands E_1 and E_2 of graphene near the Fermi level as a function of \vec{k} . The vertical axis is energy in Hückel units and the horizontal axes are momentum in the x and y directions. The conduction band (upper cone) and the valence band (lower cone) meet at six points known as Dirac points that lie at the corners of the Brillouin zone.

From Fig(4.4) one can see that the valence and conduction bands touch each other at six points, which are the six points at the corners of the hexagonal Brillouin zone(BZ), as in Fig(4.2). A cone is formed at each point where the bands touch each other. The cones are equivalent to one another with respect to the reciprocal lattice vectors. One-third of each of the cone is inside the first BZ which gives rise to two whole but inequivalent cones per BZ. At the corners where the bands touch,

the electrons in graphene have a linear energy dispersion due to the shape of the energy band structure in the vicinity of the cone vertex points. The two sets of the equivalent cones occur at the corner points K and K' that are equivalent and these points are called Dirac points as shown in Fig(4.4) and Fig(4.5).

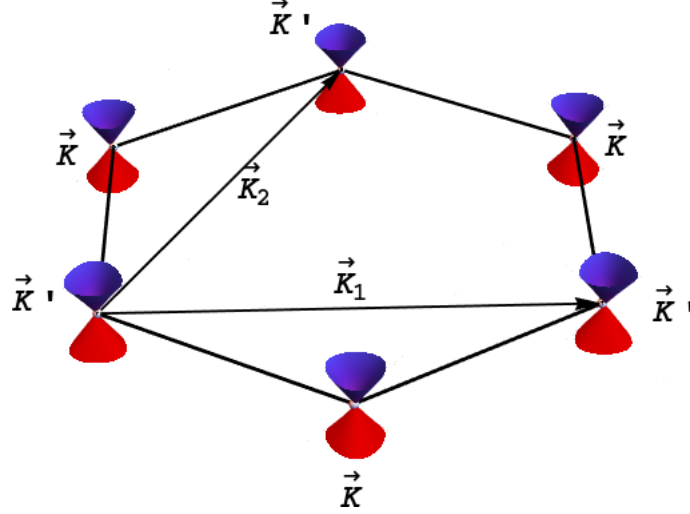


Figure 4.5: Positions of the Dirac cones in the zone. Two of the cone-shaped structures (K and K') are independent and the others are constructed translating by reciprocal basis vectors.

If the eigenvalue problem is expanded in momentum space, centering on the cone points, one proceeds to a theory that resembles the 2D Dirac equation. This Dirac equation describe a the zero mass particle with two possible values for the pseudo-spin.

There are two inequivalent cones that are located at the points k_1 and k_2 in the Brillouin zone that correspond to the momenta,

$$\vec{k}_1 = \frac{2\pi}{a} \left(\frac{1}{3\sqrt{3}}, \frac{1}{3}, 0 \right) \text{ and } \vec{k}_2 = \frac{2\pi}{a} \left(\frac{1}{3\sqrt{3}}, -\frac{1}{3}, 0 \right).$$

One can expand the Hamiltonian $H(\vec{k})$ around those points hence near ($\langle \hat{H}(\vec{k}) \rangle = E = 0$),

$$H(\vec{k}_{1,2} + \delta\vec{k}) = H_{1,2}(\delta\vec{k}) = \frac{3}{2} (\pm\sigma_x\delta k_x - \sigma_y\delta k_y) \quad (4.11)$$

where

$$H_{1,2} \psi(\vec{r}, t) = i \frac{\partial}{\partial t} \psi(\vec{r}, t). \quad (4.12)$$

Next, one can write the wavefunction in terms of a slowly varying Wannier 2-spinor envelope,

$$\psi(\vec{r}, t) = \begin{pmatrix} \psi_1(\vec{r}, t) \\ \psi_2(\vec{r}, t) \end{pmatrix} \quad (4.13)$$

which can be further simplified to

$$i \frac{3}{2} \left(\pm \sigma_x \frac{\partial}{\partial x} - \sigma_y \frac{\partial}{\partial y} \right) \psi(\vec{r}, t) = i \frac{\partial}{\partial t} \psi(\vec{r}, t), \quad (4.14)$$

where σ_x and σ_y are Pauli spin matrices. The π -theory predicts that the electron in a graphene sheet behaves as if they have a zero effective mass, similar to the results for its Dirac equation for a 2D massless particle, provided there is no perturbation. This behavior can be observed since the bands are not parabolic but linear near the Dirac points. The π -theory leads to provide the evidence that there is a very infinite electron mobility and zero charge carrier concentration near the Fermi-energy. However, at a low (non-zero) temperature, one can expect high mobility and a very small carrier concentration with almost zero gap²⁷.

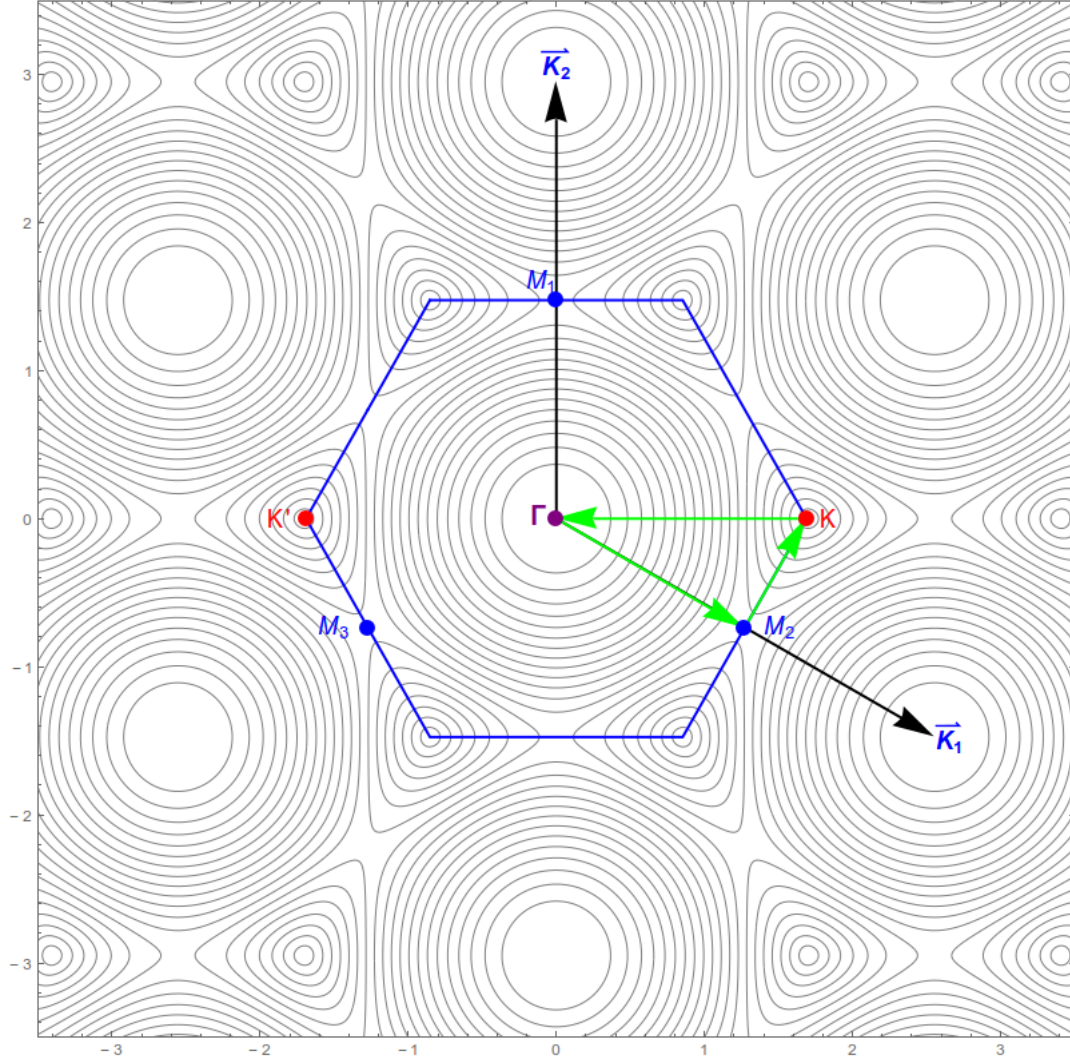


Figure 4.6: ΓMK Irreducible Brillouin zone (IBZ). Band energies of the lower band are shown as superimposed local contours. The energy zero corresponds to the Dirac cones at the K, K' points and the sharp peaks in the DOS come from saddle points at M_1, M_2 and M_3 . The points Γ, K, M , are called zone center, the corner and the center of the edge respectively. The green lines show the borders of the irreducible BZ along which the extrema occur. One moves along these lines to get the energy that an electron can have within the solid. The \vec{k} grid is replaced with a list of high symmetry points along the $\Gamma - M - K - \Gamma$ path in \vec{k} space.

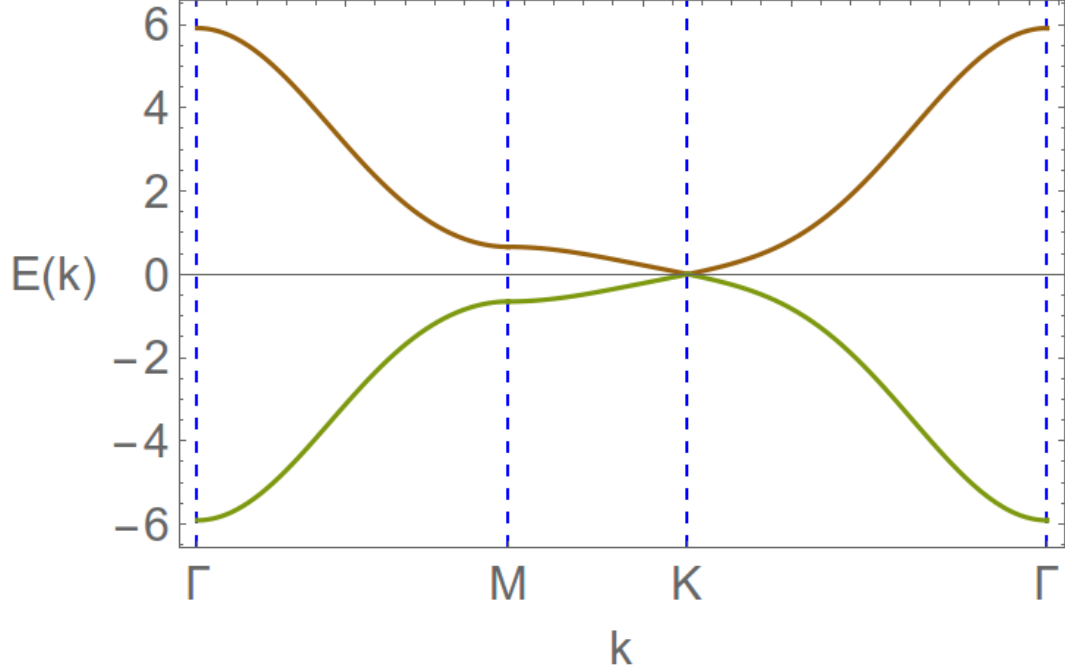


Figure 4.7: Band diagram for graphene in π orbital theory. The vertical axis is energy and the horizontal axis is the momentum in x and y directions. M , K and Γ are the symmetry points inside a first Brillouin zone given as $\vec{\Gamma} = (0, 0, 0)$, $\vec{M} = \frac{1}{2} \frac{2\pi}{a} (0, \frac{2}{3}, 0)$, $\vec{K} = \frac{2\pi}{a} (\frac{1}{3\sqrt{3}}, \frac{1}{3}, 0)$. The Dirac point is at the Fermi-level, energy, which occurs at point K . The saddle points are at M .

4.3 LCAO model

An absolutely minimal approximate basis set for mobile electron on the carbon atom consists of $2s, 2p_x, 2p_y$ and $2p_z$ wavefunction. There are eight basis orbitals per unit cell and the Bloch symmetrized Hamiltonian for a unit cell is given by

$$H = \begin{pmatrix} H_{AA} & H_{AB} \\ H_{BA} & H_{BB} \end{pmatrix} \quad (4.15)$$

Let's drop the \vec{k} argument for simplicity. Then,

$$H_{AA} = \begin{pmatrix} \langle 1, 2s|H|1, 2s \rangle & \langle 1, 2s|H|1, 2p_x \rangle & \langle 1, 2s|H|1, 2p_y \rangle & \langle 1, 2s|H|1, 2p_z \rangle \\ \langle 1, 2p_x|H|1, 2s \rangle & \langle 1, 2p_x|H|1, 2p_x \rangle & \langle 1, 2p_x|H|1, 2p_y \rangle & \langle 1, 2p_x|H|1, 2p_z \rangle \\ \langle 1, 2p_y|H|1, 2s \rangle & \langle 1, 2p_y|H|1, 2p_x \rangle & \langle 1, 2p_y|H|1, 2p_y \rangle & \langle 1, 2p_y|H|1, 2p_z \rangle \\ \langle 1, 2p_z|H|1, 2s \rangle & \langle 1, 2p_z|H|1, 2p_x \rangle & \langle 1, 2p_z|H|1, 2p_y \rangle & \langle 1, 2p_z|H|1, 2p_z \rangle \end{pmatrix} \quad (4.16)$$

and

$$H_{AB} = \begin{pmatrix} \langle 1, 2s|H|2, 2s \rangle & \langle 1, 2s|H|2, 2p_x \rangle & \langle 1, 2s|H|2, 2p_y \rangle & \langle 1, 2s|H|2, 2p_z \rangle \\ \langle 1, 2p_x|H|2, 2s \rangle & \langle 1, 2p_x|H|2, 2p_x \rangle & \langle 1, 2p_x|H|2, 2p_y \rangle & \langle 1, 2p_x|H|2, 2p_z \rangle \\ \langle 1, 2p_y|H|2, 2s \rangle & \langle 1, 2p_y|H|2, 2p_x \rangle & \langle 1, 2p_y|H|2, 2p_y \rangle & \langle 1, 2p_y|H|2, 2p_z \rangle \\ \langle 1, 2p_z|H|2, 2s \rangle & \langle 1, 2p_z|H|2, 2p_x \rangle & \langle 1, 2p_z|H|2, 2p_y \rangle & \langle 1, 2p_z|H|2, 2p_z \rangle \end{pmatrix}. \quad (4.17)$$

The matrix H_{AA} is diagonal and takes the value of the ionization energies α from the FAKE method explained above. In case of graphene, $H_{BB} = H_{AA}$. Also $H_{BA} = H_{AB}^\dagger$. The matrix elements of H_{AB} are also calculated using the FAKE method given by

$$H_{\nu,\mu}^{A,B}(\vec{k}) = \sum_B e^{i\vec{k} \cdot (\vec{R}_B + \vec{\rho}_j)} \langle \phi_\nu(\vec{r}) | H | \phi_\mu(\vec{r} - (\vec{R}_B + \vec{\rho}_j)) \rangle, \quad (4.18)$$

where ϕ_ν is on lattice site A and ϕ_μ is on the nearest neighbors B centered at $\vec{\rho}_j$ with respect to A .

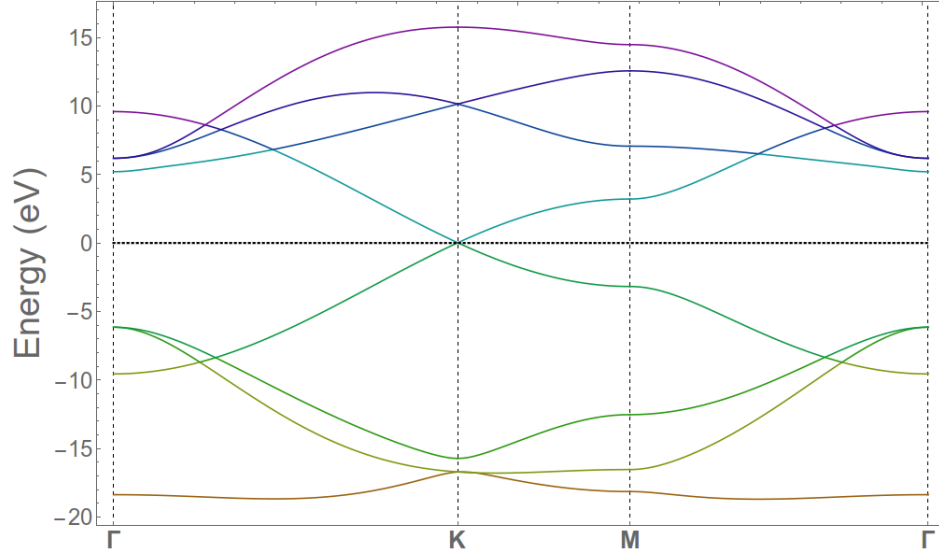


Figure 4.8: Band diagram for graphene using LCAO with a Bloch symmetrized basis of $2s, 2p_x, 2p_y$ and $2p_z$ orbitals for a unit cell. The vertical axis is energy in eV and the horizontal axis is momentum in the x and y directions.

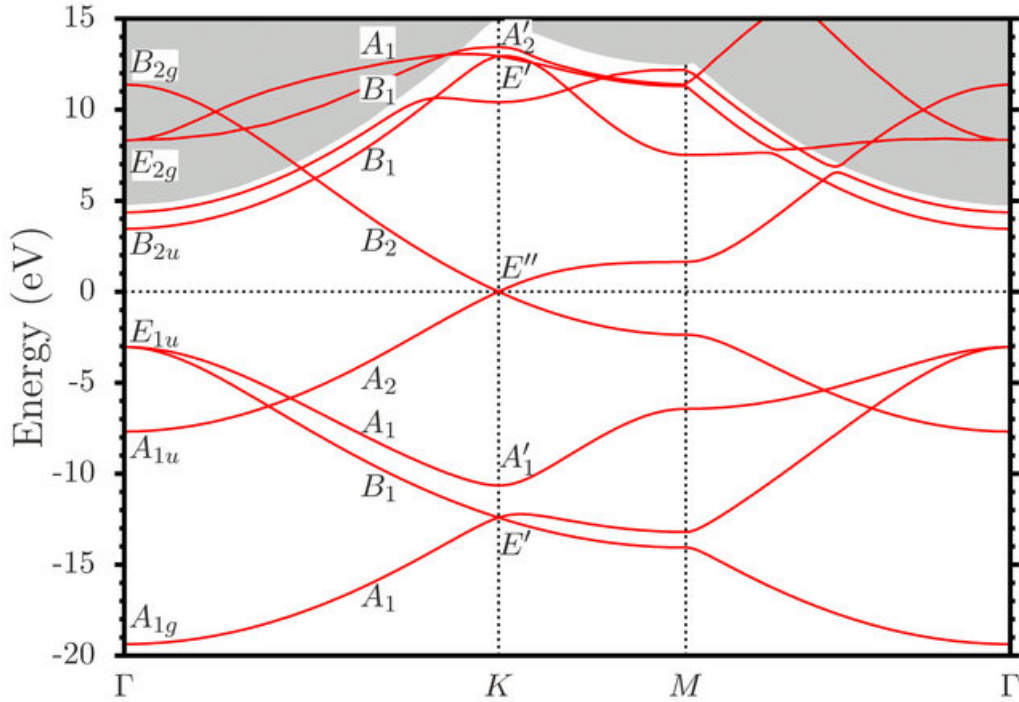


Figure 4.9: Graphene band structure from first principles-LAPW method².

The band structures obtained from FAKE using only α_0 as an adjustable parameter give qualitatively correct features, consistent with symmetry and reasonable

agreement with DFT and first principle LAPW calculations². The adjustment of α reflects a chemical shift due to charge redistribution in the ordered layer as well as higher order multipole Madelung-like electrostatic effects^{32,33}. The lowest band appears to be flat in the FAKE model. One of the possible reason for that would be is that the approximation only considers first neighbors. If one were to extend it to more neighbors, the energy in the Γ point will be going down.

CHAPTER V

GREENIAN AND LOCAL DENSITY OF STATES

5.1 Green functions

The spectral representation of any function of H is

$$f(\hat{H}) = \sum_{\alpha} |\psi_{\alpha}\rangle f(E_{\alpha}) \langle\psi_{\alpha}|, \quad (5.1)$$

where $|\psi_{\alpha}\rangle$ is an eigenfunction of \hat{H} and α runs over the whole spectrum. When one adds a driving term to make the Schrödinger's equation inhomogeneous,

$$\left(i\hbar \frac{\partial}{\partial t} - H\right) |\psi(t)\rangle = |F(t)\rangle, \quad (5.2)$$

the solution of this type of equation is given in terms of Green functions. When \hat{H} is time independent, any state function $|\psi(t)\rangle$ is,

$$\begin{aligned} |\psi(t)\rangle &= e^{-\frac{iH\Delta t}{\hbar}} |\psi(t_0)\rangle \\ &= e^{-\frac{iH(t-t_0)}{\hbar}} |\psi(t_0)\rangle, \end{aligned} \quad (5.3)$$

where, $\exp(-\frac{iH(t-t_0)}{\hbar})$ is a propagator is also a time-evolution operator or a Green function. Actually $\langle\phi_i| \exp(-\frac{iH(t-t_0)}{\hbar}) |\phi_j\rangle$ is the propagator from ϕ_j at time t_0 to ϕ_i

at time t . Define a propagator matrix to be

$$U(t, t_0) = e^{-\frac{iH(t-t_0)}{\hbar}} \quad (5.4)$$

and normalized such that

$$U(t_0, t_0) = 1, \quad (5.5)$$

and it is also an operator solution to Schrodinger's equation with $|F(t)\rangle \rightarrow 0$,

$$\left(i\hbar \frac{\partial}{\partial t} - H \right) U(t_0, t_0) = 0. \quad (5.6)$$

Since the driving term $|F(t)\rangle \neq 0$, a new operator \tilde{G} is introduced,

$$\tilde{G}(t, t_0) = -\frac{i}{\hbar} \theta(t - t_0) U(t, t_0) \quad (5.7)$$

such that

$$\left(i\hbar \frac{\partial}{\partial t} - H \right) \tilde{G}(t, t_0) = \delta(t - t_0) I. \quad (5.8)$$

Since \hat{H} is time independent, $U(t, t_0) = e^{-\frac{iH(t-t_0)}{\hbar}}$ is a propagator. The spectral representation of U is,

$$U(t, t_0) = \sum_{\alpha} |\psi_{\alpha}\rangle e^{-\frac{iE_{\alpha}(t-t_0)}{\hbar}} \langle \psi_{\alpha}|. \quad (5.9)$$

The substitution of $U(t, t_0)$ of Eq(5.9) in Eq(5.7) yields,

$$\tilde{G}(t, 0) = -\frac{i}{\hbar} \theta(t) \sum_{\alpha} |\psi_{\alpha}\rangle e^{-\frac{iE_{\alpha}t}{\hbar}} \langle \psi_{\alpha}|. \quad (5.10)$$

Since $\tilde{G}(t)$ represents a physical system, the Fourier transform of it must lead to a Fourier representation for any $t > 0$. If $\tilde{G}(t)$ is a representation in Fourier space,

$$\tilde{G}(t) = \frac{1}{2\pi} \int_{-\infty}^{\infty} \tilde{G}(E) e^{-\frac{iEt}{\hbar}} dE \quad (5.11)$$

and the inverse transform of $\tilde{G}(t)$ is $\tilde{G}(E)$, then

$$\begin{aligned} \tilde{G}(E) &= \int_{-\infty}^{\infty} \tilde{G}(t) e^{\frac{iEt}{\hbar}} dt \\ &= \int_{-\infty}^{\infty} -\frac{i\theta(t)}{\hbar} e^{-\frac{iHt}{\hbar}} e^{\frac{iEt}{\hbar}} dt \\ &= -\frac{i}{\hbar} \int_{-\infty}^{\infty} \theta(t) e^{\frac{i(E\hat{I}-H)t}{\hbar}} dt \\ &= -\frac{i}{\hbar} \int_0^{\infty} e^{\frac{i(E\hat{I}-H)t}{\hbar}} dt. \end{aligned} \quad (5.12)$$

Because the integrand $e^{\frac{i(E\hat{I}-H)t}{\hbar}}$ is always oscillating, $\tilde{G}(E)$ does not converge. One needs to introduce real damping exponentials in time to damp the oscillating complex exponentials of the Fourier transform. Finally one takes the small-damping limit. Let $e^{-\eta t}$ be the damping, then

$$\begin{aligned} \tilde{G}(E + i\eta) &= -\frac{i}{\hbar} \int_0^{\infty} e^{\frac{i(E\hat{I}-H)t}{\hbar}} e^{-\eta t} dt \\ &= -\frac{i}{\hbar} \int_0^{\infty} e^{\frac{i((E\hat{I}-H)+i\eta)t}{\hbar}} dt \\ &= -((E\hat{I} - H) + i\eta)^{-1} \left[e^{\frac{i((E\hat{I}-H)+i\eta)t}{\hbar}} \right]_0^{\infty} \\ &= -((E\hat{I} - H) + i\eta)^{-1} (-\hat{I}) \\ &= \left((E\hat{I} - H) + i\eta \right)^{-1} \end{aligned} \quad (5.13)$$

for E and η real and positive. In practice, instead of letting $\eta \rightarrow 0$, one takes η to be some small positive fixed value. Since $\tilde{G}(E) = \int_{-\infty}^{\infty} \tilde{G}(t) e^{\frac{iEt}{\hbar}} dt$ does not converge

for real E , the integral is expanded to a more general integral representation as,

$$G(z) = \int_{-\infty}^{\infty} \tilde{G}(t) e^{izt} dt \quad (5.14)$$

where z must be above the real axis. If z is a complex variable such that

$$z = E + i\eta \text{ with } E, \eta \in \Re \text{ and } \eta > 0, \quad (5.15)$$

then

$$G(z) = G(E + i\eta) = \int_{-\infty}^{\infty} \tilde{G}(t) e^{\frac{iEt}{\hbar}} e^{-\eta t} dt. \quad (5.16)$$

In general $G(z)$ converges in the upper half plane so that the matrix elements of $G(z)$ are analytic there. Then by substituting $\tilde{G}(t) = -\frac{i}{\hbar} \theta(t) e^{-\frac{iHt}{\hbar}}$,

$$\begin{aligned} G(z) &= \int_{-\infty}^{\infty} \theta(t) e^{\frac{izt}{\hbar}} \tilde{G}(t) dt \\ &= \sum_{\alpha} \frac{-i}{\hbar} \int_{-\infty}^{\infty} \theta(t) e^{\frac{izt}{\hbar}} e^{-\frac{iE_{\alpha}t}{\hbar}} |\psi_{\alpha}\rangle \langle \psi_{\alpha}| dt \\ &= \sum_{\alpha} \left(\frac{-i}{\hbar} \right) \int_0^{\infty} e^{\frac{i(z-E_{\alpha})t}{\hbar}} |\psi_{\alpha}\rangle \langle \psi_{\alpha}| dt \\ &= \sum_{\alpha} \left(\frac{-i}{\hbar} \right) \left(\frac{\hbar}{i} \right) \frac{1}{(z\hat{I} - E_{\alpha})} \left[e^{\frac{i(z\hat{I}-E_{\alpha})t}{\hbar}} \right]_0^{\infty} |\psi_{\alpha}\rangle \langle \psi_{\alpha}| \\ &= \sum_{\alpha} |\psi_{\alpha}\rangle (z\hat{I} - E_{\alpha})^{-1} \langle \psi_{\alpha}| \\ &= (z - H)^{-1}. \end{aligned} \quad (5.17)$$

This is the Greenian or a resolvent operator with complex energy $z = E + i\eta$, with η the adjustment of the width of pseudo-delta function peaks and Hamiltonian \tilde{H} such that the Greenian is singular when z is an eigenvalue. This extends $G(z)$ to the whole z plane except for the spectrum of \tilde{H} .

5.2 Local density of states

There exists a connection between a resolvent operator and the density of states (DOS). One defines a normalized density of state as,

$$D(E) = \frac{1}{N} \sum_{\alpha}^N \delta(E - E_{\alpha}) \quad (5.18)$$

where N is the total number of finite energy eigenstates and the sum is over all distinct states. The infinite peak in the delta function $\delta(E - E_{\alpha})$ can be replaced by peak of approximate finite width $\approx 2\eta$,

$$\begin{aligned} \delta(E - E_{\alpha}) &\approx \frac{1}{\pi} \frac{\eta}{(E - E_{\alpha})^2 + \eta^2} \\ &= \frac{1}{\pi} \frac{\eta}{(E - E_{\alpha} + i\eta)(E - E_{\alpha} - i\eta)} \\ &= -\frac{1}{\pi} \text{Im} \left(\frac{(E - E_{\alpha} - i\eta)}{(E - E_{\alpha} + i\eta)(E - E_{\alpha} - i\eta)} \right) \\ &= -\frac{1}{\pi} \text{Im} \left(\frac{1}{(E - E_{\alpha} + i\eta)} \right) \\ &= -\frac{1}{\pi} \text{Im} \left(\frac{1}{(E + i\eta) - E_{\alpha}} \right). \end{aligned} \quad (5.19)$$

If $\{|\tilde{\phi}_i\rangle\}$ is an orthogonal basis, so that $|\tilde{\phi}_i\rangle$ is a Löwdin basis function,

$$|\tilde{\phi}_i\rangle = S_{ij}^{-\frac{1}{2}} |\phi_j\rangle, \quad (5.20)$$

the local density of states for electrons is the relative probability per unit energy that an electron will have energy between E and $E + dE$, and be found on site with basis orbital ϕ_i . The local density of states for any basis state ϕ_i is given by,

$$D_i(E) = \sum_{\alpha=1}^N |\langle i|\alpha\rangle|^2 \delta(E - E_{\alpha}) \quad (5.21)$$

where α indexes the energy eigen-state and N is the number of basis functions used. One can replace the delta function peaks by peaks of finite width,

$$\begin{aligned}
D_i(E) &= -\frac{1}{\pi} \text{Im} \sum_{\alpha=1}^N |\langle i|\alpha\rangle|^2 \left(\frac{1}{E + i\eta - E_\alpha} \right) \\
&= -\frac{1}{\pi} \text{Im} \sum_{\alpha=1}^N \langle \tilde{\phi}_i | \psi_\alpha \rangle \left(\frac{1}{E + i\eta - E_\alpha} \right) \langle \psi_\alpha | \tilde{\phi}_i \rangle \\
&= -\frac{1}{\pi} \text{Im} \langle \tilde{\phi}_i | (E + i\eta - H)^{-1} | \tilde{\phi}_i \rangle \\
&= -\frac{1}{\pi} \text{Im} \langle \tilde{\phi}_i | G(E + i\eta) | \tilde{\phi}_i \rangle
\end{aligned} \tag{5.22}$$

5.3 Monkhorst-Pack method

The aim of this study is to develop a simple model for understanding electronic properties of adsorbates. I am looking forward to develop a formalism to work on a substrate with an infinite number of atoms. An efficient way of doing this is to use Green functions. In a π -theory model, a Green function in \vec{k} space for graphene is

$$\begin{aligned}
G(\vec{k}, z) &= \left(z\hat{I} - H(\vec{k}) \right)^{-1} \\
&= \left(z\hat{I} - \begin{pmatrix} \epsilon_1 & -(1 + \frac{1}{t} + \frac{s}{t}) \\ -(1 + t + \frac{t}{s}) & \epsilon_2 \end{pmatrix} \right)^{-1} \\
&= \begin{pmatrix} z - \epsilon_1 & (1 + \frac{1}{t} + \frac{s}{t}) \\ (1 + t + \frac{t}{s}) & z - \epsilon_2 \end{pmatrix}^{-1} \\
&= \frac{1}{D(\vec{k}, z)} \begin{pmatrix} z - \epsilon_2 & -(1 + \frac{1}{t} + \frac{s}{t}) \\ -(1 + t + \frac{t}{s}) & z - \epsilon_1 \end{pmatrix}
\end{aligned} \tag{5.23}$$

where the determinant is

$$D(\vec{k}, z) = (z - \epsilon_1)(z - \epsilon_2) - \left(1 + \frac{1}{t} + \frac{s}{t}\right)\left(1 + t + \frac{t}{s}\right).$$

The Green functions matrix elements for the periodic part are computed from H via

$$\begin{aligned} \langle m, \alpha | G | m', \beta \rangle &= \sum_{\vec{k}} \langle m, \alpha | \vec{k}, \alpha \rangle G_{\alpha, \beta}(z, \vec{k}) \langle \vec{k}, \beta | m', \beta \rangle \\ &= \frac{1}{N} \frac{A}{(2\pi)^2} \int_{\vec{k} \in \text{zone}} G_{\alpha, \beta}(z, \vec{k}) e^{i\vec{k} \cdot (\vec{R}_{m'} - \vec{R}_m)} d^2k \end{aligned} \quad (5.24)$$

The factor $\frac{A}{N}$ is the ratio of the total area to the total number of unit cells, which is the area of one unit cell that is equal to,

$$\begin{aligned} &|\vec{h}_1 \times \vec{h}_2| \cdot \hat{z} \\ &= \left(\sqrt{3} a \hat{x}\right) \times \left(\frac{\sqrt{3}}{2} a \hat{x} + \frac{3}{2} a \hat{y}\right) \cdot \hat{z} \\ &= \frac{3\sqrt{3} a^2}{2}. \end{aligned} \quad (5.25)$$

Exploiting the translational symmetry one can write,

$$m - m' = m'' \text{ and } n - n' = n'' \quad (5.26)$$

$$\begin{aligned} \therefore \langle m, \alpha | G | m', \beta \rangle &= \langle m'', \alpha | G | 0, \beta \rangle \\ &= \frac{3\sqrt{3} a^2}{2(2\pi)^2} \int_{\vec{k} \in \text{zone}} G_{\alpha, \beta}(z, \vec{k}) e^{-i\vec{k} \cdot \vec{R}_m} d^2k. \end{aligned} \quad (5.27)$$

Here, $|\vec{k}, \alpha\rangle$ is a Bloch sum of basis orbitals of translation symmetry \vec{k} , and $G_{\alpha, \beta}(z, \vec{k})$ is the α, β entry of $(z \hat{I} - H(\vec{k}))^{-1}$ with $H(\vec{k})$ the reduced Hamiltonian $H_{\alpha, \beta}(\vec{k}) = \langle \vec{k}, \alpha | H | \vec{k}, \beta \rangle$. The integration can be done analytically in closed form by doing the integrations over the Brioullin zone. Alternatively, one can use the efficient numerical method using Gaussian quadrature points by Monkhorst and Pack³⁴. For the zone

integration, the \vec{k} in the Bloch's states is expressed in terms of reciprocal basis vectors,

$$\vec{k} = p\vec{K}_1 + q\vec{K}_2. \quad (5.28)$$

The Monkhorst-Pack quadrature points are equally spaced over the zone. If there are M^2 quadrature points for $\{\vec{k}_j\}$, then

$$\begin{aligned} \frac{3\sqrt{3} a^2}{2(2\pi)^2} \int_{\vec{k} \in \text{zone}} F_{\alpha,\beta}(z, \vec{k}) d^2k &\approx \frac{3\sqrt{3} a^2}{2(2\pi)^2} \frac{\text{Recirpocal zone area}}{M^2} \sum_{j=1}^{M^2} F_{\alpha,\beta}(z, \vec{k}) \\ &= \frac{1}{M^2} \sum_{j=1}^{M^2} F_{\alpha,\beta}(z, \vec{k}). \end{aligned} \quad (5.29)$$

One can write

$$\langle m, \alpha | G | 0, \beta \rangle \approx \frac{1}{M^2} \sum_{j=1}^{M^2} G_{\alpha,\beta}(z, \vec{k}) e^{-i\vec{k} \cdot \vec{R}_{mn}}. \quad (5.30)$$

This is equivalent to approximating a finite sized lattice of $M \times M$ cells, for a given η , M with M large enough that smooth functions result. With M^2 points the calculation yields results correct for the first M^2 Fourier coefficients. The more quadrature points, the better the approximations. Let

$$\Delta\vec{k}_1 = \frac{\vec{K}_1}{M}, \quad \Delta\vec{k}_2 = \frac{\vec{K}_2}{M}, \quad (5.31)$$

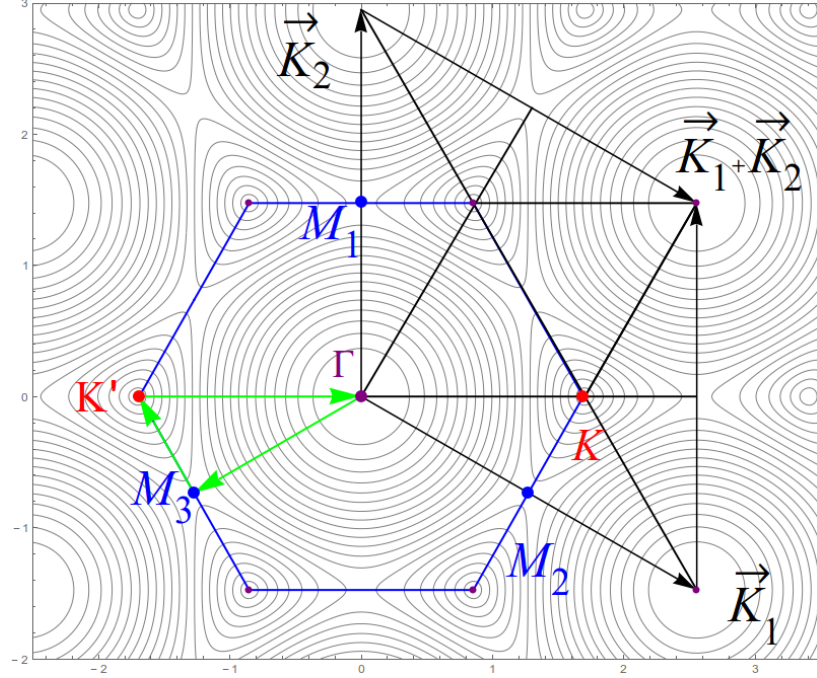


Figure 5.1: Zone transformed into a trapezoid.

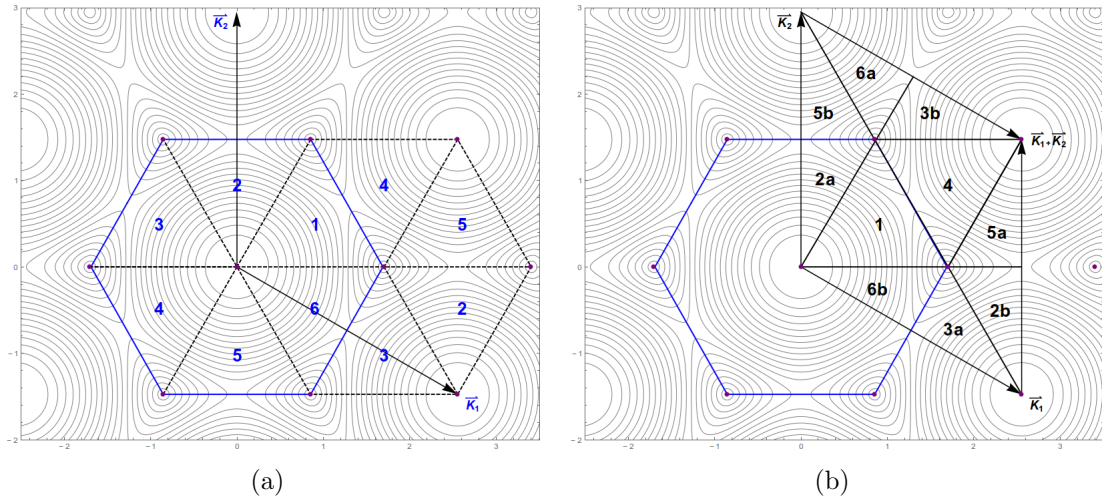


Figure 5.2: (Left) Making of the Brillouin zone (a) The symmetrized zone comprises sector 1 through 6. Other segments shown dashed are equivalent by translation (b) Translation is used to assemble an equivalent trapezoidal zone.

and then the gaussian quadrature points can be written with two index notation

as

$$\vec{k}_{pq} = (p \Delta \vec{k}_1 - \frac{1}{2} \vec{K}_1) + (q \Delta \vec{k}_2 - \frac{1}{2} \vec{K}_2),$$

where p and q are integers between 0 and $M - 1$. Thus

$$\begin{aligned}
\vec{k}_{pq} \cdot \vec{R}_{m_1 m_2} &= (p \Delta \vec{k}_1 - \frac{1}{2} \vec{K}_1) \cdot (m_1 \vec{h}_1) + (q \Delta \vec{k}_2 - \frac{1}{2} \vec{K}_2) \cdot (m_2 \vec{h}_2) \\
&= (p \frac{\vec{K}_1}{M} - \frac{1}{2} \vec{K}_1) \cdot (m_1 \vec{h}_1) + (q \frac{\vec{K}_2}{M} - \frac{1}{2} \vec{K}_2) \cdot (m_2 \vec{h}_2) \\
&= \frac{2\pi p m_1}{M} - \frac{2\pi m_1}{2} + \frac{2\pi q m_2}{M} - \frac{2\pi m_2}{2} \\
&= (2\pi) \left(\frac{2p - M}{2M} \right) m_1 + (2\pi) \left(\frac{2q - M}{2M} \right) m_2.
\end{aligned} \tag{5.32}$$

Let

$$\theta_1 = \theta_p = \pi \left(\frac{2p - M}{M} \right), \quad \theta_2 = \theta_q = \pi \left(\frac{2q - M}{M} \right), \tag{5.33}$$

so that

$$e^{i \vec{k}_{pq} \cdot \vec{R}_{m_1 m_2}} = (e^{i\theta_1})^{m_1} (e^{i\theta_2})^{m_2}$$

and hence the Green function can be written as

$$\langle m, \alpha | G | 0, \beta \rangle \approx \frac{1}{M^2} \sum_{j=1}^{M^2} G_{\alpha, \beta}(z, \theta_1, \theta_2) (e^{-i\theta_1})^{m_1} (e^{-i\theta_2})^{m_2} \tag{5.34}$$

and the range of integration over the BZ is

$$0 < \theta_1 < 2\pi \quad \text{and} \quad 0 < \theta_2 < 2\pi.$$

5.3.1 Results

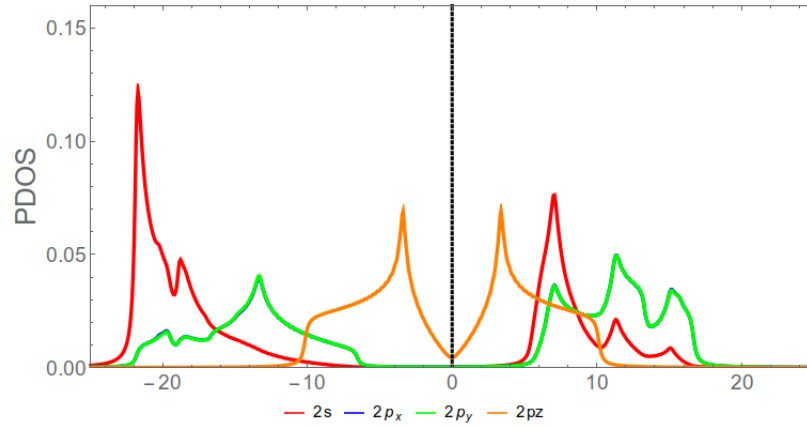


Figure 5.3: PDOS of an infinite graphene sheet for different valence orbitals using solid state matrix elements from FAKE method.

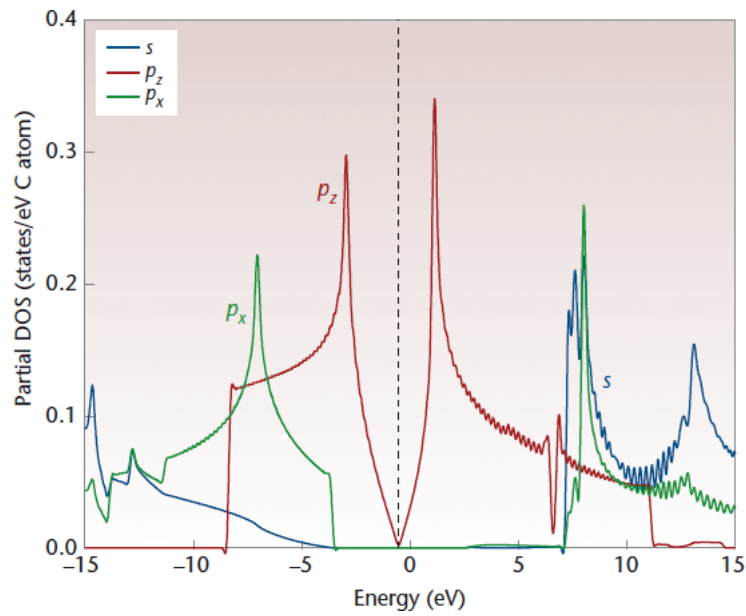


Figure 5.4: DOS of a graphene by DFT study using two basis sets for graphene by Stewart and Derek³ to study how the choice of basis functions impacts characterization techniques and calculated electronic transport properties.

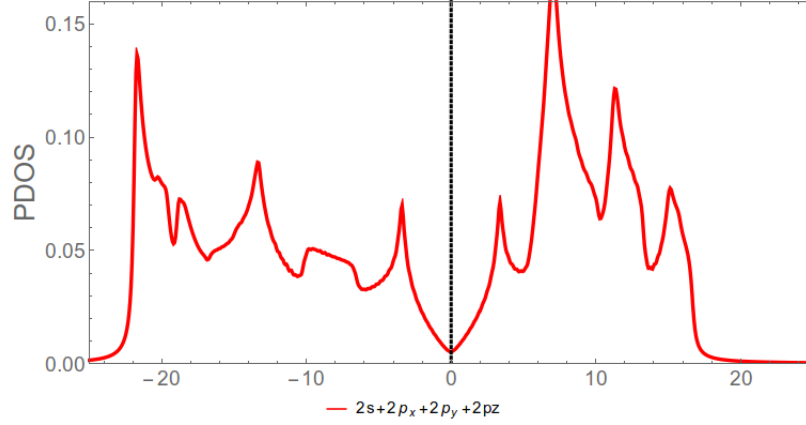


Figure 5.5: DOS of an infinite graphene sheet with all four valence orbitals combined using FAKE method.

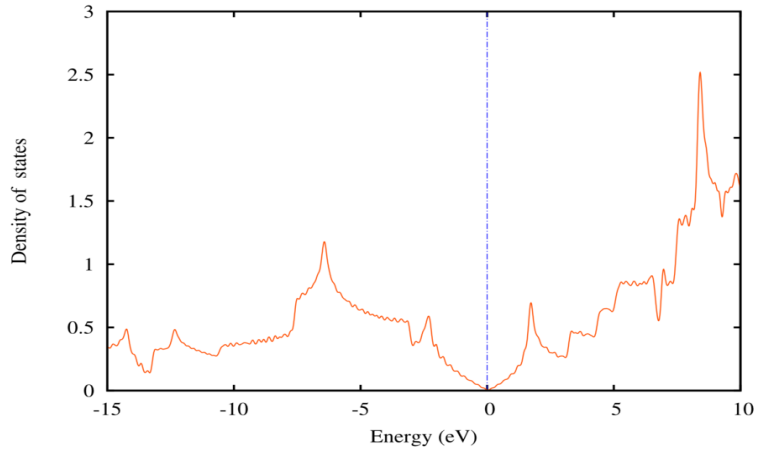


Figure 5.6: DOS of a graphene using QUANTUM ESPRESSO⁴

As expected for graphene, the DOS vanishes at the Fermi-level. Near the Fermi-level, all states are composed of the π orbitals of the carbons, the σ orbitals only contribute to energetically much lower and higher states. The wiggles in the DOS are artifacts that can be smoothed out using more \vec{k} points for the Brioullin zone sampling or using wider broadening functions i.e., large η .

Fig(5.3) shows the partial density of states calculated using the FAKE method. The density of states is zero at the Fermi level. Near the Fermi-level, the main contribution to the DOS is from the p_z state but the contribution from all other states is flat or zero. The π state is symmetric about the Fermi level whereas σ states

are not. Fig(5.4) is the DOS for a unit cell of graphene calculated using DFT with two basis sets of graphene by Stewart and Derek³. There are qualitative similarities between the FAKE DOS and DFT DOS. The van Hove singularities are about the same in both figures. It can be seen that the p_x and p_y PDOS overlap each other. Fig(5.5) and Fig(5.6) are the LDOS for an infinite graphene using the FAKE method and QUANTUM ESPRESSO⁴ respectively. The LDOS look qualitatively same near and below the Fermi level.

CHAPTER VI

EDGE SHEET OF GRAPHENE

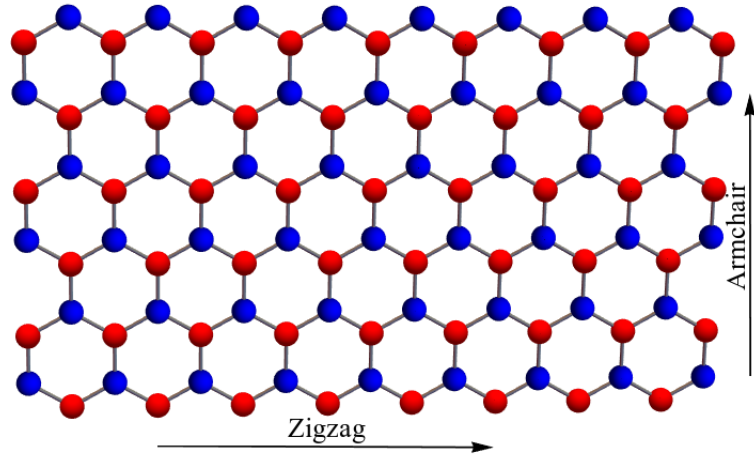


Figure 6.1: The two simple edge geometries of graphene. The armchair termination consists of both the sub-lattice sites but the zigzag termination is made of only one sub-lattice and the edge atoms are all equivalent to one another chemically. In the picture above, one can see the red sites in zigzag termination.

Graphene sheets grown in the laboratories have edges and tears so it is interesting to look at the LDOS of graphene along an edge. Let n index the horizontal row of atoms that are parallel to the zigzag edge shown in Fig(6.1). Thus $n = 1$ for atoms on the edge and $n = 2$ for the atoms on the next row. The graphene sheet is arranged in such a way that it extends infinitely in the direction parallel to the edge which is in the horizontal direction.

One can see that $n = 1, 3, \dots$ are rows of red atoms ($\alpha = 1$) which lies in the bulk of a sheet referred as $\alpha = 1$ type of sublattice. Let the horizontal axis be the x axis

(\hat{x}). One can define a Bloch symmetrized basis orbital for row n by

$$|n, k_{\parallel}\rangle = \frac{1}{N_x} \sum_{m=1}^{N_x} e^{i\vec{k}\cdot(m\vec{h}_1+n\vec{h}_2)} |m, n\rangle. \quad (6.1)$$

6.1 An effective dimer method

It is reasonable to only consider the π DOS separately from the σ DOS because the wavefunctions have a very small overlap. I make the π -orbital approximation. The Hamiltonian is block diagonal as a function of k_{\parallel} and the matrix elements are calculated in accordance to Fig(6.2). For an uncoupled dimer, the Green function matrix is

$$g = \left(z \begin{pmatrix} 1 & 0 \\ 0 & 1 \end{pmatrix} - \begin{pmatrix} 0 & -1 \\ -1 & 0 \end{pmatrix} \right)^{-1}. \quad (6.2)$$

Let

$$g_{11}(z) = g_{22}(z) = \frac{z}{z^2 - 1}, \text{ and } g_{12}(z) = g_{21}(z) = \frac{1}{1 - z^2}. \quad (6.3)$$

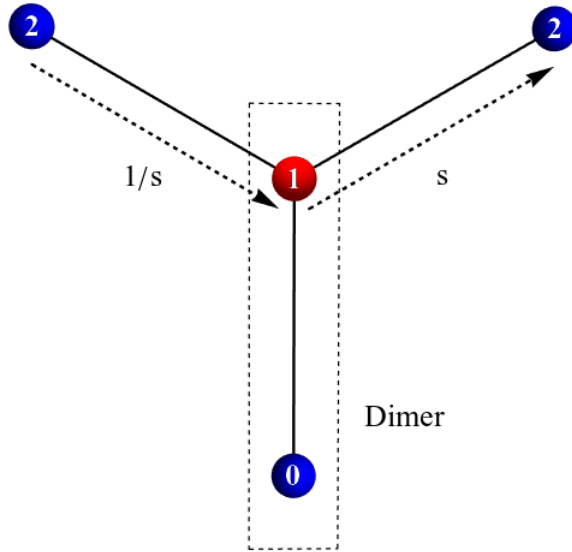


Figure 6.2: Effective dimer used to calculate the matrix elements.

Using Dyson's equation, $G = g + g V G$, one gets

$$\begin{aligned} G_{11} &= g_{11} + g_{12} V_{23} G_{31} \\ &= g_{11} - g_{12} \left(s + \frac{1}{s}\right) G_{31} \end{aligned} \quad (6.4)$$

$$\begin{aligned} G_{31} &= g_{31} + g_{33} V_{32} G_{21} \\ &= -g_{33} \left(s + \frac{1}{s}\right) G_{21} \end{aligned} \quad (6.5)$$

$$\begin{aligned} G_{21} &= g_{21} + g_{22} V_{23} G_{31} \\ &= g_{21} - g_{22} \left(s + \frac{1}{s}\right) G_{31} \end{aligned} \quad (6.6)$$

After the connection $g_{33} = G_{11}$. Then one can solve the above equations simultaneously. Putting $s = e^{i\vec{k} \cdot \frac{\vec{h}_1}{2}} = e^{i\frac{\sqrt{3}}{2} k_x a}$, we have

$$\left(s + \frac{1}{s}\right) = 2 \cos\left[\frac{\sqrt{3}}{2} k_x a\right] = 2c, \text{ and} \quad (6.7)$$

$$G_{11} = -\frac{-1 - 4 c^2 g_{11}^2 + 4 c^2 g_{12}^2 + \sqrt{-64 c^4 g_{11}^2 g_{12}^2 + (1 - 4 c^2 (g_{11}^2 + g_{12}^2))^2}}{8 c^2 g_{11}} \quad (6.8)$$

Substituting g_{11} and g_{12} from Eq(6.3), the term inside the square root becomes,

$$-64 c^4 g_{11}^2 g_{12}^2 + (1 - 4 c^2 (g_{11}^2 + g_{12}^2))^2 = \frac{16 c^4 + (z^2 - 1)^2 - 8 c^2 (z^2 + 1)}{(z^2 - 1)^2}. \quad (6.9)$$

The numerator on the above equation can be solved for z with four different roots, hence

$$G_{11}(z, c) = \frac{z^2 - 1 + 4 c^2 - \sqrt{z - 2c - 1}\sqrt{z - 2c + 1}\sqrt{z + 2c - 1}\sqrt{z + 2c + 1}}{8 c^2 z}. \quad (6.10)$$

In the same way, one can calculate the Green function matrix element G_{22} ,

$$\begin{aligned} G_{22} &= g_{22} - g_{22} \left(s + \frac{1}{s} \right) G_{32} \\ G_{32} &= -g_{33} \left(s + \frac{1}{s} \right) G_{22}. \end{aligned} \tag{6.11}$$

After solving the simultaneous equations,

$$G_{22} = \frac{g_{22}}{1 - 4 c^2 g_{22} G_{11}}. \tag{6.12}$$

Now I want to remove site 1 so there will be a dangling bond state at site 2. Next I look at the local density of states at site 2. Let F be the new Green function. Then,

$$\begin{aligned} F_{11} &= G_{11} + G_{11} V_{11} F_{11}, \\ F_{22} &= G_{22} + G_{21} V_{11} F_{12}, \\ \text{and } F_{12} &= G_{12} + G_{11} V_{11} F_{12}, \end{aligned} \tag{6.13}$$

After solving the simultaneous equations above,

$$F_{22} = G_{22} + G_{21} V_{11} (1 - G_{11} V_{11})^{-1} G_{12}. \tag{6.14}$$

In order to remove the site 1, I put a repulsive potential on the atom:

$$V_{11} = \frac{1}{\epsilon} \tag{6.15}$$

such that $\epsilon \rightarrow 0$. Then

$$F_{22} = G_{22} - G_{21} G_{11}^{-1} G_{12}. \tag{6.16}$$

6.1.1 Results and Discussion

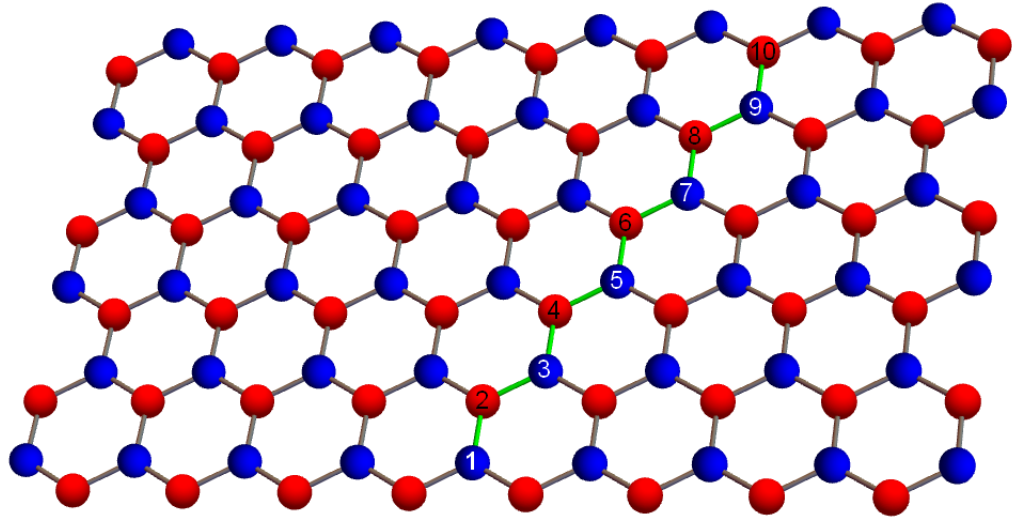


Figure 6.3: Schematic diagram showing the zigzag states for different values of n .

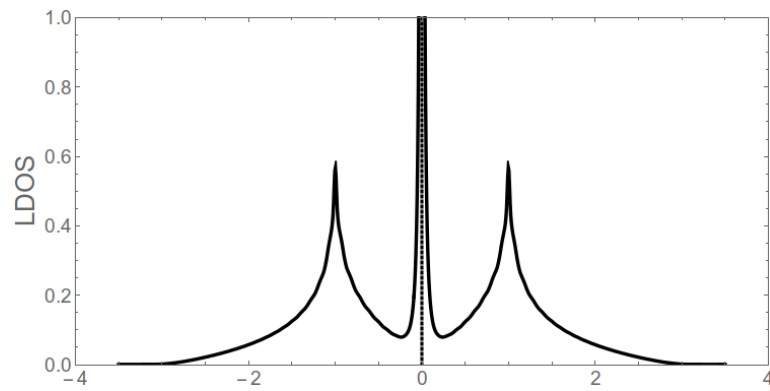


Figure 6.4: π orbital DOS at site 1 of Fig(6.2) a zigzag state representing α sub-lattice before removing site 1.

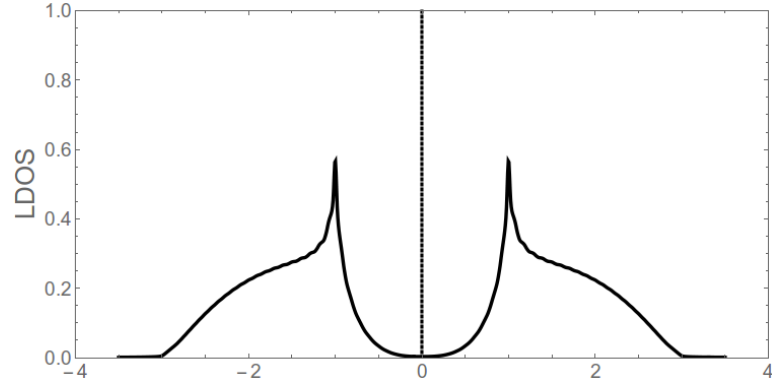


Figure 6.5: π orbital DOS at site 2 of Fig(6.2) a zigzag state representing β sub-lattice before removal of site 1.

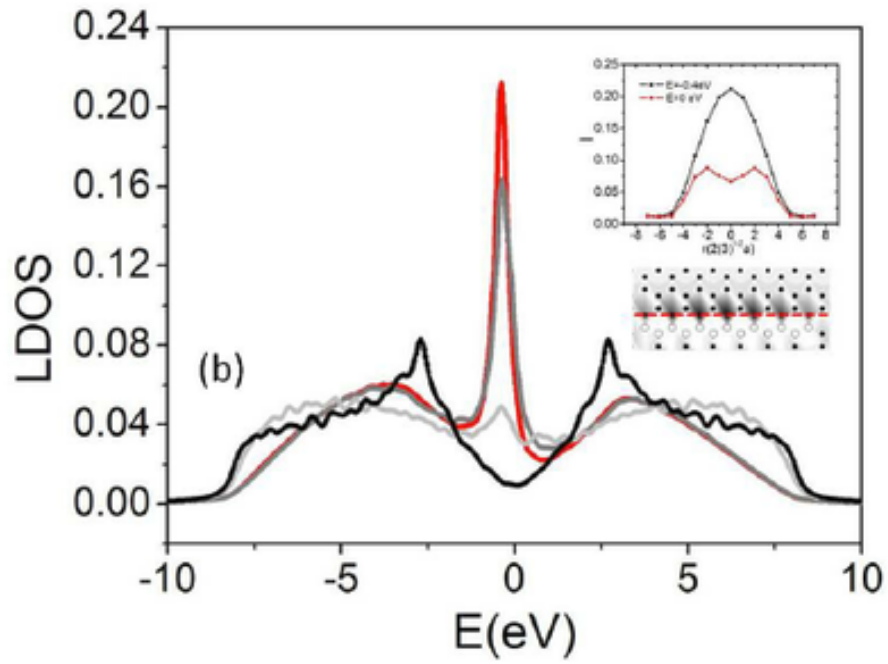


Figure 6.6: π LDOS of sites in the vicinity of a zigzag line defect⁵.

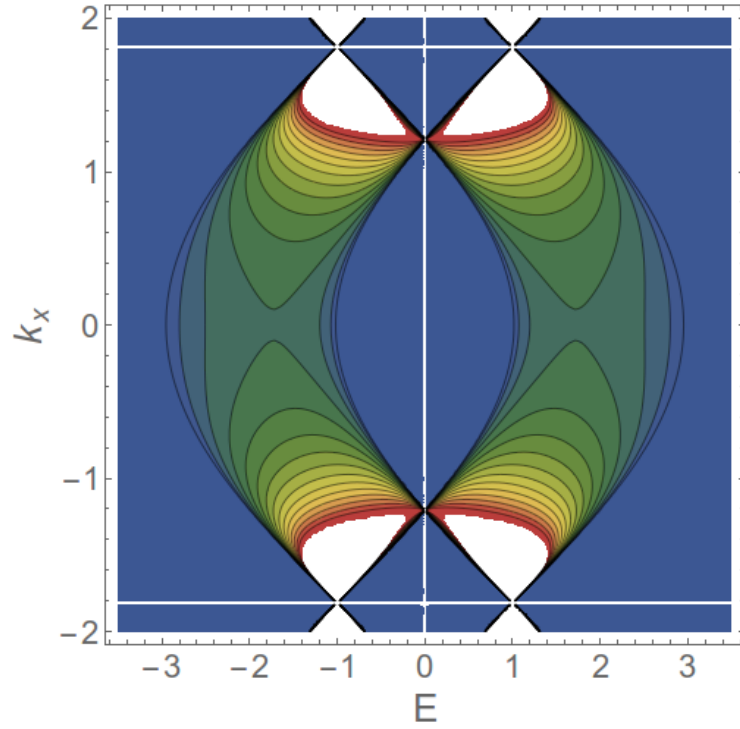


Figure 6.7: Contour plot of spectral density of Fig(6.2) at site 1 before its removal. The white area is where the probability of finding the electron is maximum and darker the area lesser the probability is.

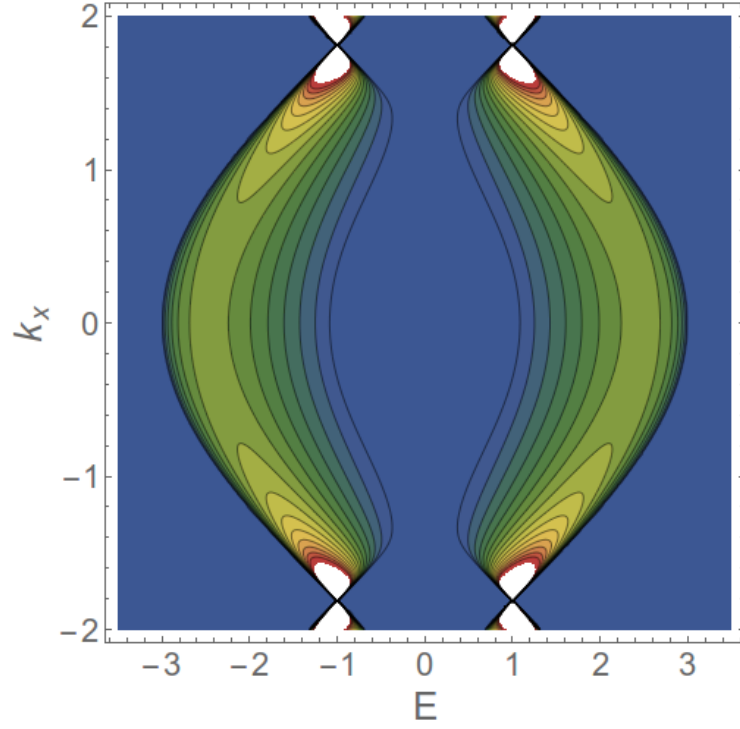


Figure 6.8: Contour plot of spectral density at site 2 before removal of site 1.

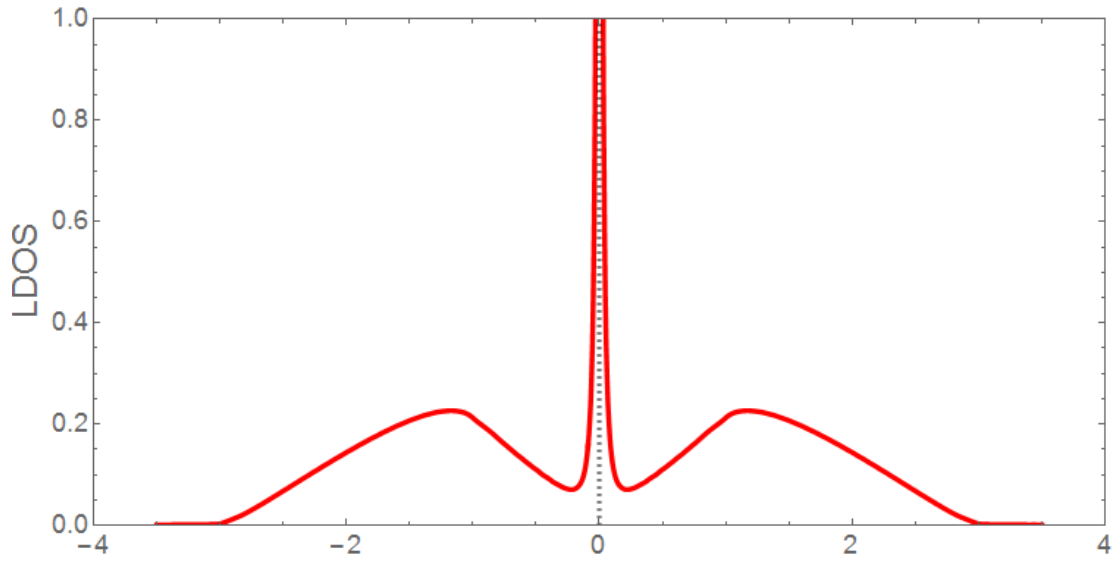


Figure 6.9: π LDOS at site 2 after removing site 1 from Fig(6.2).

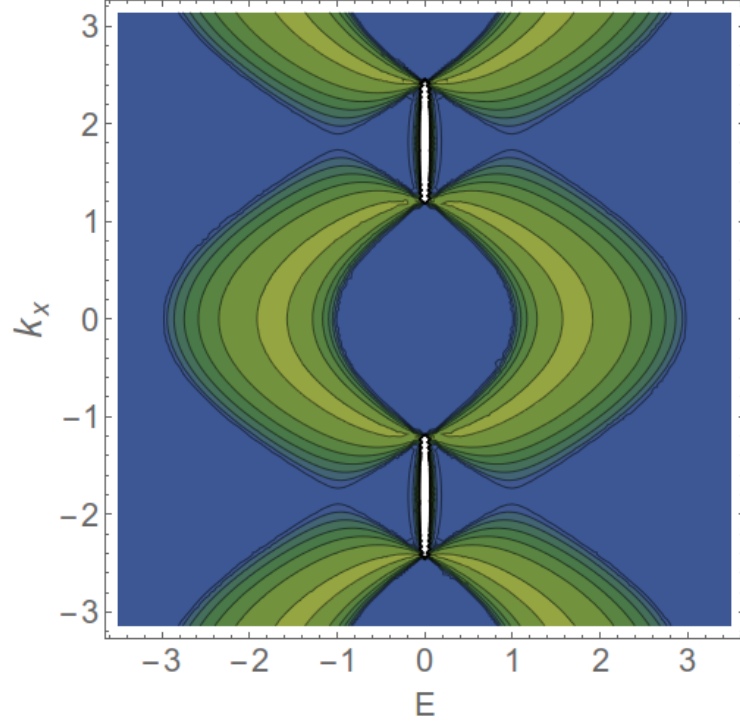


Figure 6.10: Spectral density at the edge state after the removal of site 1.

Fig(6.7) shows the projected electron density on the first row of atoms, $n = 1$, as a function of energy in the horizontal axis and momentum $k_{||}$ to the edge on the vertical axis. There is a strong peak at the Fermi level in Fig(6.4), in contrast to the LDOS of a graphene for an infinite sheet. This represents a dangling bond state. In pristine graphene a carbon atom has a coordination number of 3 whereas a carbon atom at the edge has a coordination number of 2 that leaves one non-bonding π -orbital creating a dangling bond edge state³⁵.

The white area in the contour plot Fig(6.7) and Fig(6.8) is the region that has a high probability of finding the electrons whereas the darker area has less probability. Also, one can see that the bands are partly flat at the Fermi level ($E = 0$). One can conclude that the electrons are strongly localized near zigzag states. One strong feature of such states is that they have a non-bonding character. They are also not responsible for electron transport because the current operator acting on the non-bonding orbitals has vanishing expectation value³⁵.

CHAPTER VII

HOLES AND DEFECTS ON GRAPHENE

The interesting feature in a real graphene sheet is to look at the electronic structure near a missing carbon atom causing a graphene sheet to have a vacancy. Let H_0 be the Hamiltonian of an infinite sheet of graphene with no imperfections. Now assume that the same sheet has a single vacancy at a random site of any unit cell. So one is interested in calculating the LDOS near the site where there is a hole.

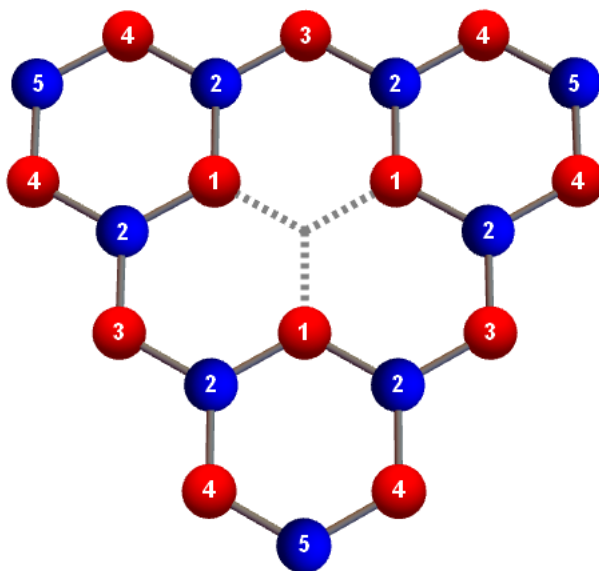


Figure 7.1: Schematic diagram of a graphene where a carbon (β) sublattice is removed, the numbers are the neighboring atoms with respect to the vacancy.

So, a carbon atom has been removed from an infinite graphene sheet and the electronic properties are to be observed in the neighborhood of the vacancy. Let A and B represent lattice region of an unaltered infinite set and an altered finite set of the graphene lattice respectively. The Green's function of this model after alteration

can be calculated using Dyson's equation,

$$G = g + gVG \quad (7.1)$$

and the Green's function matrix elements are

$$G_{ij} = \langle i|G|j \rangle = g_{ij} + \sum_{kl} g_{ik} V_{kl} G_{lj}. \quad (7.2)$$

For simplicity only p_z orbital is used as a Bloch symmetrized basis function as described in Chap(V). The interaction matrix element V_{ij} is zero unless both the basis orbitals i and j belong to B . So if B is a deleted carbon then, G_{AA} can be calculated with respect to the alteration made with B .

$$G_{AA} = g_{AA} + g_{AA}V_{AA}G_{AA} + g_{AB}V_{BB}G_{BA} + g_{AB}V_{BA}G_{AA} \quad (7.3)$$

Since V_{BB} is constrained to be non-zero while V_{AA} and V_{AB} are all zero so,

$$G_{AA} = g_{AA} + g_{AB}V_{BB}G_{BA}. \quad (7.4)$$

Similarly,

$$\begin{aligned} G_{BA} &= g_{BA} + g_{BB}V_{BB}G_{BA}, \\ G_{BA} - g_{BB}V_{BB}G_{BA} &= g_{BA}, \\ \left(I_{BB} - g_{BB}V_{BB} \right) G_{BA} &= g_{BA}, \\ G_{BA} &= \left(I_{BB} - g_{BB}V_{BB} \right)^{-1} g_{BA}. \end{aligned} \quad (7.5)$$

Then substituting G_{BA} into the Eq(7.4) containing G_{AA} gives,

$$G_{AA} = g_{AA} + g_{AB}V_{BB} \left(I_{BB} - g_{BB}V_{BB} \right)^{-1} g_{BA}. \quad (7.6)$$

For a single vacancy, B contains only one site. Let $V_{BB} = \frac{1}{\epsilon} \hat{I}_{BB}$, so when one takes the limit $\epsilon \rightarrow 0$, V_{BB} is infinite so as to push the electron out of the region B making it as a hole. So by removing the carbon as described, the Green functions G_{AA} with respect to the vacant site can be calculated anywhere in the graphene sheet.

$$\begin{aligned} G_{AA} &= g_{AA} + g_{AB} \left(\frac{1}{\epsilon} I_{BB} \right) \left(I_{BB} - g_{BB} \left(\frac{1}{\epsilon} I_{BB} \right) \right)^{-1} g_{BA} \\ &= g_{AA} + \frac{1}{\epsilon} g_{AB} \left(I_{BB} - \frac{1}{\epsilon} g_{BB} \right)^{-1} g_{BA} \end{aligned} \quad (7.7)$$

Take the limit $\epsilon \rightarrow 0$,

$$G_{AA} = g_{AA} - g_{AB} (g_{BB})^{-1} g_{BA} \quad (7.8)$$

where g_{AA} , g_{AB} , g_{BB} and g_{BA} are the unperturbed green function of a pristine graphene.

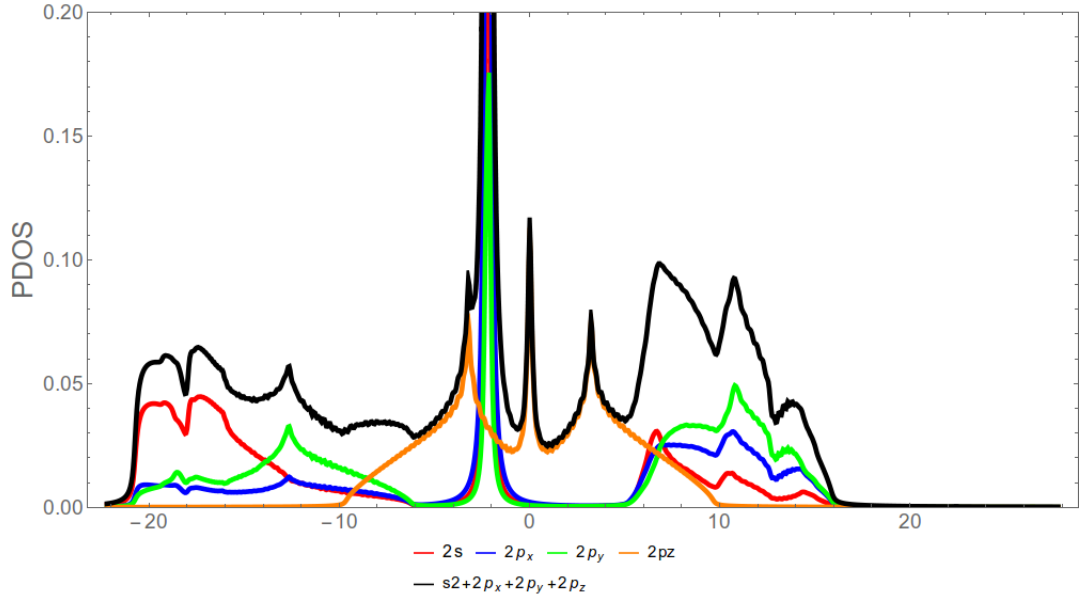


Figure 7.2: LDOS for an adjacent site to the vacancy, site 1 (α) sublattice in Fig(7.1). The red, blue, green and orange curves are PDOS for $2s$, $2p_x$, $2p_y$ and $2p_z$ respectively. The black curve is the total DOS at site 1. There is a peak at Fermi level that is caused due to the vacancy.

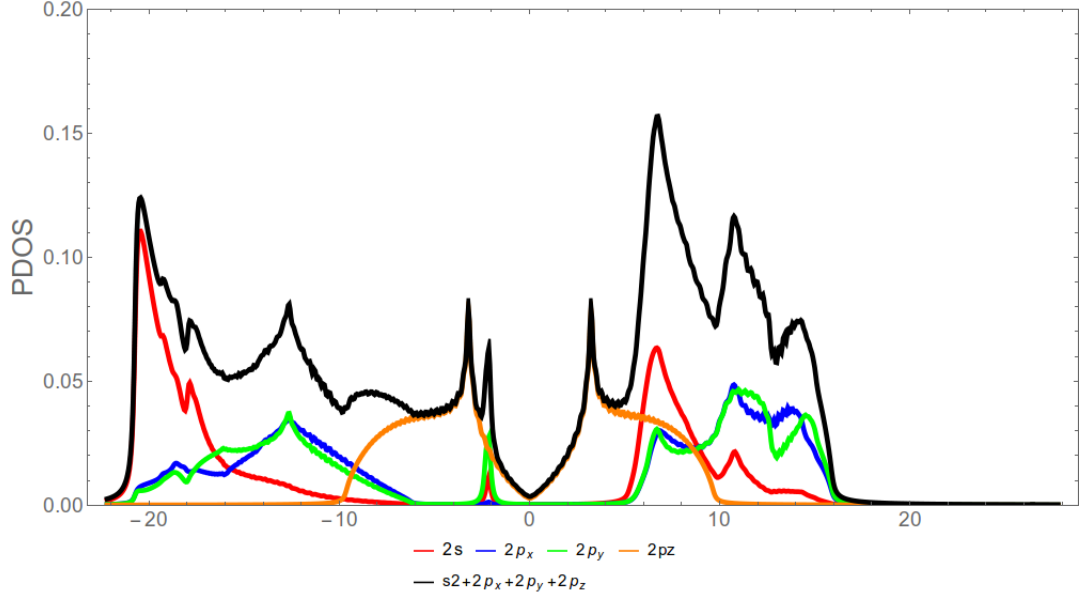


Figure 7.3: LDOS for an adjacent site to the vacancy, site 2 (β) in Fig(7.1). The red, blue, green and orange curves are PDOS for $2s$, $2p_x$, $2p_y$ and $2p_z$ respectively. The black curve is the total DOS at site 2. There is a zero DOS at fermi level. The site is the same sublattice as the vacancy.

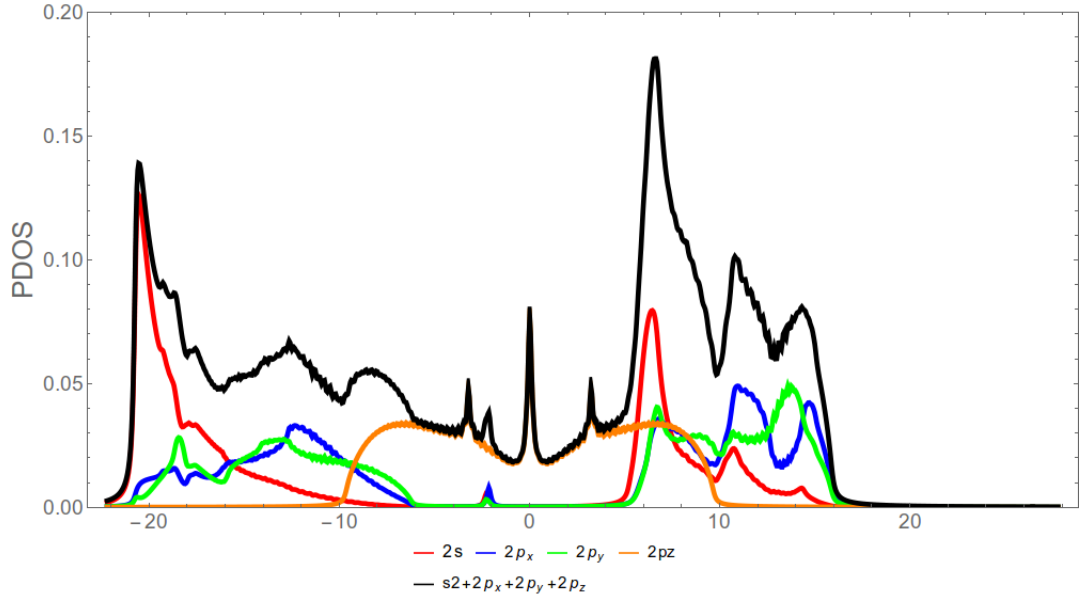


Figure 7.4: LDOS for an adjacent site to the vacancy, site 3 (α) sub lattice in Fig(7.1). The red, blue, green and orange curves are PDOS for $2s$, $2p_x$, $2p_y$ and $2p_z$ respectively. The black curve is the total DOS at site 3 which is the third nearest neighbor with respect to the vacancy. Because it is an α sublattice, one can see a peak in a Fermi level as we saw from site 1.

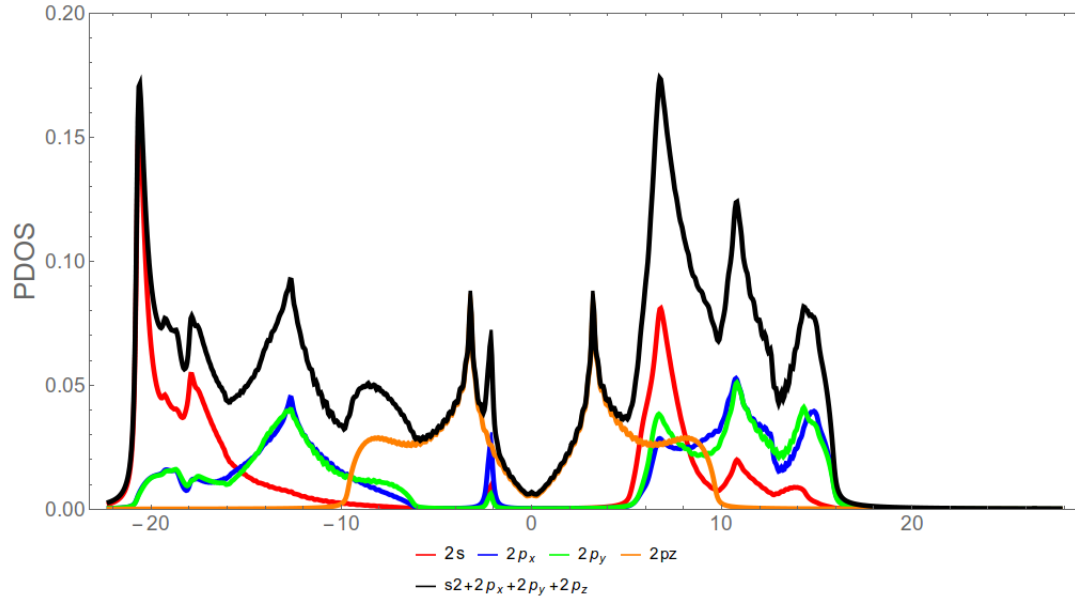


Figure 7.5: LDOS for an adjacent site to the vacancy, site 4 (α) sub lattice in Fig(7.1). The red, blue, green and orange curves are PDOS for $2s$, $2p_x$, $2p_y$ and $2p_z$ respectively. The black curve is the total DOS at site 4. Because site 4 is α sublattice in the graphene system, it can be seen there is a very small peak in the Fermi level. However it is not as big we saw on 1st and 3rd neighbor DOS.

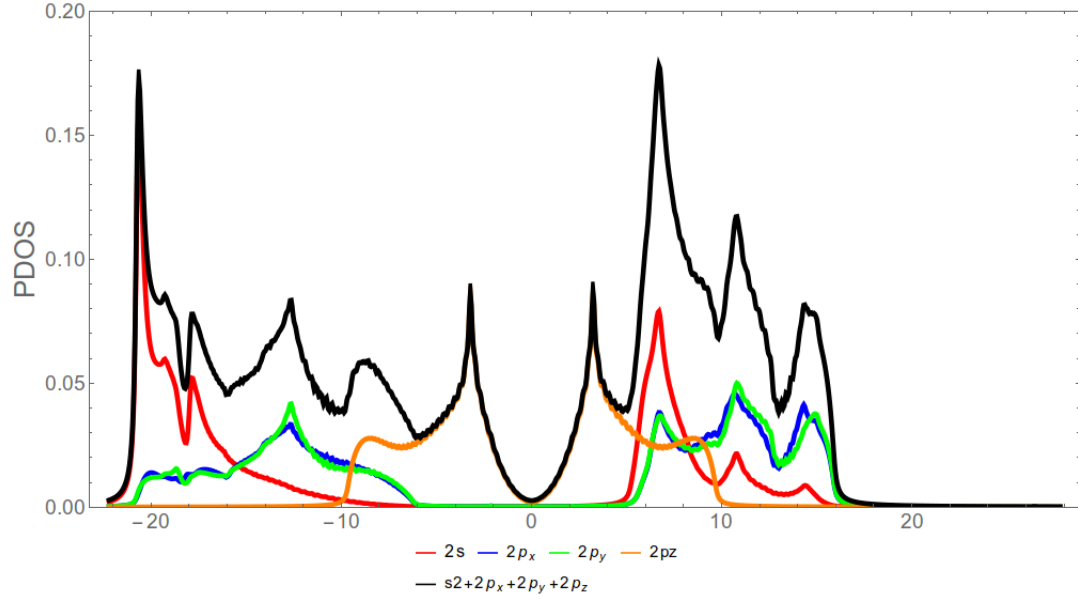


Figure 7.6: LDOS for an adjacent site to the vacancy, site 5 (β) sub lattice in Fig(7.1). The red, blue, green and orange curves are PDOS for $2s$, $2p_x$, $2p_y$ and $2p_z$ respectively. The black curve is the total DOS at site 5. It is the fifth nearest neighbor from the vacancy and is a β sublattice. The effect of vacancy is significantly less here compared to other sites. However, the DOS at Fermi level looks flat compared to the original one.

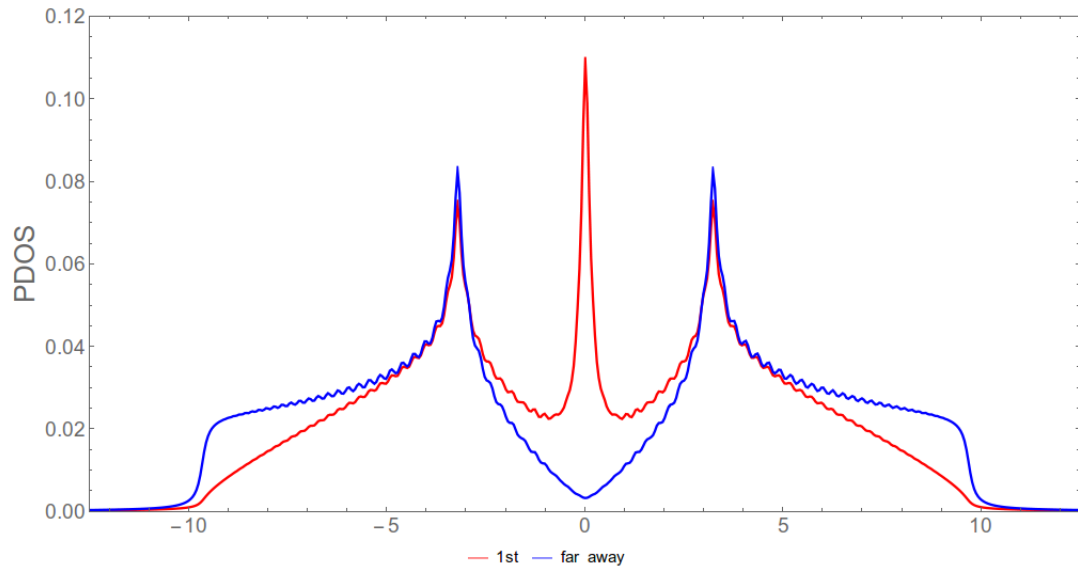


Figure 7.7: Only π LDOS at a site next to vacancy (Red) and at a site far-far away from it (Blue).

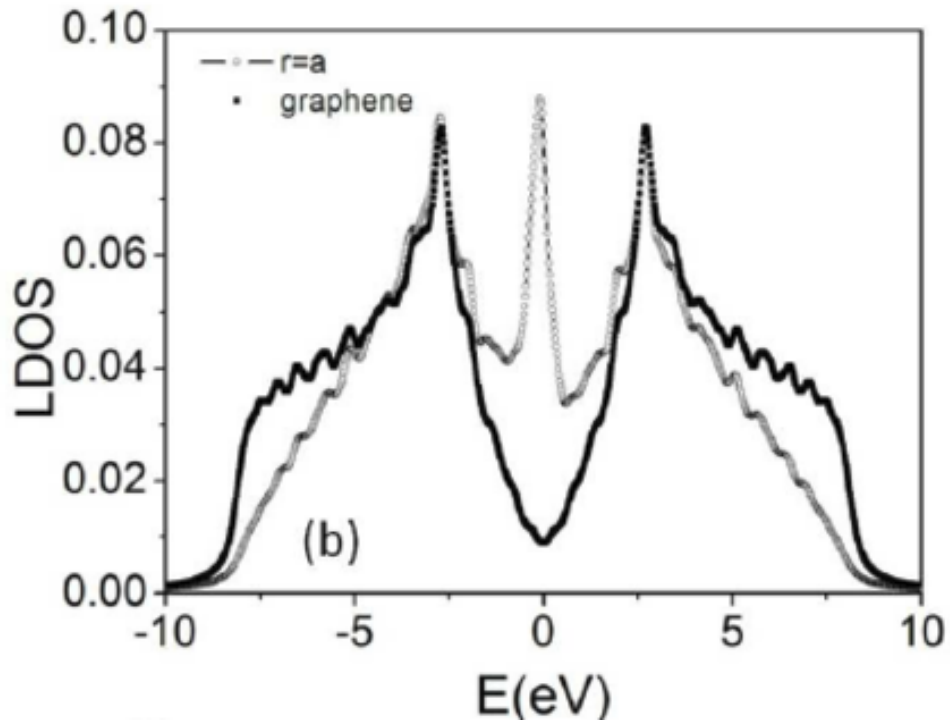


Figure 7.8: π LDOS at a lattice site next to the vacancy ($r = a$) and at a site far away from vacancy (black solid line)⁵.

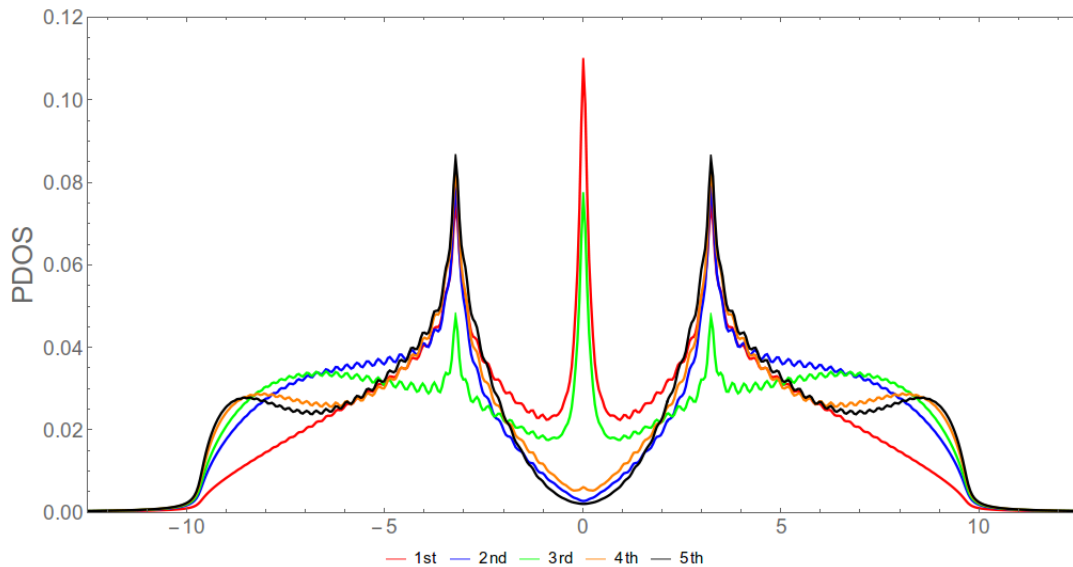


Figure 7.9: Only π LDOS of first five neighboring sites due to vacancy. Red, blue, green, orange and black are 1st, 2nd, 3rd, 4th and 5th neighbors respectively. Red, green and orange represent α sublattice whereas blue and black represent the β sublattice, the same kind where the vacancy was made.

Fig(7.9) above shows the π LDOS for first five neighboring sites that are adjacent to the vacancy. The LDOS at any site in the graphene can be found using Eqn(7.8). There is a peak that appears to be in the vicinity of Fermi energy in the energy spectrum. The local density of states shows a pronounced low-energy peak in the vicinity of the vacancy, indicating that the charge carriers are localized there⁵. There are no such peaks elsewhere in the bulk of the graphene sheet. This is similar to the dangling bond state that was observed at the edge. It occurs that the bond with the adjacent sites also behave as similar to that of a dangling bond because each neighboring sites are two-fold coordinated. The three-fold neighbor (site 3) LDOS graph is similar to the LDOS deep in the bulk of the graphene sheet except at the Van Hove singularities.

CHAPTER VIII

A SIMPLE MODEL OF GRAPHITE

8.1 Introduction

In this chapter I consider briefly the interaction of graphene layers in different graphite structures. Although the simple hexagonal graphite with layers stacked directly above one another does not necessarily occur in nature⁶, it is always useful to compare the theoretical model for the properties with other forms that exist. The interaction between layers in graphite-like materials dramatically changes their electronic properties due to the shift of the planes which makes it of interest to study the simple models, which can be extended later to explain different systems. I will limit my calculation to the π bands here too.

8.2 Method

In the model of Chap(V), the interaction between a site and any of its neighbors in a $2D$ plane is represented by the Hückel parameter. Fig(8.4) shows four different parameters for three different graphite structures. I will be using the Green's function technique to determine the DOS. The Hamiltonian is⁶:

$$\hat{H} = \sum_i |\phi_i\rangle \epsilon_i \langle \phi_i| + \sum_{i,j} |\phi_i\rangle V_{ij} \langle \phi_j| \quad (8.1)$$

where $|\phi_i\rangle$ is a Bloch symmetrized basis function that is localized at site i . The π calculation in this section involve V_{ij} being nonzero only for nearest and next nearest

neighbors. The quantity ϵ is the usual Hückel parameter which is taken to be $\epsilon_i = 0$.

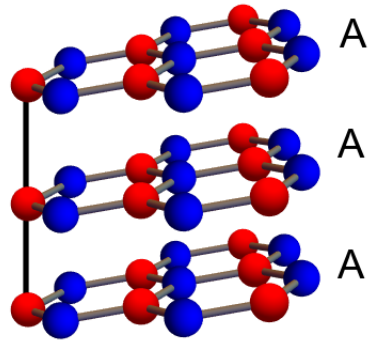


Figure 8.1: AA stacked graphene where two layers aren't shifted horizontally.

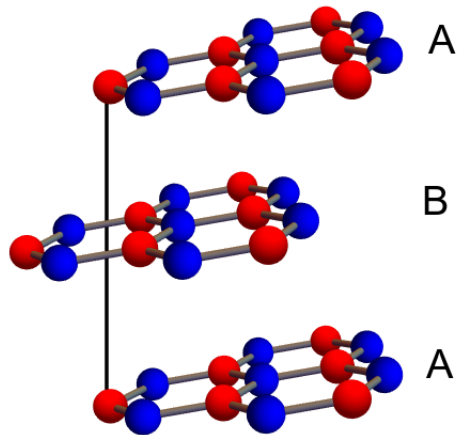


Figure 8.2: AB stacked graphene where two layers are shifted horizontally.

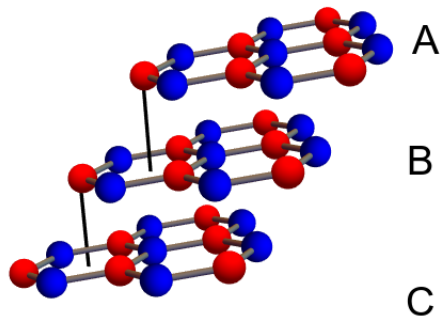


Figure 8.3: ABC stacked graphene where two layers are shifted horizontally.

I have already calculated the familiar π -orbital DOS for a graphene (graphite monolayer) where the nearest neighbor interaction described earlier in section of Chapter(5.5) to be V_1 as shown in Fig(8.4). After looking at the features of LDOS for a single layer, I see how the DOS changes after an addition of another layer using a transfer matrix method Dyson's equation,

$$G = G_0 + G_0 V G \quad (8.2)$$

where G_0 is the Green function matrix of a single layer graphene involving two Bloch symmetrized ($2p_z$) orbitals per unit cell, and G is the Green function matrix after a second layer is added through a connecting matrix V_2 . The layers 1 and 2 are identical to one another and are connected in a fashion shown in Fig(8.4). However, the calculation is still two dimensional. After the connection, the system is built up from a unit cell of four atoms, so this new matrix with dimensions 4×4 is obtained given as,

$$G_0 = \begin{pmatrix} g_{11} & g_{12} & 0 & 0 \\ g_{21} & g_{22} & 0 & 0 \\ 0 & 0 & g_{33} & g_{34} \\ 0 & 0 & g_{43} & g_{44} \end{pmatrix} \quad (8.3)$$

where,

$$g_{33} = g_{11}, \quad g_{34} = g_{12}, \quad g_{43} = g_{21}, \quad \text{and} \quad g_{44} = g_{22}.$$

The matrix G_0 is an uncoupled Green function matrix with block diagonals consist

of single layer graphene's unit cell Green functions as,

$$G_0 = \begin{pmatrix} g_{AA} & g_{AB} & 0 & 0 \\ g_{BA} & g_{BB} & 0 & 0 \\ 0 & 0 & g_{BB} & g_{BA} \\ 0 & 0 & g_{AB} & g_{BB} \end{pmatrix} \quad (8.4)$$

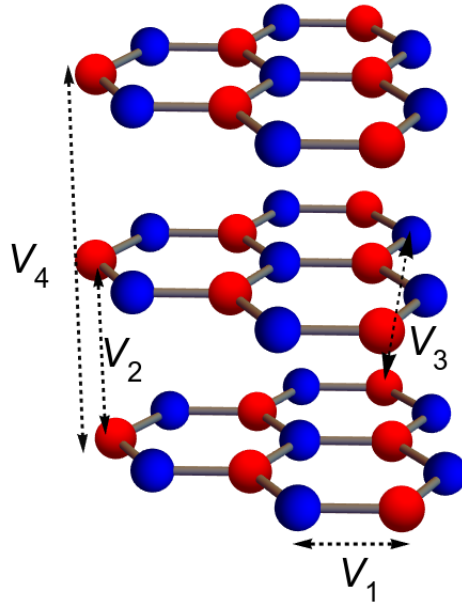


Figure 8.4: Tight binding matrix element V 's reproduced from (B. A. McKinnon)⁶

Fig(8.4) is a model that is reproduced from McKinnon⁶ which is a AA stacked graphene three layers. There are four different matrix elements V_1, V_2, V_3 and V_4 that represent the interaction between the layers. The term V_1 is tunneling matrix element inside the 2D graphene plane, which is the same as Hückel parameter I have been using in previous chapters. The term V_2 is the matrix element of the coupling between same sub lattices for two different layers in AA stacking mode whereas V_3 represents the coupling between different sublattices. The term V_4 is the coupling between first and third layer of same type sublattices.

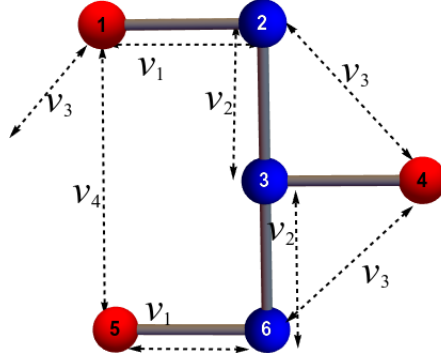


Figure 8.5: Schematic diagram of the connection.

Fig(8.5) represents a schematic diagram of the atoms involved during the calculation. The atomic sites 1 and 2 are connected by matrix element v_1 . The same argument allows for the atomic sites 5 and 6. The matrix element v_2 is used to interconnect two layers; site 2 with 3 and 3 with 4. Similarly, the matrix element v_3 is used to connect 2 with 4, 4 with 6 but with different sublattices. Finally, the term v_4 connects the first and third layer between the same atomic sublattices.

8.2.1 Two layers

First I will do the calculation based on only two layers. For that, the bridge or the connection matrix V is going to be only 4×4 ,

$$V = \begin{pmatrix} 0 & v_1 & 0 & 0 \\ v_1 & 0 & v_2 & v_3 \\ 0 & v_2 & 0 & v_1 \\ 0 & v_3 & v_1 & 0 \end{pmatrix} \quad (8.5)$$

The quantity v_2 is in fact the matrix element of the Hamiltonian between $2p_z$ states of two AA stacked grahene layers where the interplane spacing is found to be of 3.35\AA ⁶. So if G is the new matrix after the connection has been made which has a dimensions

of 4×4 ,

$$G(z, \vec{k}) = \left(\hat{I} - G_0 V \right)^{-1} \cdot G_0 \quad (8.6)$$

The $g_{11}(z)$ and $g_{12}(z)$ are the Green function matrix elements of an unperturbed unit cell of graphene given as in Eq(5.23),

$$g_{22} = g_{11} = \frac{z}{D(\vec{k}, z)(z^2 - 1)} \text{ and } g_{12} = g_{21} = \frac{1}{D(\vec{k}, z)(1 - z^2)}. \quad (8.7)$$

8.2.2 Three layers

Let's assume a system that is made of three layers of graphene. In such a case, the Green function matrix element made for two layers above can be used to build the Green function that would be made of 6 atoms with a dimensions of 6×6 ,

$$G_0 = \begin{pmatrix} G_{11} & G_{12} & G_{13} & G_{14} & 0 & 0 \\ G_{21} & G_{22} & G_{23} & G_{24} & 0 & 0 \\ G_{31} & G_{32} & G_{33} & G_{34} & 0 & 0 \\ G_{41} & G_{42} & G_{43} & G_{44} & 0 & 0 \\ 0 & 0 & 0 & 0 & g_{11} & g_{12} \\ 0 & 0 & 0 & 0 & g_{21} & g_{22} \end{pmatrix} \quad (8.8)$$

Let W be the connecting matrix between them which is given as,

$$W = \begin{pmatrix} 0 & 0 & 0 & 0 & v_4 & 0 \\ 0 & 0 & 0 & 0 & 0 & 0 \\ 0 & 0 & 0 & 0 & v_3 & v_2 \\ 0 & 0 & 0 & 0 & 0 & v_3 \\ v_4 & 0 & v_3 & 0 & 0 & 0 \\ 0 & 0 & v_2 & v_3 & 0 & 0 \end{pmatrix} \quad (8.9)$$

8.2.3 Results and Discussion

The values of v' s used are taken to be $v_2 = 0.35, v_3 = 0.035$ and $v_4 = 0.035$ from McKinnon⁶. The matrix is sparse and thus the new perturbed Green function matrix is given as,

$$\mathbf{G} = \left(\hat{I} - G_0 W \right)^{-1} \cdot G_0 \quad (8.10)$$

Thus obtained \mathbf{G} would be G_0 if one wants to add more layers.

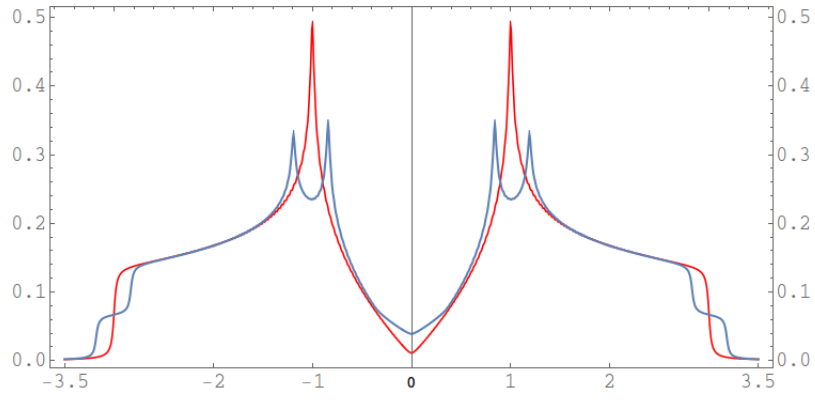


Figure 8.6: Density of states for one layer (Red) and two layers (Blue): $v_1 = 1$ and $v_2 = 0.35$ in Hückel units.

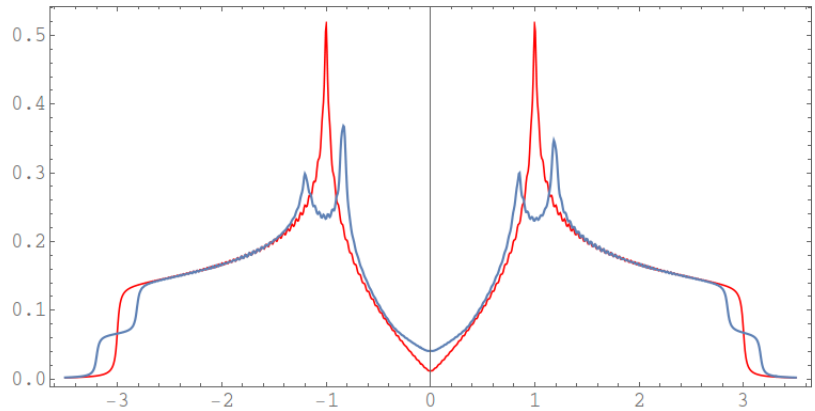


Figure 8.7: Density of states for one layer (Red) and three layers (Blue): $v_1 = 1$, $v_2 = 0.35$, $v_3 = 0.035$ and $v_4 = 0.035$ in Hückel units.

One can see from Fig(8.6), that the DOS contains the sum of two single-layer DOS, one shifted by $+v_2$ and another by $-v_2$ respectively. From this, one can expect

that when large number of layers are stacked directly upon each other above the first layer, the DOS would be the sum over an infinite number of monolayers shifted from $-v_2$ to v_2 . Also the DOS at the Fermi level is nonzero with respect to the single monolayer, thus making it semi-metallic to metallic. The larger value of the interaction v_2 increases the bandwidth by $2v_2$ ⁶. The higher interaction also increases the value of DOS at Fermi level making it nonzero. The interaction v_3 makes the DOS asymmetric as shown in Fig(8.7) about the fermi energy, which results from the fact that the lattice is no longer bipartite⁶. The parameter v_4 is the interplane interaction strength, which increases the effect that is already coming from v_2 .

CHAPTER IX

EXTENSION THEORY FOR GRAPHENE

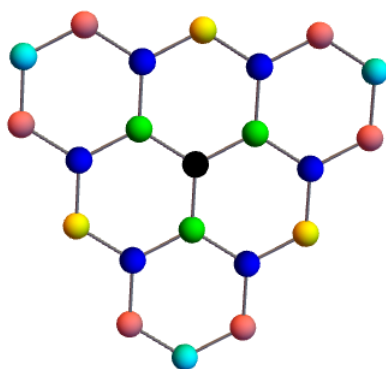


Figure 9.1: Schematic diagram of graphene showing its first five neighbors.

9.1 Extended Hamiltonian

In this Chapter, a method is adapted of using the known Green function for a given Hamiltonian H in order to find the Green function of a lattice Hamiltonian \tilde{H} in the algebra of H . The method does not depend on translational symmetry but on spectral methods³⁶. In Fig(9.1) is shown an atom (black) in a graphene sheet of infinite extent. Its first neighbors are green and second neighbors are dark blue. The yellow atoms are third neighbors in the chemical or graphical sense, but two different distances are involved. They are the third and fourth neighbors in terms of radial distance. The Green functions for the resolvent

$$G = (z - H)^{-1} \tag{9.1}$$

where H is nearest neighbor Hamiltonian are already known. In a simple π theory, the non-zero H entries scaled to are -1 for adjacent atoms and 0 for non-adjacent ones. Notice that the matrix H^p , or the p^{th} power of H , has non-zero entries only between the sites that are visualized in terms of p steps. In fact, the entry $(H^p)_{mn}$ is

$$(H^p)_{mn} = (-1)^p (\# \text{ of walks of exactly } p \text{ steps connecting } m \text{ to } n). \quad (9.2)$$

The adjacency matrix on the honeycomb lattice is $H^{(1)}$. This is zero except for sites adjacent. When i is adjacent to j , $H_{ij}^{(1)}$ is 1 , the π theory matrix element is $H_{ij} = -1$. Thus the normalized Hückel Hamiltonian is H is minus the adjacency matrix

$$H^1 = -H^{(1)}. \quad (9.3)$$

From Fig(9.1) there are ways, starting at the central atom, that one can take two steps. One way is going from the black atom to green and then to blue, the other way is going to green and coming back. All two steps walk are of one of these two types. This gives,

$$H^2 = H^{(2)} + 3I. \quad (9.4)$$

To take three steps, one can start from black, go to green then blue and come back to green. There are five different ways one can do it. The successive three steps would take you to the nearest third neighbor two times and one way to the nearest fourth neighbor one time.

$$H^3 = 5H - 2H^{(3)} - H^{(4)} \quad (9.5)$$

where $H^{(1)}$, $H^{(2)}$, $H^{(3)}$ and $H^{(4)}$ contain only first, second, third and fourth neighbor interactions respectively. Then,

$$H^{(1)} = -H, \quad H^{(2)} = H^2 - 3I, \quad \text{and} \quad H^{(3)} + \frac{1}{2}H^{(4)} = \frac{5}{2}H - \frac{1}{2}H^3$$

and so a more general Hamiltonian

$$\begin{aligned}\tilde{H} &= H + \alpha H^{(2)} + \beta \left(H^{(3)} + \frac{1}{2} H^{(4)} \right) \\ &= H + \alpha (H^2 - 3I) + \frac{\beta}{2} (5H - H^3).\end{aligned}\tag{9.6}$$

Further simplifying,

$$\tilde{H} = -3\alpha I + \left(1 + \frac{5}{2}\beta\right)H + \alpha H^2 - \frac{\beta}{2}H^3 = F(H).\tag{9.7}$$

9.1.1 Extended Green functions

The idea here³⁶ is to do the extension to a particular set of Hamiltonians having the same eigenfunctions as H . More generally the algebra generated by H consists of all Hamiltonians of the polynomial form

$$\tilde{H} = F(H) = a_0 + a_1 H + \dots + a_n H^n = \sum_{k=1}^n a_k H^k,\tag{9.8}$$

where the coefficients are real and the sum is over all independent powers of H up to some maximum n . It is assumed that the singularities of $f(z)$ lie outside a circle in the complex plane containing the eigenvalues of H . Consider $\tilde{G}(z)$ be the Greenian for the extended Hamiltonian \tilde{H} of Eq(9.7). Then,

$$\tilde{G}_{ij}(z) = \left\langle \phi_i \left| (z - \tilde{H})^{-1} \right| \phi_j \right\rangle\tag{9.9}$$

where \tilde{H} is indeed a polynomial in H . Since the extended Hamiltonian has the same eigenfunction as H ,

$$\tilde{H} |\psi_\mu\rangle = \left(-3\alpha + \left(1 + \frac{5}{2}\beta\right)E_\mu + \alpha E_\mu^2 - \frac{\beta}{2}E_\mu^3 \right) |\psi_\mu\rangle\tag{9.10}$$

And so,

$$\tilde{G}(z) = \sum_{\mu} |\psi_{\mu}\rangle \frac{1}{(z - (-3\alpha + (1 + \frac{5}{2}\beta)E_{\mu} + \alpha E_{\mu}^2 - \frac{\beta}{2}E_{\mu}^3))} \langle \psi_{\mu}| \quad (9.11)$$

which is the Greenian for the extended Hamiltonian. Thus, the Green function matrix elements are given by the spectral representation

$$\langle \phi_i | \tilde{G}(z) | \phi_j \rangle = \sum_{\mu} \langle \phi_i | \psi_{\mu} \rangle \frac{1}{(z - (-3\alpha + (1 + \frac{5}{2}\beta)E_{\mu} + \alpha E_{\mu}^2 - \frac{\beta}{2}E_{\mu}^3))} \langle \psi_{\mu} | \phi_j \rangle \quad (9.12)$$

Because $\tilde{G}(z)$ is analytic except where z enters the spectrum of \tilde{H} , the Cauchy formula gives,

$$\begin{aligned} \tilde{G}_{ij}(z) &= \frac{1}{2\pi i} \oint_{C_{\mu}} \sum_{\mu} \langle \phi_i | \psi_{\mu} \rangle \frac{dh}{(z - (-3\alpha + (1 + \frac{5}{2}\beta)h + \alpha h^2 - \frac{\beta}{2}h^3))} \frac{1}{h - E_{\mu}} \langle \psi_{\mu} | \phi_j \rangle \\ &= \frac{1}{2\pi i} \oint \frac{dh}{(z - (-3\alpha + (1 + \frac{5}{2}\beta)h + \alpha h^2 - \frac{\beta}{2}h^3))} \sum_{\mu} \langle \phi_i | \psi_{\mu} \rangle \frac{1}{h - E_{\mu}} \langle \psi_{\mu} | \phi_j \rangle \\ &= \frac{1}{2\pi i} \oint \frac{dh}{(z - (-3\alpha + (1 + \frac{5}{2}\beta)h + \alpha h^2 - \frac{\beta}{2}h^3))} G_{ij}(h) \\ &= \frac{1}{2\pi i} \oint \frac{G_{ij}(h) dh}{(z - (-3\alpha + (1 + \frac{5}{2}\beta)h + \alpha h^2 - \frac{\beta}{2}h^3))} \end{aligned} \quad (9.13)$$

In the later expression, the contour enclosed each singularity E_{μ} due to the eigenvalues of H but no zeros or singularities of $(z - F(h))^{-1}$. Deforming the contour, effectively turning it inside out, we can make the integral into one over a curve that encloses only the (much smaller number of) zeros of the denominator or singularities of $(z - F(h))^{-1}$ where in this case $F(h)$ is defined in Eq(9.7). Thus, including a minus, one has an integral counter-clockwise about the poles formed by the denominator

$$\tilde{G}_{ij}(z) = -\frac{1}{2\pi i} \oint \frac{G_{ij}(h) dh}{z - F(h)} \quad (9.14)$$

Consider $f(h, z)$ as a polynomial in h , the roots are then functions of z . Let $h_k(z)$ be the k^{th} root of $f(h, z) = 0$ where,

$$f(h, z) = (z - F(h)) = \frac{\beta}{2}h^3 - \alpha h^2 - \left(1 + \frac{5\beta}{2}\right)h + z + 3\alpha. \quad (9.15)$$

In general one can assume the poles are simple and treat the cases when this is not so as exceptional. Confluence of poles leads to additional van Hove singularities. Then assuming the singularities are all due to simple zeros of the denominator, one has

$$\tilde{G}_{ij}(z) = -\frac{1}{2\pi i} \oint \frac{G_{ij}(h)}{f(h, z)} dh = -\sum_{k=1}^n \frac{G_{ij}(h_k(z))}{f'(h_k(z))} \quad (9.16)$$

where

$$f'(h_k(z)) = \left. \frac{\partial f(h, z)}{\partial h} \right|_{h \rightarrow h_k(z)}. \quad (9.17)$$

9.1.2 Boundary region

To find the boundary between the region in (α, β) at fixed z where there are three real roots and the region where there is one, find the h discriminant by eliminating h between f and $\frac{\partial f}{\partial h}$ where

$$f = \frac{\beta}{2} h^3 - \alpha h^2 - \left(1 + \frac{5\beta}{2}\right) h + z + 3\alpha \quad (9.18)$$

$$\frac{\partial f}{\partial h} = \frac{3\beta}{2} h^2 - 2\alpha h - \left(1 + \frac{5\beta}{2}\right). \quad (9.19)$$

If the two polynomials have the common root h then the polynomial resultant of eliminating h between them has to be zero which gives the conditions for this:

$$\begin{aligned} g = & 27\beta^3 z^2 - \beta(16\alpha^3 + 36\alpha\beta(1 - 2\beta)) \\ & z - \beta(48\alpha^4 + 8\beta + 60\beta^2 + 150\beta^3 + 125\beta^4 + 4\alpha^2(1 + 32\beta + 13\beta^2)) = 0. \end{aligned} \quad (9.20)$$

Each real root z signifies an additional van Hove singularity. The zero set marks boundaries between where there are three real h roots and where there is only one h root.

There will be multiple roots of $g = 0$ in Eq(9.20) where the number of van Hove singularities changes by two. Further, it is appropriate to resolve the boundary between regions in $\alpha-\beta$ where there are two critical z values merge and become complex. The transitions where the critical z -values (van Hove singularities) merge are found from the discriminant of the quadratic:

$$g = 27\beta^3 z^2 - \beta(16\alpha^3 + 36\alpha\beta(1 - 2\beta))z - \beta(48\alpha^4 + 8\beta + 60\beta^2 + 150\beta^3 + 125\beta^4 + 4\alpha^2(1 + 32\beta + 13\beta^2)) = 0 \quad (9.21)$$

$$\frac{\partial g}{\partial z} = 54\beta^3 z - \beta(16\alpha^3 + 36\alpha(1 - 2\beta)) = 0 \quad (9.22)$$

and thus eliminating z altogether I get,

$$\beta^5 (4\alpha^2 + 6\beta + 15\beta^2) = 0 \quad (9.23)$$

The Eqn(9.23) gives the information about where the number of van Hove points changes and how many of the van Hove singularities exist for that particular model (α, β) . Thus there is a quintuple root along the line $\beta = 0$, and a simple root on the ellipse,

$$\beta^5 \left(\frac{4}{15} \alpha^2 + \left(\beta + \frac{3}{15} \right)^2 - \left(\frac{3}{5} \right)^2 \right) = 0 \quad (9.24)$$

9.1.3 Extended lattice results

The ellipse is centered at $(\alpha, \beta) = (0, -\frac{3}{15})$ with radii $r_\alpha = \sqrt{\frac{3}{20}}$, $r_\beta = \frac{3}{5}$. At the center of the ellipse $(\alpha, \beta) = (0, -\frac{3}{15})$, there is no transition as a function of z .

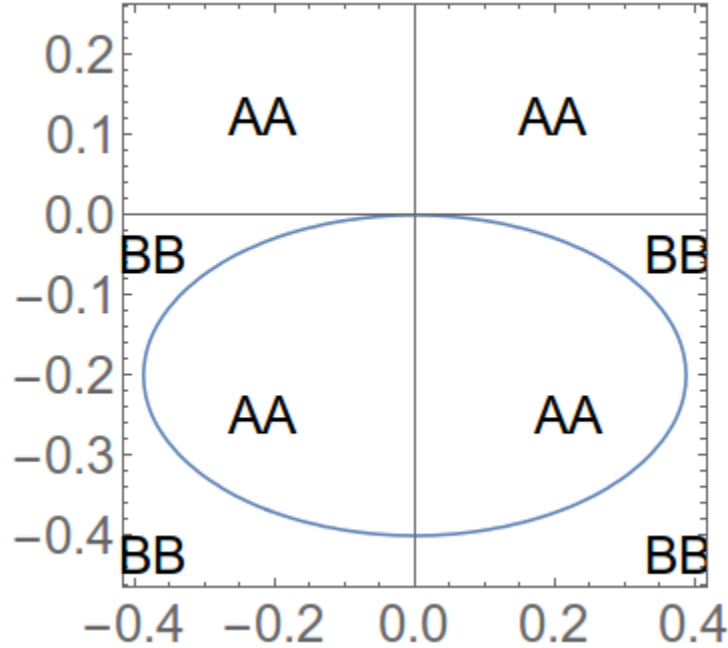


Figure 9.2: Contour plot of the ellipse formed by the resultant of g . The x -axis is α and y -axis is β .

Fig(9.2) represents the contour plot of the ellipse formed by the resultant of g centered at r_α and r_β . The number of van Hove singularities depends whether the α and β are taken inside or outside of the ellipse, i.e, region AA or BB.

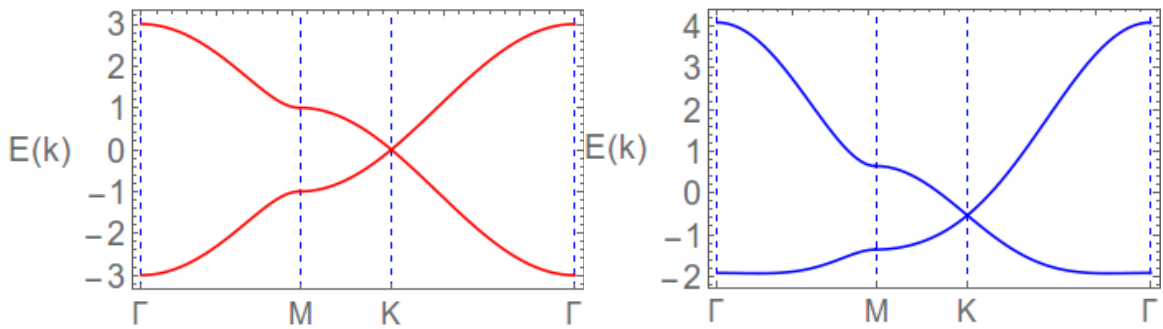


Figure 9.3: π -theory bands for an extended Hamiltonian. Red is when $(\alpha, \beta) = (0, 0)$ and blue is when $(\alpha, \beta) = (0.18, 0.003)$.

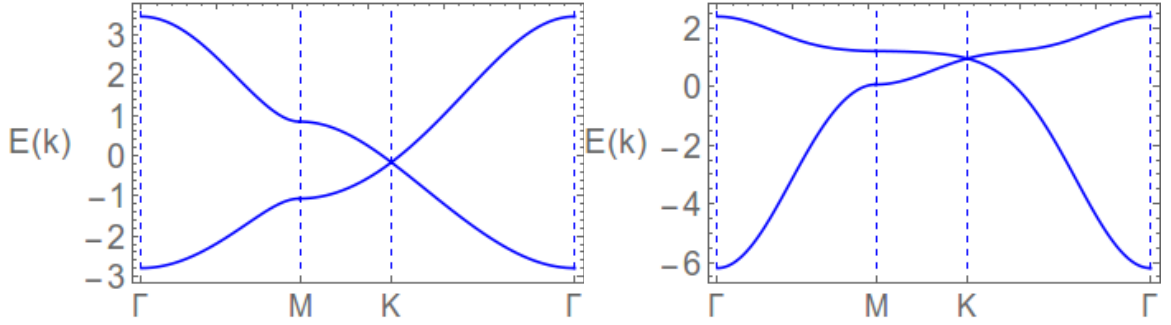


Figure 9.4: π -theory bands for an extended Hamiltonian. Left is when $(\alpha, \beta) = (0.055, -0.0215)$ and right is when $(\alpha, \beta) = (-0.3178, -0.2152)$.

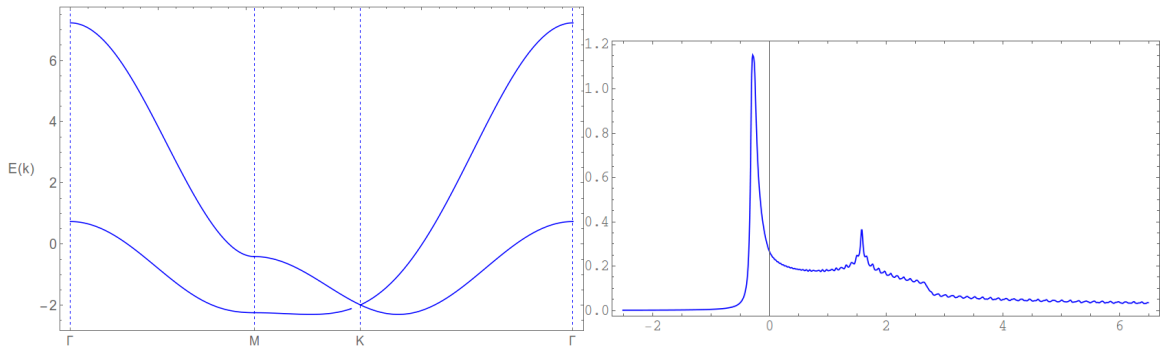


Figure 9.5: π -theory bands for an extended Hamiltonian in the BB region. On the left is some extra dips in the band so the number of van Hove singularities on the right changes at those points.

Fig(9.3) and Fig(9.4) represent four different bands for different values of α and β inside and outside the ellipse on the region AA. One can see how the band structures change for the chosen model parameters. This structural change in bands determines the number of van Hove singularities in the DOS curves. Now we will be looking at the DOS curves for those corresponding values of α and β .

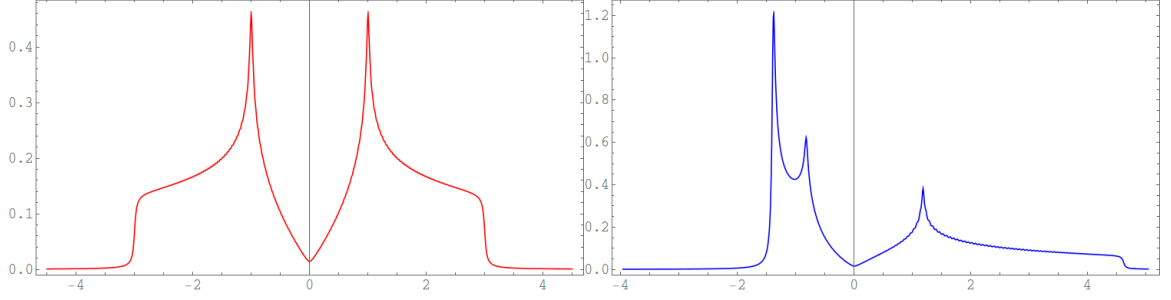


Figure 9.6: π theory bands for an extended Hamiltonian. Left is when $(\alpha, \beta) = (0, 0)$ and right is when $(\alpha, \beta) = (0.1798, 0.0002958)$ outside the ellipse.

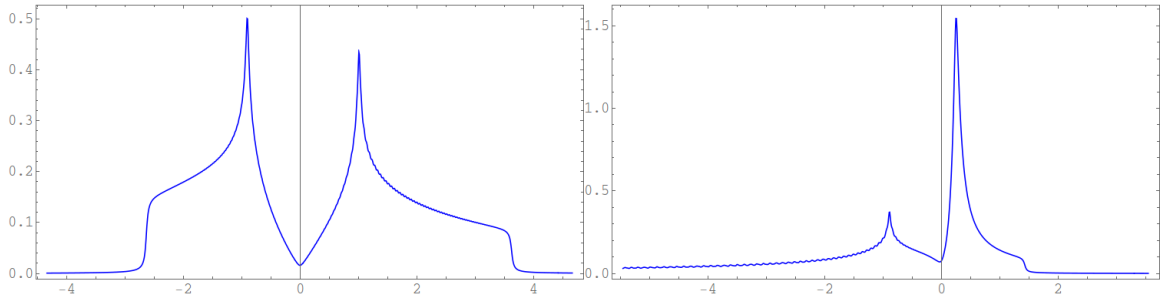


Figure 9.7: π theory bands for an extended Hamiltonian. Left is when $(\alpha, \beta) = (0.055, -0.0215)$ and right is when $(\alpha, \beta) = (-0.3178, -0.2152)$ inside the ellipse.

Inside the ellipse in region AA is contained the Hückel model $\alpha = \beta = 0$. All models inside the ellipse have bands similar to the Hückel model with no extra dips in the band structure as one can see in Fig(9.3) and Fig(9.4). Also there were no extra van Hove singularities induced for the range of the model parameters in the Fig(9.6) and Fig(9.7). In Fig(9.5), the value of $\alpha - \beta$ is taken outside the ellipse at region BB, thus giving a change in structure in the band with some extra dips. The bands show that they behave fictitiously metallic for that particular value of β . Also, one can notice that the number of van Hove singularities are changed as expected.

CHAPTER X

ADSORBATE SYSTEMS

Recently, there is interest in properties that are manifested on the nanometer scale of adsorbate systems. The project, preliminary results of which are reported here, is to study approximate electronic properties of molecules adsorbed on planar crystalline surfaces. The FAKE method or simply the π -orbital method provide a real space picture of the electronic interactions. So, I adapted these methods, which in principle can handle large, complex molecular structures with less computational effort, to calculate properties of adsorbed molecules.

An approximate one-electron Green function based on the FAKE method is constructed and used to find properties including the local or projected densities of states (LDOS or PDOS) of the adsorbates and substrates. So here for example, in this model, we look at the adsorption of an isolated hydrogen atom in various registries on the graphene surface. It is useful to see the effect of registry of the adsorbate atom in order to interpret experimental results and to explore graphene's potential applications. So the Green formalism is used to calculate PDOS including interactions of the hydrogen with the graphene. This is done by Löwdin partitioning of the FAKE Hamiltonian. Now I will describe the partitioning method.

10.1 Löwdin partitioning technique

If the Greenian $G(z)$ of the Hamiltonian H is split to a zero-order part $H^{(0)}$ representing a clean graphene sheet and a perturbation part V representing the adsorbate,

where $G^{(0)}(z)$ is for $H^{(0)}$, then the full $G(z)$ has to satisfy a Dyson-like relation $G(z) = G^{(0)} + G^{(0)}(z) V G(z)$ for which the solution is, $G(z) = \left(1 - G^{(0)} V\right)^{-1} G^{(0)}$. This solution reflects the partitioning of the Hamiltonian $H = H^{(0)} + V$ where V is the matrix that connects from one sub system of $H^{(0)}$ to other sub system. Quite generally, if A is a substrate and B is the set of atoms where V is non-zero or an adsorbate, in this case, then A and B represents two independent parts of the Hamiltonian, the Löwdin's partition technique³⁷ is,

$$\hat{H} = \begin{pmatrix} H_{AA} & V_{AB} \\ V_{BA} & H_{BB} \end{pmatrix} = \begin{pmatrix} H_{AA} & H_{AB} \\ H_{BA} & H_{BB} \end{pmatrix}, \quad (z\hat{I} - \hat{H})\hat{G} = \hat{I} \quad (10.1)$$

so that,

$$\begin{aligned} \left(z \begin{pmatrix} I_{AA} & 0 \\ 0 & I_{BB} \end{pmatrix} - \begin{pmatrix} H_{AA} & H_{AB} \\ H_{BA} & H_{BB} \end{pmatrix} \right) \begin{pmatrix} G_{AA} & G_{AB} \\ G_{BA} & G_{BB} \end{pmatrix} &= \begin{pmatrix} I_{AA} & 0 \\ 0 & I_{BB} \end{pmatrix}, \\ \begin{pmatrix} zI_{AA} - H_{AA} & -H_{AB} \\ -H_{BA} & zI_{BB} - H_{BB} \end{pmatrix} \begin{pmatrix} G_{AA} & G_{AB} \\ G_{BA} & G_{BB} \end{pmatrix} &= \begin{pmatrix} I_{AA} & 0 \\ 0 & I_{BB} \end{pmatrix}. \end{aligned} \quad (10.2)$$

H_{AA} , H_{BB} are the unperturbed Hamiltonians of A and B where as H_{AB} and H_{BA} the interaction Hamiltonians (perturbations of some kind). They are also V_{AB} and V_{BA} in the matrix V which is purely off diagonal with $V_{AB} = V_{BA}^\dagger$. Then,

$$\begin{aligned} (zI_{AA} - H_{AA})G_{AA} - H_{AB}G_{BA} &= I_{AA}, \\ (zI_{AA} - H_{AA})G_{AB} - H_{AB}G_{BB} &= 0, \\ -H_{BA}G_{AA} + (zI_{BB} - H_{BB})G_{BA} &= 0, \\ -H_{BA}G_{AB} + (zI_{BB} - H_{BB})G_{BB} &= I_{BB}. \end{aligned} \quad (10.3)$$

From Eq(10.3)(line 3),

$$\begin{aligned}
-H_{BA}G_{AA} + (zI_{BB} - H_{BB})G_{BA} &= 0, \\
(zI_{BB} - H_{BB})G_{BA} &= H_{BA}G_{AA}, \\
G_{BA} &= (zI_{BB} - H_{BB})^{-1}H_{BA}G_{AA}.
\end{aligned} \tag{10.4}$$

Putting G_{BA} back into Eq(10.3)(line 1),

$$\begin{aligned}
(zI_{AA} - H_{AA})G_{AA} - H_{AB}(zI_{BB} - H_{BB})^{-1}H_{BA}G_{AA} &= I_{AA}, \\
\left((zI_{AA} - H_{AA}) - H_{AB}(zI_{BB} - H_{BB})^{-1}H_{BA}\right)G_{AA} &= I_{AA}.
\end{aligned} \tag{10.5}$$

But ,

$$\begin{aligned}
(zI_{BB} - H_{BB})^{-1} &= g_{BB} \\
\therefore \left((zI_{AA} - H_{AA}) - H_{AB}g_{BB}H_{BA}\right)G_{AA} &= I_{AA} \\
(zI_{AA} - H_{AA})\left(I_{AA} - \frac{1}{zI_{AA} - H_{AA}}H_{AB}g_{BB}H_{BA}\right)G_{AA} &= I_{AA} \\
(zI_{AA} - H_{AA})\left(I_{AA} - g_{AA}H_{AB}g_{BB}H_{BA}\right)G_{AA} &= I_{AA} \\
\left(I_{AA} - g_{AA}H_{AB}g_{BB}H_{BA}\right)G_{AA} &= (zI_{AA} - H_{AA})^{-1} = g_{AA} \\
G_{AA} &= \left(I_{AA} - g_{AA}H_{AB}g_{BB}H_{BA}\right)^{-1}g_{AA}
\end{aligned} \tag{10.7}$$

Similary replacing $A \rightarrow B$ and $B \rightarrow A$ yields

$$G_{BB} = \left(I_{BB} - g_{BB}H_{BA}g_{AA}H_{AB}\right)^{-1}g_{BB}. \tag{10.8}$$

Therefore one has the two complementary equations,

$$G_{AA} = \left(I_{AA} - g_{AA}H_{AB}g_{BB}H_{BA}\right)^{-1}g_{AA}, \tag{10.9}$$

and

$$G_{BB} = \left(I_{BB} - g_{BB} H_{BA} g_{AA} H_{AB} \right)^{-1} g_{BB}. \quad (10.10)$$

10.2 Chemisorption of Hydrogen

10.2.1 Hydrogen right on top of carbon

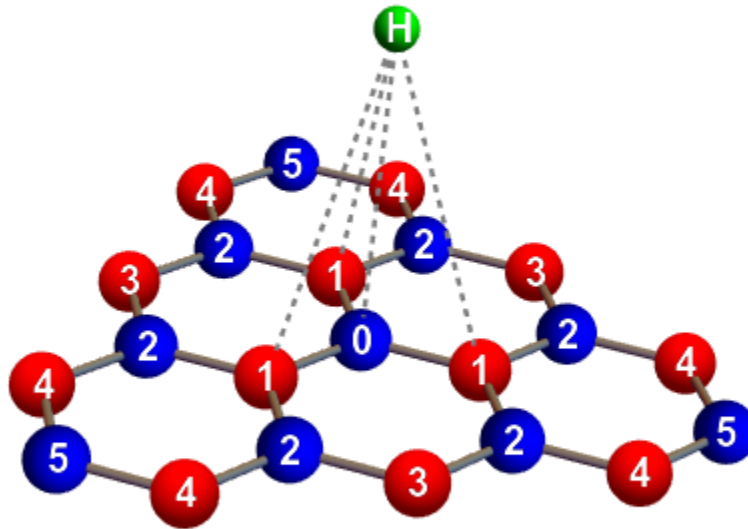


Figure 10.1: Schematic diagram of a Hydrogen atom placed right on top of a carbon atom, namely atom 0. The labels 1,2,3,4,5 are the first, second, third, fourth and fifth neighbors with respect to carbon 0.

The adsorption of a single H atom on graphene-like surfaces has been well studied both at experimental and theoretical levels³⁸⁻⁴¹. Here, we look at adsorption of an isolated Hydrogen atom in various positions on the graphene surface. For this calculation, Hydrogen was placed at a distance of 2.5\AA above the carbon, corresponding

to measurement, and we studied the characteristic patterns induced in the electronic projected density of states of both hydrogen and various graphene orbitals.

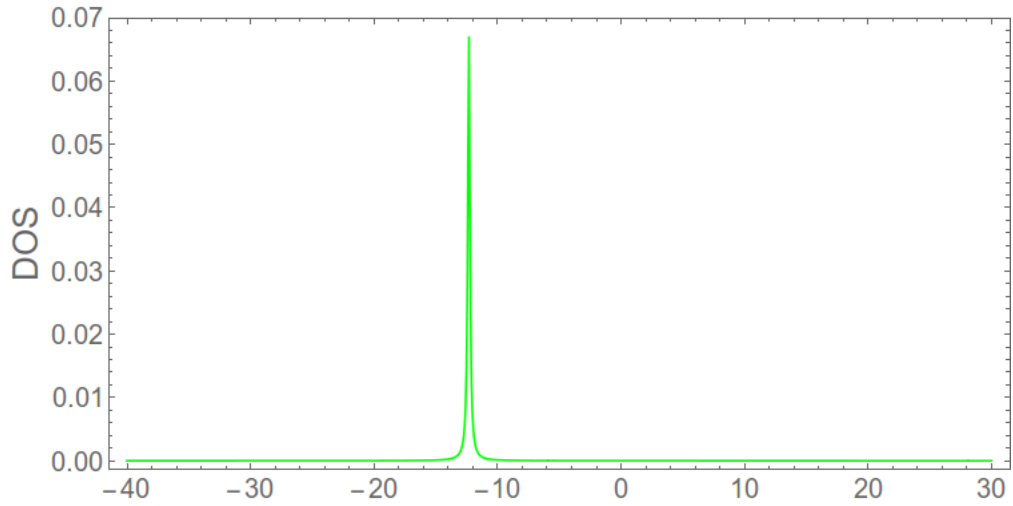


Figure 10.2: FAKE DOS for a single isolated hydrogen atom without coupling to the substrate.

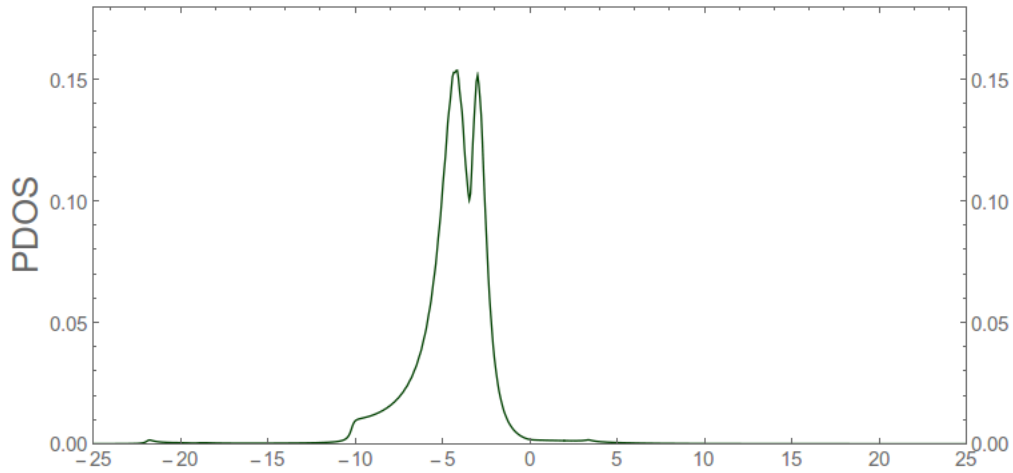


Figure 10.3: FAKE PDOS of hydrogen atom that is located at a distance of 2.5\AA . A splitting in its energy level can be seen when it is coupled to a carbon atom as shown in Fig(10.1). The H atom is directly on top of carbon 0 is allowed to interact with 22 carbon atoms as shown.

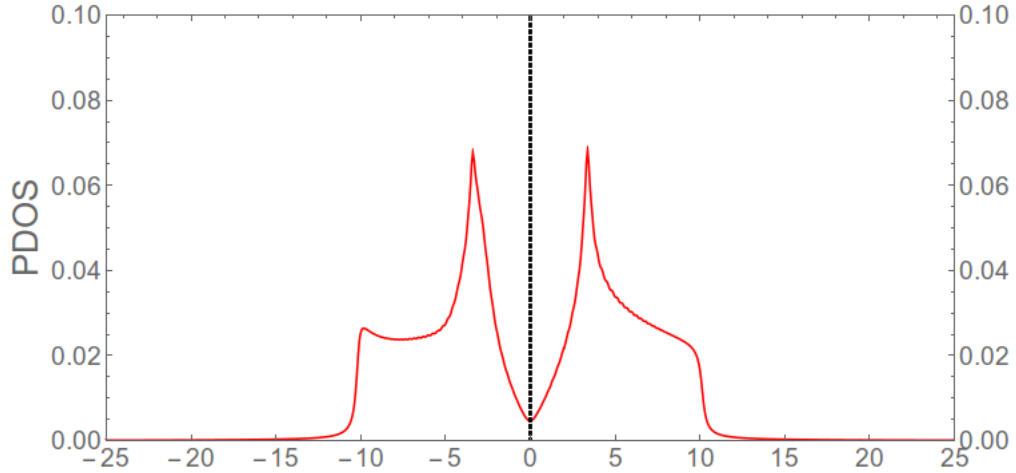


Figure 10.4: π theory: p_z PDOS of an adjacent carbon atom, site 1 at Fig(10.1). Here the zero of the DOS is still located at the Fermi energy, which is taken as zero on the graphene. There is also a change in van Hove singularity on the valence band.

In the figures shown from the calculations presented here, you will notice the DOS does not appear to go to zero at the energy of the Dirac cone ($E = 0$). This is due in part to a numerical error in zone integration but mostly to curve smoothing inherent in the graphics software. When both of these are taken into account the DOS goes to zero at the cone energy.

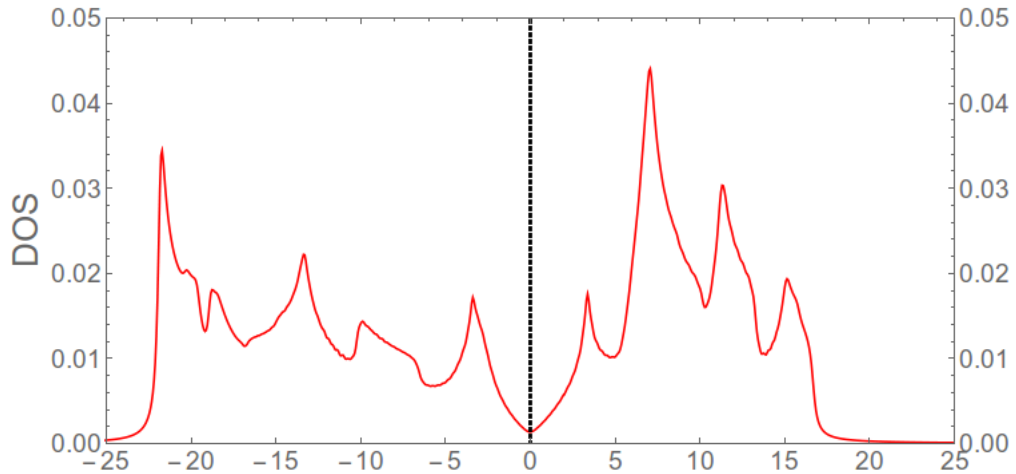


Figure 10.5: FAKE DOS of an adjacent carbon atom, site 1 at Fig(10.1). The DOS is not significantly changed anywhere in the energy spectrum.

Here, we try to study those effects of such defects on LDOS that are found to be

related to magnetization on a graphene sheet⁵. Within the FAKE model, the mean charge density is computed self-consistently,

$$\langle q_i \rangle = \int \rho_i f(E - E_f) dE \quad (10.11)$$

where ρ_i is the partial density of states, and $f(E - E_f)$ is the Fermi function. This self-consistent charge provides the local density of states on each atom. In essence the charge dependent part of H_{ii} is an on-site Hubbard interaction⁴². During the self-consistent calculation, the number of spin-up and spin-down electrons are fixed for graphene. In a pristine graphene, the number of A and B sublattices are equal to each other. So the net charge is equal to zero. By putting a hydrogen above graphene, the lattice distortion takes place. There is an amount of charge transfer that takes place between the two subsystems. The adsorbent carbon is pushed a little above by its neighbors towards hydrogen changing the hybridization to sp^3 . In a 2D graphene plane, a vacancy is created at a site where the carbon was previously localized. This implies that the number of atoms $A(N_A)$ and $B(N_B)$ are not equal anymore. The total spin of the ground state is given by Lieb's theorem⁴³

$$S = \frac{1}{2}(N_A - N_B). \quad (10.12)$$

Lieb's theorem shows that in the attractive Hubbard model, the ground state has the spin angular momentum $S = 0$ for every electron filling. However in the repulsive case, with a bipartite lattice and a half-filled band the spin is given by Eq(10.12) and the ground states are unique in both the cases.

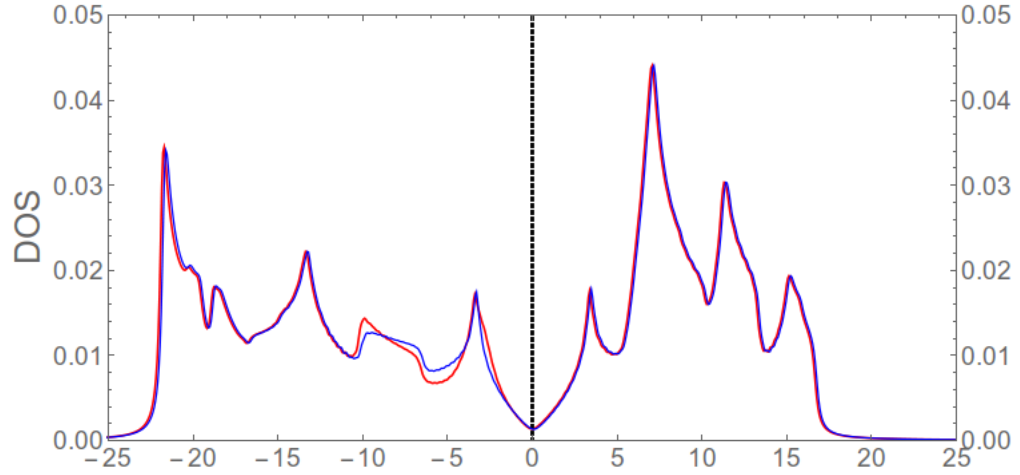


Figure 10.6: The DOS of the first neighbor is changed from blue to red. The change is coming from p_z contribution that was seen in Fig(10.4).

So this induces the magnetic moment that will be localized around the distortion plane. If the attachment carbon is in sublattice A , the magnitude of the induced magnetic moment in sublattice B is larger than in A ⁵. This tells that the effective magnetic interactions between spins in opposite sublattices is antiferromagnetic but on the same sublattice is ferromagnetic.⁴⁴⁻⁴⁷.

10.2.2 Hydrogen above the center of a ring

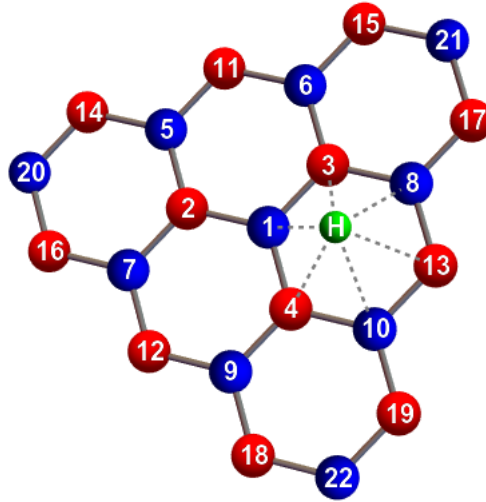


Figure 10.7: An isolated atomic hydrogen is placed at a distance of 2.5 \AA above from the center of 2D graphene ring.

In this section, I computed the LDOS of graphene and hydrogen when the hydrogen was positioned to be at 2.5 \AA above the center of the cyclic ring as opposed to directly on top of a carbon. Thus induced different DOS at different sites is shown as follows:

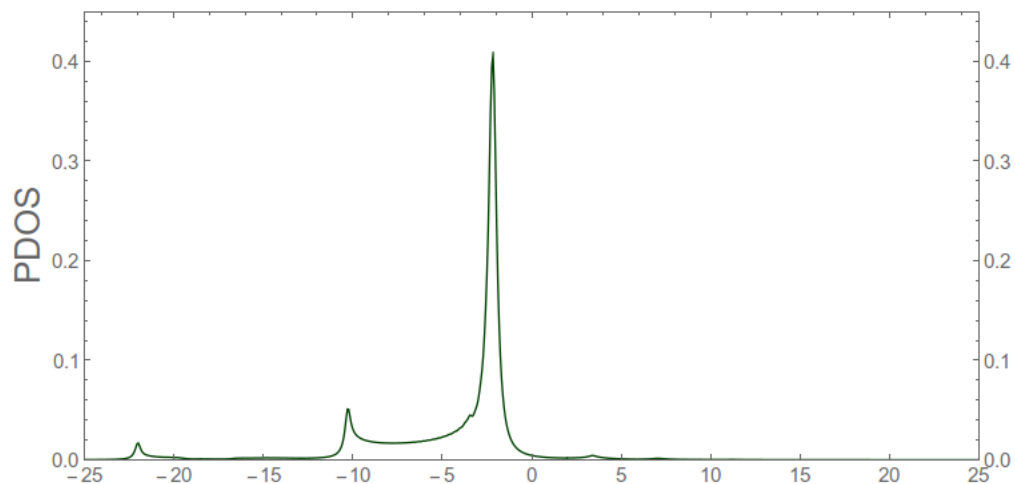


Figure 10.8: FAKE PDOS on hydrogen. There are two more peaks that have arisen in the valence part after the coupling of hydrogen with graphene.

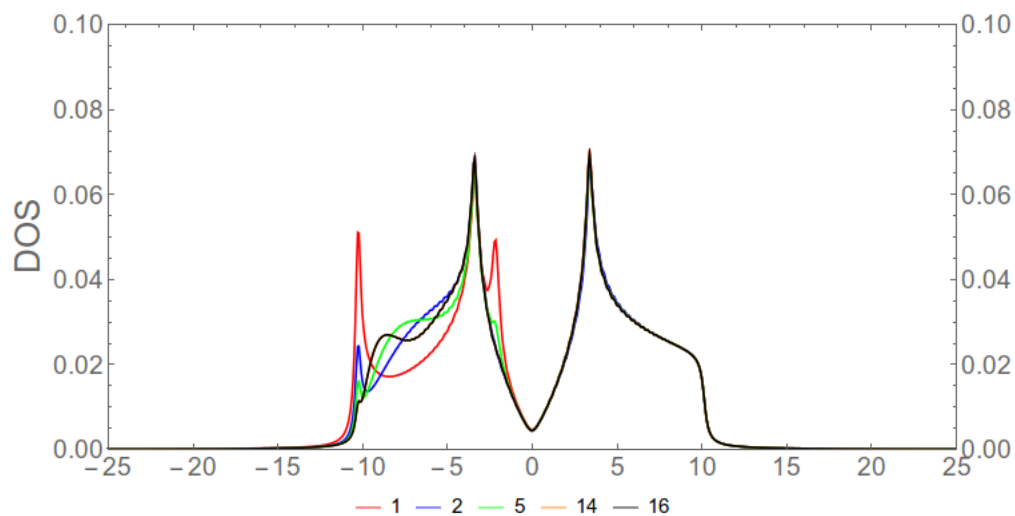


Figure 10.9: π theory. The induced π DOS on adjacent carbon atoms due to the coupling of hydrogen at a distance of 2.5\AA above the center of the ring in the sites 1, 2, 5, 14, and 16 as shown in Fig(10.7).

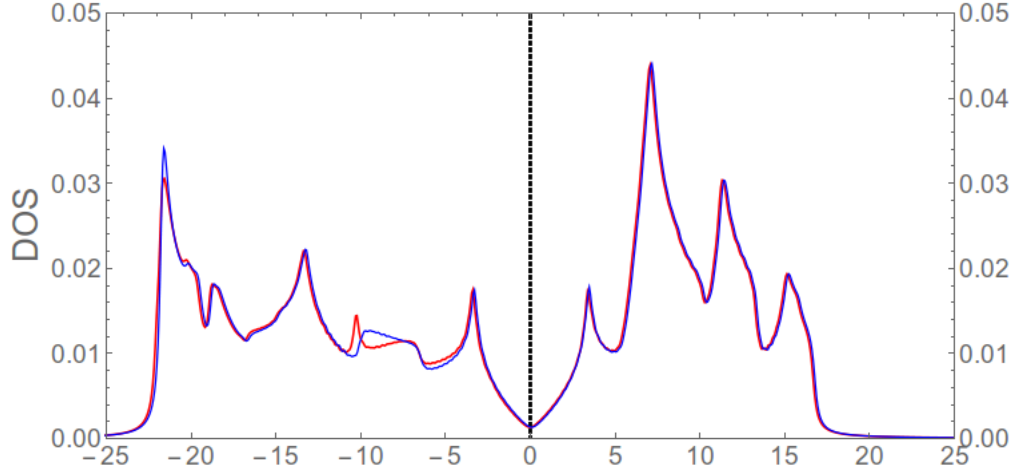


Figure 10.10: FAKE DOS: The DOS of one of the carbon site inside the ring has changed from blue to red. It is seen that there is a small change in DOS which is coming from the contribution of p_z orbital. The other PDOS stays the same.

In Fig(10.8), Fig(10.9), Fig(10.10), the DOS that is induced after the substrate is coupled with an isolated H as shown in Fig(10.7) is shown. There are two new peaks that appear below the peak for hydrogen in Fig(10.8). In the substrate, there is a splitting of energy in the previous van Hove singularity in the valence band. There is another new peak appearing in the neck of the DOS. Looking at the FAKE DOS, the σ states haven't changed significantly. The red peak shows that it is appearing from the π contribution that we explained above.

10.2.3 Hydrogen above and in between the bonds

In this section, the hydrogen was placed at a distance of $2.5A^\circ$ above the bond between the two sublattices as shown in Fig(10.11).

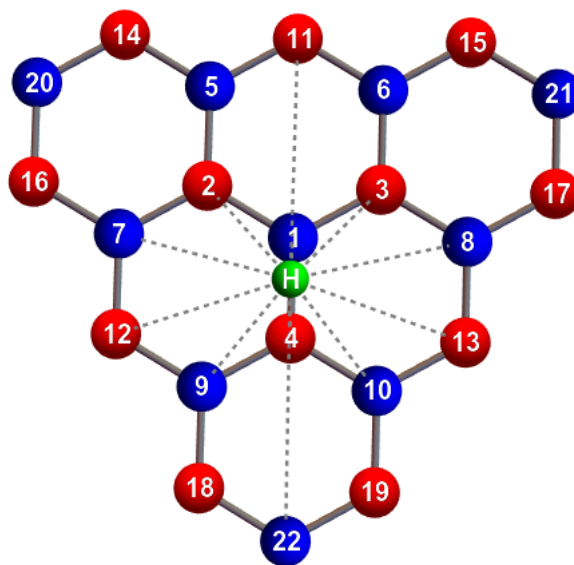


Figure 10.11: An isolated hydrogen placed 2.5\AA above the mid distance between site 1 and 4.

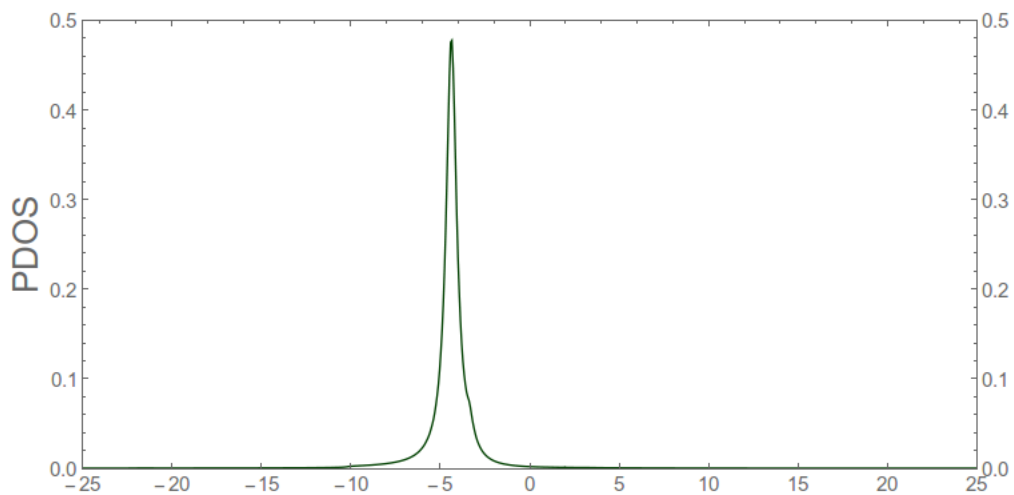


Figure 10.12: The PDOS of the hydrogen from the kind of configuration described in Fig(10.11) is only shifted and broadened from atomic hydrogen .

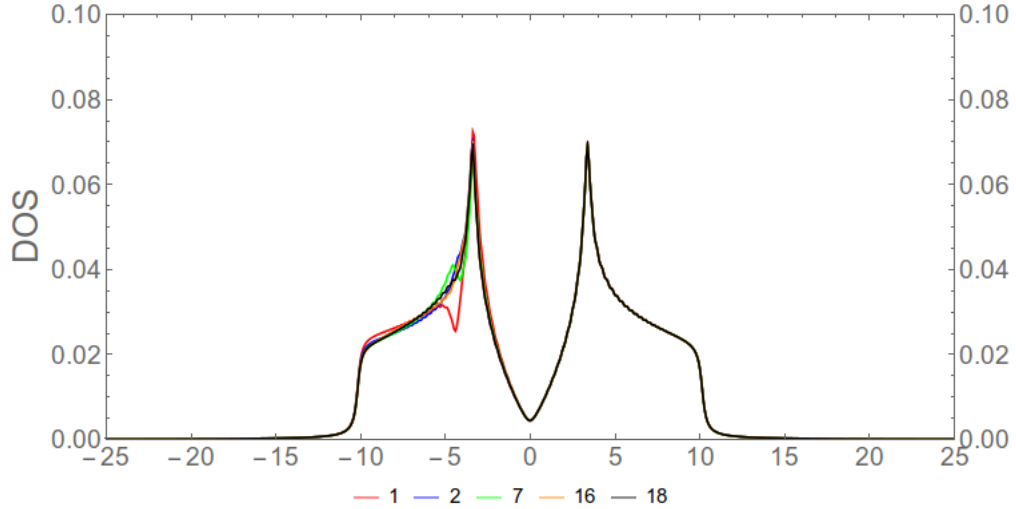


Figure 10.13: The π DOS at sites 1, 2, 7, 16, and 18. Only the first neighbor seems to change its shape. However, the change is not as significant as from other registries shown above.

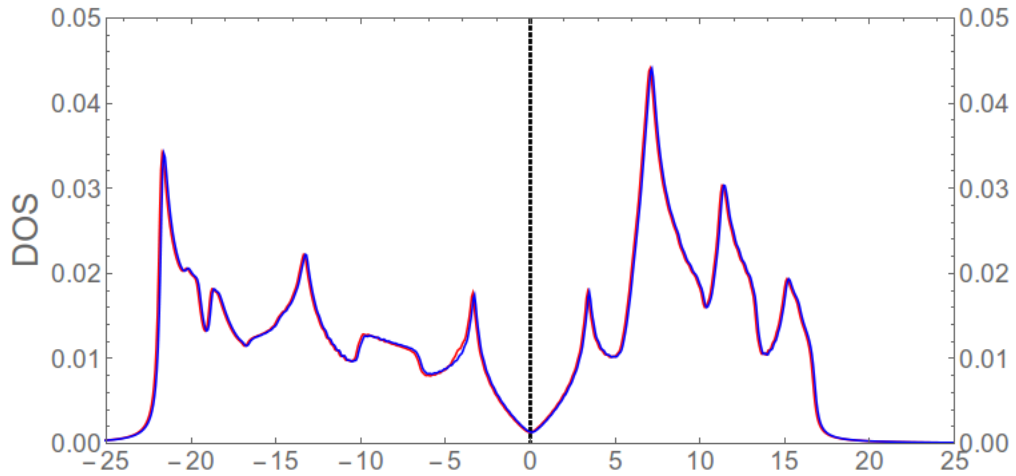


Figure 10.14: The total DOS at site 1. Blue is the uncoupled DOS whereas the red is new coupled DOS. There is no change in total DOS for this kind of registry at all.

Fig(10.12), Fig(10.13), Fig(10.14), show the DOS of hydrogen and carbons after the coupling with the registry described above is made. The DOS for hydrogen doesn't change significantly, still being the same. Also for carbon, only the first neighbor DOS changes in between the neck and the van Hove singularity observed before in the valence band. The other characteristics remain the same. The changed contribution is mainly coming from π state. The FAKE DOS shows that the total DOS remains

unchanged with this type of registry because the DOS before and after adsorbing the hydrogen appear to be the same.

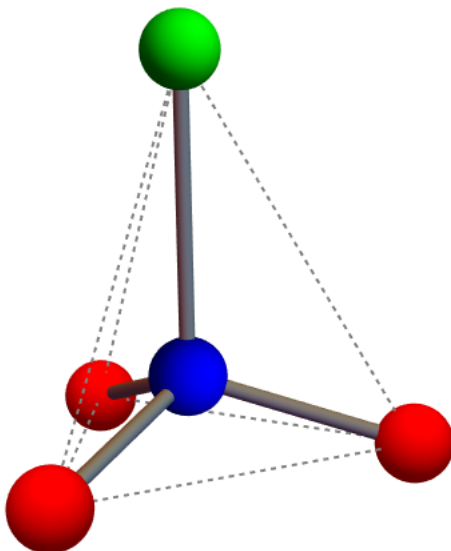


Figure 10.15: The distortion of the lattice due to displacement of the adsorbent carbon atom and rehybridization from its initial sp^2 hybridization to sp^3 . The H atom (above) distorts the carbon lattice and causes rehybridization. The rehybridization describes approximately the local change in the Hamiltonian

It was anticipated that at very low temperature ($<30\text{K}$), H atoms would not stick to pristine graphene⁴⁸. However, it was shown experimentally that hydrogen atoms do stick on graphene surface when emitted from a 2000 K thermal source⁴⁹. Most of the experiments use a hot (1600 K - 2200 K) H atomic beam to chemisorb H atoms to graphene^{50,51}. In a recent study of adsorbate-induced magnetization, Gonzalez et al²⁸ removed effectively a p_z orbital from the π manifold via this rehybridization mechanism at the location of a single carbon atom by adsorption of a single H atom experimentally. Doing this, the initial sp^2 hybridization plus p_z of the corresponding carbon atom was effectively changed due to lattice distortion to sp^3 hybridization⁵²⁻⁵⁶. The new configuration makes a path for charge transfer through an initially stable graphene. It is important to model and observe the smallest structural change that is thus induced in the substrate. The defects that arise from the chemisorption have

been expected to lead to a better theoretical understanding of graphene⁵.

In more detail, it was assumed that the chemi-adsorbed H atom causes an effective vacancy in the π manifold of the unperturbed graphene plane. This vacancy fails to preserve the three-fold symmetry of the individual adjacent atoms reducing it to two-fold. So I have studied the characteristics of such graphene lattice irregularities by including an adsorbed hydrogen atom on a graphene substrate within a FAKE calculation and also in just the π -orbital approximation. In a study of long-range electronic effects on graphene due to adsorbed hydrogen atoms, Ruffieux et al.^{40,57} deposited a single atom of hydrogen at an apparent height of $2.5A$, as suggested by the scanning tunneling microscopy, which showed surrounded by a complex threefold pattern. By comparing with the DFT studies and simulated STM images, the resolution was good enough to identify the adsorbate as a single H site with either the $\alpha = 1$ or 2 atomic sublattices of the graphene. Actually, I think this means they were able to identify which sublattice the H was on and call that, let's say the $\alpha = 1$ sublattice. Then they could compare neighbors on the $\alpha = 1$ or $\alpha = 2$ sublattices with the pure graphene case. The narrow peaks in the density of states can be observed also at E_f from the DFT calculations⁵². This motivates us studying DOS on different sites within the area of FAKE calculation.

CHAPTER XI

SUMMARY AND DISCUSSIONS

In Chapter I, implemented the FAKE method developed by Frank Harris et. al to form a model Hamiltonian for molecules and solids that contain carbon, hydrogen, oxygen, nitrogen and fluorine. The results are then compared with those of Snyder and Basch²⁴ first-principle methods and are found to be satisfactory. The method is advantageous over other methods like DFT and Monte Carlo simulations because it requires less time to study large molecules and is expected to be advantageous also for solids.

In Chapter II, I used the method of Least Squares to express a standard Slater-type atomic orbital (STO) basis in terms of three gaussian type orbitals. The exponents and coefficients for $1s$, $2s$, $2p$ and $3d$ orbitals are optimized and are given in Table(2.1). Also, I found generating functions for computing the overlap and kinetic energy integrals for gaussian type orbitals in three dimensions.

Chapter III focuses on tight-binding method in general which is an approximation method that prove to be useful especially for qualitative understanding of the eigenfunctions. I have applied it as a formalism to study graphene which is the substrate solid for my research on adsorbate because tight binding gives a localized description of the valence and low-lying conduction bands and states appropriately. The FAKE method is adapted to give the solid state matrix elements.

In Chapter IV, I study electronic properties of a simple 2D graphene using tight-binding within the FAKE model. This chapter reviews the use of lattice translation and reciprocal lattice vectors. I have used Bloch's theorem to write eigenstates us-

ing a symmetry-reduced lattice Hamiltonian. The resulting band diagrams compare reasonably well with first principle linear augmented plane wave(LAPW) method calculations by Kogan and Nazarov².

In Chapter V, the Green functions are applied to a Schrödinger equation that becomes a matrix representation in a Bloch symmetrized atomic orbital basis set in the LCAO formalism. The Green functions are used to compute local or projected densities of states. I have applied the method of Brillouin zone Gaussian quadrature points of Monkhorst and Pack to compute charge and produce LDOS graphs for graphene.

In Chapter VI, I looked at a projection method for the LDOS of a graphene with edges and tears. LDOS and spectral density graphs Fig(6.9) and Fig(6.10) were found for the edge states and compared to others' results in the literature. The strong peak right at the Fermi level was observed in contrast to the LDOS of a graphene for an infinite sheet. The contour plot of the spectral densities shows an area that has a high probability of finding the electrons.

In Chapter VII, a model calculation was developed for an imperfection in graphene. I have looked at the electronic structure near a missing carbon atom resulting in a vacancy in the graphene sheet. In order to create a vacancy, the potential at that site is allowed to be infinite so as to push the electrons out the region making a hole. In this way, the induced local density of states at any site in the lattice can be observed.

In Chapter VIII, I consider briefly the interaction of graphene layers in different graphite structures or graphene multilayers. I have studied the response in electronic properties of graphene for more than one layers in an AA stacked model. For such a model when a number of layers are added, the response DOS on a top is the sum of that number of layers shifted by the coupling parameter. Also, the DOS at Fermi level is found to be non-zero making graphite metallic from semi-metallic.

In Chapter IX, I applied a Green function extension theory³⁶ to study a π theory

model Hamiltonian studied a model Hamiltonian that is extended up to its first four neighbors. The matrix power p of the Hamiltonian H was visualized in terms of walks of p steps. So a Green function was computed from the extended Hamiltonian as a function of five different parameters. Assuming that the resulting poles in the complex energy plane of the integrands were simple, they were treated in the cases where they were not exceptional. Thus the density of states for a graphene was computed based on an extended π theory. There were no extra van Hove singularities induced for the range of model parameters studied and hence no extra dips in the band structures the α and β parameter values of the model were inside a certain region.

In Chapter X, I studied the chemisorption of atomic hydrogen on a graphene substrate. I used the self-consistent one-electron atomic Hamiltonian to couple the substrate and the adsorbate. Then I computed the one-electron Green functions using Löwdin partitioning technique to find the local density of states. I looked at the adsorption of an isolated hydrogen atom in various registries. The observed DOS in hydrogen shows an energy splitting. By putting the hydrogen, the graphene lattice is distorted, and the lattice is not bipartite anymore. The total number of spin in the 2D plane is not zero anymore and there must be some magnetic moment induced in the periphery due to the adsorption.

In summary, I have studied one-electron properties associated with zigzag edge states, lattice defects, doping and multilayers of graphene within the simple π theory and or FAKE model. When a molecule is adsorbed on an infinite graphene substrate, electrons tunnel back and forth between substrate and adsorbate. Since the LDOS of the substrate atoms has a spectral continuum, the LDOS of the adsorbate will broaden and shift, via Fano effect⁵⁸. That is, where an isolated molecular state of the adsorbate is stationary and hence an energy eigenstate with a single well-defined energy, coupling it to the substrate permits it to decay, and hence causes a shift and acquire a finite lifetime broadening $\Delta E \Delta t \sim \hbar$ where ΔE is the energy width and Δt

is the decay time.

The method used reasonably predicts qualitative feature of the local density of states and other measurable properties of interest. The advantage of this method is to obtain efficiently qualitative suggestions of spectral features that appear in the experiments. This way, it relates such features conceptually to the physics of adsorbate systems. The formalism is also useful to study electronic behavior in response to the perturbations such as alterations of molecular configurations. The theory provides some qualitative insight into properties of complex adsorbed molecules. My study has shown that the results agree qualitatively with experimental measurement on such adsorbate systems. The Green-function based formalism are directly related to the angle-resolved photoemission spectroscopy (ARPES). The data collected in ARPES probes the properties on the band structures, Fermi surface, energy gaps etc.

So my study leads me to believe that the chemisorption of an isolated H atom is indeed possible. This study reproduces the theoretical prediction of DFT in agreement with experiments that the spectral effects of adsorbed atomic hydrogen are closely related to the effects of a lattice vacancy. This fact, and the related fact that the perturbation affects one sublattice preferentially over the other is most easily understood in the LCAO context of the current study. The difference between the DOS with respect to different positions of carbon atoms: on top of a carbon atom, on top of the hexagonal ring, on top of the carbon-carbon bond are significantly different from one another. The isolated hydrogen atom does have an influence on the graphene plane. Such small in-differences can be related with different electronic properties of the adsorbates.

REFERENCES

- [1] Attila Szabo and Neil S Ostlund. *Modern quantum chemistry: introduction to advanced electronic structure theory*. Courier Corporation, 2012.
- [2] E. Kogan and V. U. Nazarov. Symmetry classification of energy bands in graphene. *Phys. Rev. B*, 85:115418, Mar 2012. doi: 10.1103/PhysRevB.85.115418. URL <http://link.aps.org/doi/10.1103/PhysRevB.85.115418>.
- [3] Derek Stewart. A cautionary tale of two basis sets and graphene. *Computing in Science & Engineering*, 14:55–59, 2012.
- [4] Paolo Giannozzi, Stefano Baroni, Nicola Bonini, Matteo Calandra, Roberto Car, Carlo Cavazzoni, Davide Ceresoli, Guido L Chiarotti, Matteo Cococcioni, Ismaila Dabo, Andrea Dal Corso, Stefano de Gironcoli, Stefano Fabris, Guido Fratesi, Ralph Gebauer, Uwe Gerstmann, Christos Gougoussis, Anton Kokalj, Michele Lazzeri, Layla Martin-Samos, Nicola Marzari, Francesco Mauri, Riccardo Mazzarello, Stefano Paolini, Alfredo Pasquarello, Lorenzo Paulatto, Carlo Sbraccia, Sandro Scandolo, Gabriele Sclauzero, Ari P Seitsonen, Alexander Smogunov, Paolo Umari, and Renata M Wentzcovitch. Quantum espresso: a modular and open-source software project for quantum simulations of materials. *Journal of Physics: Condensed Matter*, 21(39):395502 (19pp), 2009. URL <http://www.quantum-espresso.org>.
- [5] Yi Chen Chang and Stephan Haas. Defect-induced resonances and magnetic patterns in graphene. *Physical Review B*, 83(8):085406, 2011.

- [6] BA McKinnon and TC Choy. A tight binding model for the density of states of graphite-like structures, calculated using green's functions. *Australian journal of physics*, 46(5):601–612, 1993.
- [7] Neil W. Ashcroft and N. David Mermin. *Solid state physics*. Holt, Reinhart and Winston, 1976, Page 330-333.
- [8] Hans A. Bethe. *Intermediate Quantum Mechanics*. W. A. Benjamin Inc, 1964, Page 42-49.
- [9] John C. Slater. *Quantum theory of atomic structure I*. McGraw-Hill Book company, Inc., 1960, Page 110-115.
- [10] John C. Slater. *Quantum theory of atomic structure II*. McGraw-Hill Book company, Inc., 1960, Page 1-6.
- [11] Frank E. Harris. Self-consistent methods in huckel theory. *The Journal of Chemical Physics*, 48(9):4027–4028, October 1968.
- [12] Frank E. Harris, Joseph Delhalle, and Alfred Trautwein. Fake molecular orbital calculations. *Chemical Physics Letters*, 72(2):315–318, June 1980.
- [13] Max Wolfsberg and Lindsay Helmholz. The spectra and electronic structure of the tetrahedral ions MnO_4^{--} . *Journal of Chemical Physics*, 20:837, 1952.
- [14] Louis Chopin Cusachs. Semiempirical molecular orbitals for general polyatomic molecules ii one electron model prediction of the h-o-h angle. *Journal of Chemical Physics*, 43:S157, 1965.
- [15] Alfred E. Anderson and Roald Hoffman. Description of diatomic molecules using one electron configuration energies with two body interactions. *Journal of Chemical Physics*, 60(11):4271–4273, June 1974.

- [16] Robert Rein, Nubuo Fukuda, Htain Win, and Frank E. Harris. Iterative extended huckel theory. *Journal of Chemical Physics*, 45:4743–4744, June 1966.
- [17] Louis Chopin Cusachs and James Ward Reynolds. Selection of molecular matrix elements from atomic data. *Journal of Chemical Physics*, 43:S160, 1965.
- [18] A. Streitwieser. *Molecular orbital theory for organic chemists*. Wiley, New York, 1959.
- [19] R. Rein, G.A. Clarke, and F.E. Harris. *Quantum aspects of heterocyclic compounds in chemistry and biochemistry*. The Israel Academy of Science and Humanities Jerusalem, 1970, Page 86-115.
- [20] Nuboru Mataga and Kitisuke Nishimoto. Electronic structure and spectra of nitrogen heterocycles. *Zeitschrift fur Physikalische Chemie Neue Folge*, 13(S): 140–157, June 1957.
- [21] H. Chojnacki. Repulsion integral parametrization of the scf lcao mo ci method for nitrogen heteroaromates. *Theoretica Chimica Acta (Berl.)*, 11:458–464, 1968.
- [22] S. C. Mathur and E.C. McKannan. The omega technique LCAO-MO Calculations for the Hydrogen Pthalocyanine Molecules. *International Journal of Quantum Chemistry*, IS:247–250, 1967.
- [23] C. E. Moore. *Atomic energy levels*. National Bureau of Standards Circular No 467, 2, 1952.
- [24] L.C. Snyder and H. Basch. *Molecular wavefunction and properties*. Wiley, New York, 1972.
- [25] C. Kittel. *Introduction to Solid State Physics*. Wiley, 2005.
- [26] E. Kaxiras. *Atomic and electronic structure of solids*. Cambridge University Press, 2003.

- [27] Andre K Geim and Konstantin S Novoselov. The rise of graphene. *Nature materials*, 6(3):183–191, 2007.
- [28] Héctor González-Herrero, José M Gómez-Rodríguez, Pierre Mallet, Mohamed Moaied, Juan José Palacios, Carlos Salgado, Miguel M Ugeda, Jean-Yves Veillen, Félix Yndurain, and Iván Brihuega. Atomic-scale control of graphene magnetism by using hydrogen atoms. *American Association for the Advancement of Science*, 352(6284):437–441, 2016.
- [29] P. R. Wallace. The band theory of graphite. *Phys. Rev.*, 71:622–634, May 1947. doi: 10.1103/PhysRev.71.622. URL <https://link.aps.org/doi/10.1103/PhysRev.71.622>.
- [30] Riichiro Saito, Gene Dresselhaus, and Mildred S Dresselhaus. *Physical properties of carbon nanotubes*. World scientific, 1998.
- [31] DE Ellis and GS Painter. Discrete variational method for the energy-band problem with general crystal potentials. *Physical Review B*, 2(8):2887, 1970.
- [32] Frank E. Harris, Hendrik J. Monkhorst, and William A. Schwalm. Hartee-fock formalism for the calculation of total energies and charge densities of thin films. *Journal of Vacuum Science and Technology*, 16(5):1318–1322, April 1979.
- [33] Hendrik J. Monkhorst and William A. Schwalm. Electrostatic for periodic films of atoms. *Physical Review B*, 23(4):1729–1742, August 1980.
- [34] Hendrik J. Monkhorst and James D. Pack. Special points for brillouin-zone integrations. *Phys. Rev. B*, 13:5188–5192, Jun 1976. doi: 10.1103/PhysRevB.13.5188. URL <http://link.aps.org/doi/10.1103/PhysRevB.13.5188>.
- [35] Maajida L.C. Murdock. Green function Huckel calculation of electronic prop-

- erties of graphene based nanostructures. Master's thesis, University of North Dakota, Grand Forks, ND, 2009.
- [36] William A Schwalm and Mizuho K Schwalm. Extension theory for lattice green functions. *Physical Review B*, 37(16):9524, 1988.
- [37] Per? Olov Lowdin. Studies in perturbation theory xiii. treatment of constants of motion in resolvent method, partitioning technique, and perturbation theory. *International Journal of Quantum Chemistry*, 2(6):867–931, 1968.
- [38] Daniel C Elias, Rahul Raveendran Nair, TMG Mohiuddin, SV Morozov, P Blake, MP Halsall, AC Ferrari, DW Boukhvalov, MI Katsnelson, AK Geim, et al. Control of graphene's properties by reversible hydrogenation: evidence for graphane. *Science*, 323(5914):610–613, 2009.
- [39] Sunmin Ryu, Melinda Y Han, Janina Maultzsch, Tony F Heinz, Philip Kim, Michael L Steigerwald, and Louis E Brus. Reversible basal plane hydrogenation of graphene. *arXiv preprint arXiv:0811.3033*, 2008.
- [40] P Ruffieux, O Gröning, P Schwaller, L Schlapbach, and P Gröning. Hydrogen atoms cause long-range electronic effects on graphite. *Physical review letters*, 84(21):4910, 2000.
- [41] Nathan P Guisinger, Gregory M Rutter, Jason N Crain, Phillip N First, and Joseph A Stroscio. Exposure of epitaxial graphene on sic (0001) to atomic hydrogen. *Nano letters*, 9(4):1462–1466, 2009.
- [42] John Hubbard. Electron correlations in narrow energy bands. iii. an improved solution. In *Proceedings of the Royal Society of London A: Mathematical, Physical and Engineering Sciences*, volume 281, pages 401–419. The Royal Society, 1964.

- [43] Elliott H Lieb. Two theorems on the hubbard model. In *Condensed Matter Physics and Exactly Soluble Models*, pages 55–58. Springer, 2004.
- [44] María P. López-Sancho, Fernando de Juan, and María A. H. Vozmediano. Magnetic moments in the presence of topological defects in graphene. *Phys. Rev. B*, 79:075413, Feb 2009. doi: 10.1103/PhysRevB.79.075413. URL <https://link.aps.org/doi/10.1103/PhysRevB.79.075413>.
- [45] Hideki Kumazaki and Dai S. Hirashima. Nonmagnetic-defect-induced magnetism in graphene. *Journal of the Physical Society of Japan*, 76(6):064713, 2007. doi: 10.1143/JPSJ.76.064713.
- [46] Annica M. Black-Schaffer. Rkky coupling in graphene. *Phys. Rev. B*, 81:205416, May 2010. doi: 10.1103/PhysRevB.81.205416.
- [47] M Sherafati and S Satpathy. Rkky interaction in graphene from the lattice green’s function. *Physical Review B*, 83(16):165425, 2011.
- [48] Gianfranco Vidali, Joe Roser, Giulio Manicó, Valerio Pirronello, Hagai B Perets, and Ofer Biham. Formation of molecular hydrogen on analogues of interstellar dust grains: experiments and modelling. In *Journal of Physics: Conference Series*, volume 6, page 36. IOP Publishing, 2005.
- [49] Thomas Zecho, Andreas Güttler, Xianwei Sha, Bret Jackson, and Jürgen Küppers. Adsorption of hydrogen and deuterium atoms on the (0001) graphite surface. *The Journal of chemical physics*, 117(18):8486–8492, 2002.
- [50] Thomas Zecho, Andreas Güttler, and Jürgen Küppers. A tds study of d adsorption on terraces and terrace edges of graphite (0001) surfaces. *Carbon*, 42(3): 609–617, 2004.

- [51] VV Ivanovskaya, A Zobelli, D Teillet-Billy, N Rougeau, V Sidis, and PR Briddon. Hydrogen adsorption on graphene: a first principles study. *The European Physical Journal B-Condensed Matter and Complex Systems*, 76(3):481–486, 2010.
- [52] Oleg V Yazyev and Lothar Helm. Defect-induced magnetism in graphene. *Physical Review B*, 75(12):125408, 2007.
- [53] L Jeloica and V Sidis. Dft investigation of the adsorption of atomic hydrogen on a cluster-model graphite surface. *Chemical Physics Letters*, 300(1):157–162, 1999.
- [54] Xianwei Sha and Bret Jackson. First-principles study of the structural and energetic properties of h atoms on a graphite (0001) surface. *Surface Science*, 496(3):318–330, 2002.
- [55] DW Boukhvalov, MI Katsnelson, and AI Lichtenstein. Hydrogen on graphene: Electronic structure, total energy, structural distortions and magnetism from first-principles calculations. *Physical Review B*, 77(3):035427, 2008.
- [56] David Soriano, Nicolas Leconte, Pablo Ordejón, Jean-Christophe Charlier, Juan-Jose Palacios, and Stephan Roche. Magnetoresistance and magnetic ordering fingerprints in hydrogenated graphene. *Physical review letters*, 107(1):016602, 2011.
- [57] HA Mizes and JS Foster. Long-range electronic perturbations caused by defects using scanning tunnelling microscopy. *Science*, 244(4904):559, 1989.
- [58] Ugo Fano. Effects of configuration interaction on intensities and phase shifts. *Physical Review*, 124(6):1866, 1961.